LONGITUDINAL ANALYSIS OF RETINAL PERFUSION IN MICE FOLLOWING ACUTE ISCHEMIA-REPERFUSION INJURY

by

Ryan Christopher Matthews

Submitted in partial fulfilment of the requirements for
the degree of Master of Science

at

Dalhousie University
Halifax, Nova Scotia
April 2023

Dalhousie University is located in Mi'kma'ki, the
ancestral and unceded territory of the Mi'kmaq.
We are all Treaty people.

Dedication

This thesis is dedicated to my family,
whose continuous support and love mean the world.
Thank you for always being in my corner
and reminding me that this too, shall pass

Table of Contents

List of Figures

Abstract

Background and Purpose

Retinal ischemia is a common pathology in many vision-threatening diseases. Optical coherence tomography angiography (OCTA) is a non-invasive imaging technique that provides images of microvasculature by measuring temporal variations in the intensity of reflected light. OCTA has been employed previously to assess changes in retinal perfusion during, or immediately after acute ischemia-reperfusion (I/R) injury, however, the longitudinal impact of I/R injury has yet to be fully explored. The goal of this study was to explore the longitudinal relationship between retinal perfusion, thickness, and retinal ganglion cell (RGC) loss using a model of acute I/R injury in mice.

Methods

24 adult female C57Bl/6 mice were divided evenly into groups receiving 15-, 30- or 45-minutes of retinal ischemia, induced by elevating intraocular pressure (IOP) with a cannula in the anterior chamber connected to a raised pressure reservoir. A non-ischemic repeatability group of 4 mice was used for comparison. Imaging sessions were performed at baseline and over a period of 10-days post-I/R injury. At all time points, perfusion density (PD) in the superficial (SVP), intermediate (ICP) and deep (DCP) capillary plexuses were computed from OCTA vascular volumes and ganglion cell complex (GCC) thickness was computed from peripapillary optical coherence tomography (OCT) B-scans. Following the last imaging session, immunohistochemistry (IHC) was performed to quantify cumulative RGC loss. Relevant statistics were performed.

Results

Longitudinal changes in retinal perfusion and GCC thickness following acute I/R injury were tracked *in vivo* with OCTA and OCT. PD was decreased in all plexuses in the 15- and 30-minute elevated IOP groups, however, changes at all time points were not significant when compared to the repeatability group. No significant differences were found in GCC thickness and RGC density between repeatability/control and the 15- and 30-minute elevated IOP groups across all time points. Due to extensive retinal damage, PD in the 45-minute elevated IOP group was computed using a custom vascular volume that combined all capillary plexuses together. PD in the 45-minute elevated IOP group was significantly lower than the repeatability group at all time points post-I/R injury. GCC thickness in the 45-minute elevated IOP group was significantly increased at 1-day, then significantly decreased at 5-, 7- and 10-days post-I/R injury, when compared to all other groups. RGC density in the 45-minute elevated IOP group was significantly lower than all other groups. There was no significant difference in PD between the SVP, ICP and DCP any time point in the 15- and 30-minute elevated IOP groups.

Conclusion

This research describes the *in vivo* use of OCTA and OCT in tracking the longitudinal changes in retinal PD and GCC thickness following acute I/R injury in mice. Data gathered from OCTA and OCT may be useful in enhancing our understanding of the time course of changes in retinal perfusion and thickness during disease. Our comparative analyses between ischemic durations and between the vascular plexuses may provide valuable insight into the pathogenesis of ischemic retinal disease.

List of Abbreviations Used

AMD	Age-Related Macular Degeneration
AMPA	Amino-Methyl-Propionic-Acid
ATP	Adenosine Triphosphate
BRAO	Branch Retinal Artery Occlusion
BRB	Blood-Retinal-Barrier
BRVO	Branch Retinal Vein Occlusion
CCAC	Canadian Council of Animal Care
CCV	Custom Combined Volume
CNV	Choroidal Neovascularization
CRA	Central Retinal Artery
CRAO	Central Retinal Artery Occlusion
CRV	Central Retinal Vein
CRVO	Central Retinal Vein Occlusion
CSLO	Confocal Scanning Laser Ophthalmoscopy
DCP	Deep Capillary Plexus
DR	Diabetic Retinopathy
FA	Fluorescein Angiography
FG	Fluoro-Gold
GABA	γ- Aminobutyric Acid
GCC	Ganglion Cell Complex
GCL	Ganglion Cell Layer
HBSS	Hanks' Balanced Salt Solution
I/R	Ischemia-Reperfusion
ICGA	Indocyanine Green Angiography
ICP	Intermediate Capillary Plexus
IHC	Immunohistochemistry
ILM	Inner Limiting Membrane
INL	Inner Nuclear Layer
IOP	Intraocular Pressure

IPL	Inner Plexiform Layer
IR	Infrared Light
LGN	Lateral Geniculate Nucleus
NDS	Normal Donkey Serum
NMDA	N-Methyl-D-Aspartate
NO	Nitric Oxide
NT	Neurotransmitter
O_2	Oxygen
OCT	Optical Coherence Tomography
OCTA	Optical Coherence Tomography Angiography
ON	Optic Nerve
ONH	Optic Nerve Head
ONL	Outer Nuclear Layer
OPL	Outer Plexiform Layer
PACG	Primary Angle Closure Glaucoma
PBS	Phosphate Buffered Solution
PD	Perfusion Density
PFA	Paraformaldehyde
POAG	Primary Open Angle Glaucoma
r	Pearson Correlation Coefficient
RBPMS	RNA-Binding Protein with Multiple Splicing
RCL	Retrograde Labelling of the Superior Colliculus
RGC	Retinal Ganglion Cell
RNFL	Retinal Nerve Fibre Layer
ROI	Region of Interest
ROS	Reactive Oxygen Species
RPCP	Radial Peripapillary Capillary Plexus
RPE	Retinal Pigment Epithelium
SC	Superior Colliculus
SD	Standard Deviation
SVP	Superficial Vascular Plexus

TNF-α	Tumor Necrosis Factor-α

Acknowledgements

When I first moved to Nova Scotia to begin this degree at Dalhousie, I had no idea what to expect. Now several years later reflecting upon my time in the Retina and Optic Nerve Laboratory, I feel incredibly lucky and grateful to have learned from and worked alongside the many incredible people who have made this degree possible.

I would like to first thank my supervisor, Dr. Balwantray Chauhan, for his guidance, instruction, and support over the past few years. Thank you for inviting me to be part of the RONL and sharing your infectious enthusiasm for research every week. I greatly appreciate the amount of time, effort, and knowledge you have invested in both me and this project. It has been an honour to be one of your graduate students.

I would also like to thank the members of my supervisory committee, Dr. Stefan Krueger, Dr. Jayme Vianna, and Dr. Melina Agosto. Thank you for offering your patience, insight, and input, all of which were invaluable to the progression of this project.

I would further like to thank Michele Hooper and Dr. Corey Smith, whose technical expertise and knowledge were instrumental in getting this project off the ground and running. I am incredibly appreciative of your efforts in contribution to this project- its completion would truly not have been possible without you.

Lastly, I would like to thank Delaney Henderson and Aliénor Jamet for offering their friendship and support over the past several years. I truly appreciate your help in navigating graduate school and keeping me sane until the finish line.

CHAPTER 1. Introduction

1.1. Vision

For those with sight, vision is an inherent sense utilized in navigating the challenges of everyday life. Through the process of conducting and converting light from objects into usable information, the eye and retina permits us to visualize and interact with our surroundings.

1.1.1. Anatomical Structure and Function of the Eye

The main function of the eye is to collect, refract, focus and transform light into information that can be used later by higher processing centres in the brain. Briefly, light collected from the environment first passes through the cornea, where most refraction occurs, then passes through the anterior chamber, pupil and crystalline lens, where it is further focussed on to the retina at the posterior wall of the eye (Figure 1.1). As the outermost coating of the eye, the cornea and sclera serve to protect the interior structures. The cornea is a transparent, avascular tissue that contributes from 66% to 80% of the refractive power of the eye (Hejtmancik & Shiels, 2015; Sridhar, 2018). The sclera is opaque and connects to the cornea at the limbus. Posterior to the cornea is the iris and pupil. The iris is a coloured, circular muscle that contracts and dilates to change the size of the pupil, the aperture through which light reaches the retina. The crystalline lens is located just posterior to the iris and pupil, suspended in place by the ligamentous zonular fibres that attach to the ciliary body. Tight packaging of numerous proteins enables lens transparency and refractive power (Hejtmancik & Shiels, 2015). The ciliary body is a

ring of tissue posterior to the iris and contains the ciliary muscle and processes, which act to control the shape of the lens and secrete aqueous humour, respectively (Donaldson et al., 2017; Glasser & Kaufman, 1999). Filling in the space posterior to the lens is the vitreous, a gel-like substance that consists almost entirely of water, but supports a network of collagen that stabilizes the vitreous and maintains the shape of the inner cavity of the eye (Pokki et al., 2015). There are three distinct fluid chambers within the eye. The anterior chamber is situated between the cornea and the iris, while the posterior chamber is located between the iris and the anterior surface of the zonule fibres. The anterior and posterior chambers are filled with aqueous humour. The final fluid chamber is the vitreous chamber, filled with vitreous and found between the zonule fibres/posterior lens and the retina.

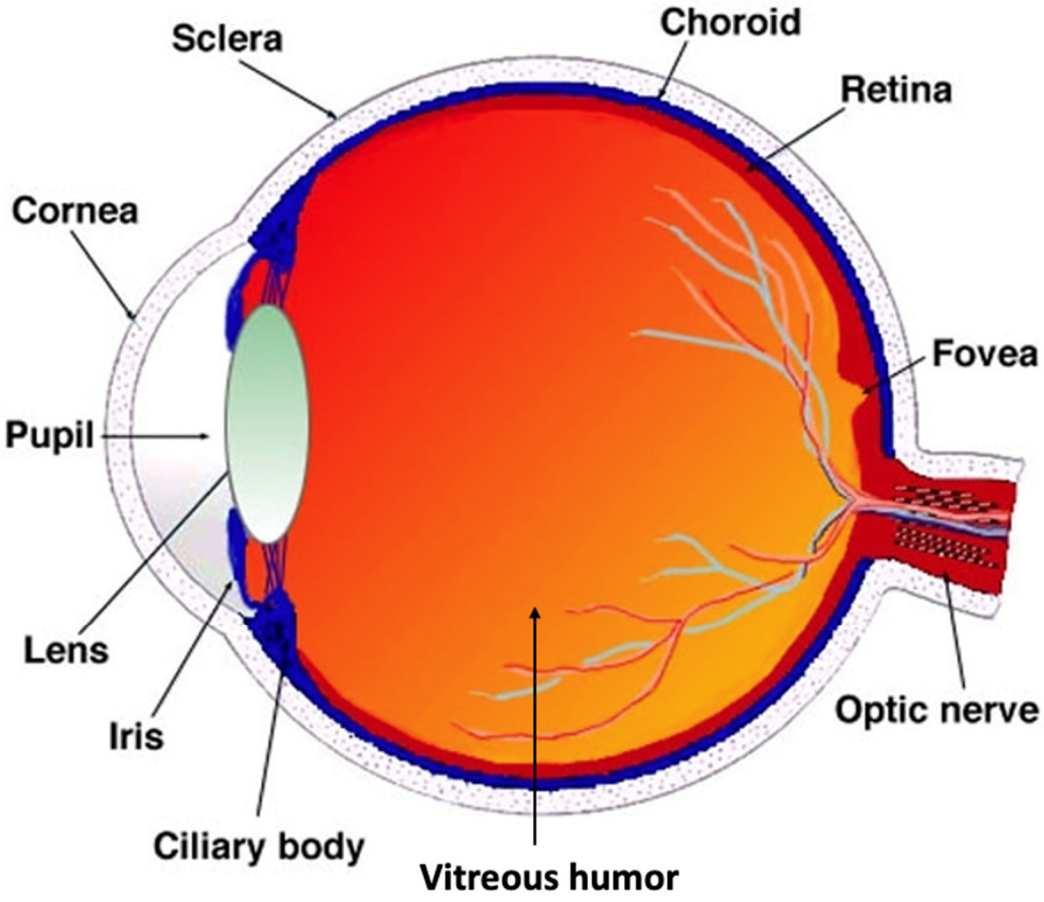

Figure 1.1. Structural anatomy of the human eye in cross-section. Relevant anatomical structures labelled. Figure adapted from Webvision (http://webvision.med.utah.edu/) and used under the non-commercial 4.0 international (CC BY-NC) creative commons license.

1.1.2. Anatomical Structure of the Retina

The retina is a stratified coat of neural tissue approximately 0.5mm thick in vertebrates (Kolb, 2011). The vertebrate retina is organized into three nuclear layers, separated by two plexiform layers (Hoon et al., 2014) (Figure 1.2). The nuclear layers contain the bodies of cells that populate the retina, with the external layer (the outer nuclear layer [ONL]) containing the rod and cone photoreceptor somas, the middle layer (the inner nuclear layer [INL]) containing primarily the amacrine, bipolar and horizontal cells, as well as Müller glial cells, and the inner layer (the ganglion cell layer [GCL]), containing primarily retinal ganglion cells (RGC) and displaced amacrine cells (Hoon et al., 2014; Kolb et al., 2001). The two plexiform layers contain synapses between cells of adjacent nuclear layers. The outer plexiform layer (OPL) is situated between the ONL and INL, and contains synaptic connections between the photoreceptors, bipolar and horizontal cells. The inner plexiform layer (IPL) is located between the INL and GCL, and contains synaptic connections between bipolar cells, amacrine cells and RGCs. Anterior to the GCL, the retinal nerve fibre layer (RNFL) contains axons of RGCs that span across the retina in nerve fibre bundles towards the optic nerve (ON), where they exit the eye.

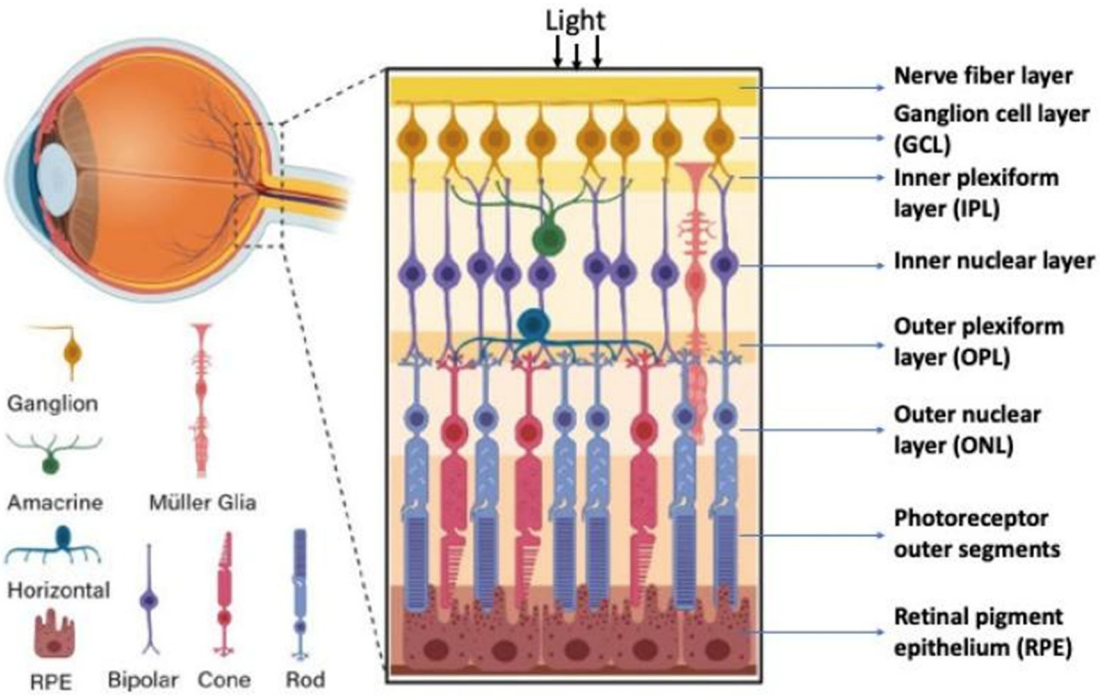

Figure 1.2. Schematic of the mammalian retina and its cell types. The three nuclear layers of the retina and the cell somas found within are labelled. The synaptic connections between cell types within the two plexiform layers are illustrated. Connection between photoreceptor outer segment and the RPE is illustrated. Figure obtained from Grigoryan, 2022 and used under the non-commercial 4.0 international (CC BY- 4.0) creative commons license (https://creativecommons.org/licenses/by/4.0/).

1.1.3. Signal Progression Through the Retina

Signal progression begins when light traverses the retina and reaches the photoreceptors, which neighbor the retinal pigment epithelium (RPE). The RPE is a single layer of cells located between the light sensitive outer segments of the photoreceptors and the choroid. Key RPE functions are to nourish the photoreceptors and absorb light, which is made possible by the heavy pigmentation of RPE cells (Pepperberg et al., 1993; Uehara et al., 1990). The RPE also plays an important role in phagocytosing and regenerating the tips of the photoreceptor outer segments after they receive photo-oxidative damage and shed off (Beatty et al., 2000; Bok, 1993; LaVail, 1983; Winkler et al., 1999).

Rods are the most abundant photoreceptor in both the human and mouse retina, contain the visual pigment rhodopsin and are primarily used for low-light vision. Cones are primarily used for light-abundant vision. Primates contain three visual pigment cone opsins, which respond maximally to light in the long (red), medium (green) and short (blue) wavelength ranges (Bowmaker & Dartnall, 1980). Cones comprise ~3% of all photoreceptors in the mouse retina and have two cone pigments, S and M, which maximally respond to light in the short (360nm) and medium (508nm) wavelength ranges, respectively (Carter-Dawson & LaVail, 1979; Fu & Yau, 2007). In darkness, open cation channels induce constant photoreceptor depolarization, permitting continuous release of the neurotransmitter (NT) glutamate (Stryer, 1991; Yau, 1994). Stimulation from a photon initiates signal transduction as light energy photo-isomerizes the 11-*cis*-retinal chromophore to all-*trans*-retinal, inducing conformational change of the G protein-coupled receptor opsin. This initiates a cascade of signals that closes cation

channels, thereby inducing cell membrane hyperpolarization and cessation of glutamate release. After isomerization, all-*trans*-retinal is reduced to all-*trans*-retinol and travels to the RPE, where it is re-oxidized to 11-*cis*-retinal before returning to the photoreceptors. (Hargrave & McDowell, 1992; Tsin et al., 2018).

Bipolar cells contribute to the vertical pathway from photoreceptors to RGCs and are reported to make up ~40% of all cells in the mouse INL (Jeon et al., 1998). Two types of bipolar cells exist, on-centre and off-centre, where light stimuli in the centre of the receptive field results in depolarization and hyperpolarization, respectively (Dacheux & Miller, 1976; Toyoda, 1973; Werblin & Dowling, 1969). Horizontal cells are retinal interneurons and comprise 3% of all INL cell bodies (Jeon et al., 1998). Across the OPL, a laterally interconnected network of horizontal cell axons enables information summation (Werblin & Dowling, 1969). Horizontal cells provide a variety of functions, one of the most important being the inhibitory modulation of photoreceptors and bipolar cells via various feedback and feedforward mechanisms (Baylor et al., 1971; Hirano et al., 2007; Kolb et al., 2001; Werblin & Dowling, 1969). Amacrine cells are retinal interneurons that make up 39% of all cells in the mouse INL. Additionally, displaced amacrine cells comprise ~59% of all cells in the mouse GCL, while in humans make up 3-80% of all GCL cells, depending on proximity to the optic nerve head (ONH) (Curcio & Allen, 1990; Jeon et al., 1998). Using γ- aminobutyric acid (GABA) and glycine, amacrine cells integrate and modulate inhibitory information sent to RGCs either directly via synaptic connections, or indirectly via reciprocal synapses with bipolar cells (Kolb & Nelson, 1993; Wässle et al., 2009).

RGCs are the terminal cells in signal progression through the retina and act to transmit the final output to the brain. Human retinas contain approximately 1.5 million RGCs, while mouse retinas contain approximately 60,000 (Albrecht May, 2008; Curcio & Allen, 1990; Jeon et al., 1998). Chemical information received by RGCs is converted into electrical potentials at the cell membrane and further integrated by the dendrites and soma into electrical spikes that are sent along RGC axons (Kolb et al., 2001). The dominant targets in the brain for RGC axons are the lateral geniculate nucleus (LGN) in humans and the superior colliculus (SC) in rodents (Calkins, 2012; Lund, 1965; Perry, 1981; Salinas-Navarro et al., 2009). Although the brain perceives the final visual signal, RGCs participate in some visual processing at the retinal level. Examples include varying RGC responses to on/off status, width and direction of light stimuli (Barlow et al., 1964; Hartline, 1938; Lettvin et al., 1959; Wiesel, 1959).

1.2. Eye Vasculature

1.2.1. Perfusion of the Eye

In humans, blood in the internal carotid artery branches into the ophthalmic artery and prior to reaching the eye, is further divided into the choroidal and retinal systems of blood supply (Anand-Apte & Hollyfield, 2010; Anderson & McIntosh, 1967; Kiel, 2010; Wright et al., 2020) (Figure 1.3).

The choroidal system receives blood from three branches of the ophthalmic artery, the anterior ciliary artery and the long and short posterior ciliary arteries, which together supply blood to the anterior tissues of the eye and the choroid. The anterior ciliary artery passes through the sclera near the limbus and joins the arterial circle of the iris, supplying

blood to the iris and ciliary body (Kiel, 2010; Wright et al., 2020). The two long posterior ciliary arteries penetrate the sclera at the posterior pole of the eye, travel anteriorly between the sclera and the choroid and give off branches that join the arterial circle of the iris, or supply the anterior portion of the choroid (Anand-Apte & Hollyfield, 2010; Kiel, 2010). In humans, 16-20 short posterior ciliary arteries penetrate the sclera around the ON and form the circle of Zinn, which give off branches that supply blood to the proximal ON and posterior choroid (Anand-Apte & Hollyfield, 2010; Kiel, 2010). The choroid is dense with interconnecting capillaries that receive 80-85% of the total ocular blood flow, supplying 79% of all oxygen (O_2) consumed by the retina (Alm & Bill, 1972, 1973; Yu et al., 2010). The choroid is an inefficient O_2 delivery system, as low arteriovenous O_2 differences have been found in choroidal circulation, likely due in part to high blood flow rates (Alm & Bill, 1972; Anderson & McIntosh, 1967). The capillary bed of choroidal circulation is the choriocapillaris and as the innermost layer of the choroid, located adjacent to Bruch's membrane. Blood vessels in the choriocapillaris are fenestrated with circular openings, permitting the passage of macromolecules and O_2 that cross Bruch's membrane to nourish the RPE and outer retina (Cunha-Vaz et al., 1966; Guyer et al., 2006). Deoxygenated blood and metabolic by-products are cleared from the iris, ciliary body and choroidal circulation via venules that empty blood into the vortex veins serving each quadrant of the eye (Anand-Apte & Hollyfield, 2010; Anderson & McIntosh, 1967; Kiel, 2010). The vortex veins empty into the superior and inferior ophthalmic veins, which drain into the cavernous sinus, carrying blood back towards the heart.

The retinal system is supplied by the central retinal artery (CRA). The CRA pierces the tissue of the ON, travels along its inferior edge and enters the eye through the ONH (Anand-Apte & Hollyfield, 2010; Kiel, 2010) (Figure 1.3). After entering the eye, the CRA divides into branch arteries that radiate outwards from the ONH to supply blood to all quadrants of the inner retina. The retinal blood supply is both terminal and exclusive, indicating that there are no arteriovenous anastomoses and blood supply to each retinal quadrant is specific to the branch vessel that delivered it (Anand-Apte & Hollyfield, 2010). The branch arteries descend into the retina to supply blood to the retinal microvasculature. Blood vessels of the inner retina are drained by retinal venules and veins, which empty into the central retinal vein (CRV) that exits the eye in the ON, parallel to the CRA. The CRV will drain into the cavernous sinus, directing blood inferiorly towards the heart (Anderson & McIntosh, 1967).

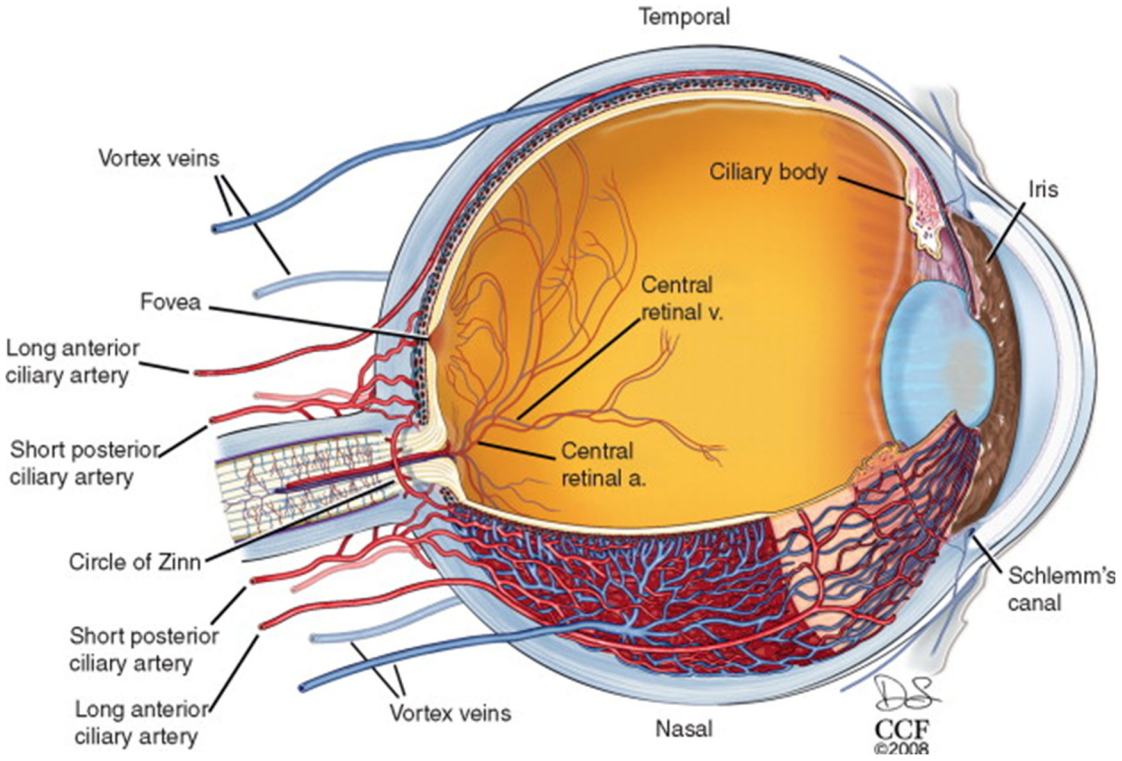

Figure 1.3. Vascular anatomy of the human eye in cross-section. Major arteries and veins perfusing the anterior structures, retina and choroid of the eye are labelled. Drawing originally by Dave Schumick, used from Anand-Apte & Hollyfield, 2010, with permission.

1.2.2. Retinal Microvasculature

The retina is one of the most metabolically active tissues in the body, consuming more O_2 per gram than the brain (Andersen & Saltzman, 1964; Chan et al., 2012; Wright et al., 2020; Yu & Cringle, 2001). The intersection of metabolic need and physiological processing presents a unique situation for perfusion within the retina. Blood vessels must be organized such that adequate light transparency is maintained, while simultaneously servicing the extensive metabolic needs of the retina (Chan et al., 2012; Funk, 1997; Wangsa-Wirawan & Linsenmeier, 2003; Wright et al., 2020; Yu et al., 2010).

The outer retina is completely avascular, therefore nourishment is required from blood circulating the choriocapillaris, which supplies the RPE and photoreceptors (Anderson & McIntosh, 1967; Germer et al., 1998; Yu et al., 2005; Yu et al., 2010). In contrast, the inner retina is characterized by a complex network of vascular beds that supply the various layers of the inner retina. Blood flow in the inner retina is slower, affording higher O_2 extraction as indicated by higher arteriovenous O_2 differences, when compared to the choroid (Anand-Apte & Hollyfield, 2010; Hickham et al., 1963).

In mice, three retinal capillary plexuses are described, the superficial vascular plexus (SVP) found in the GCL, the intermediate capillary plexus (ICP) in the IPL and the deep capillary plexus (DCP) in the OPL (Paques et al., 2003; Ramos et al., 2013). Incoming blood from CRA-derived branch retinal arteries is first received by the SVP, a capillary free zone where horizontal arterioles branch perpendicularly to form the ICP (Paques et al., 2003). The ICP is characterized by short capillary segments in the horizontal plane that also branch perpendicularly, supplying blood to the DCP. The DCP is composed mostly of post-capillary venules running horizontally and branching vertically to initiate

a venous drainage system that is symmetrical, but opposite to the arteriolar system described above (Paques et al., 2003; Ramos et al., 2013).

In humans, four capillary plexuses are described in the retinal peripapillary region (Campbell et al., 2017; Chan et al., 2012, 2015; Kurokawa et al., 2012; Spaide et al., 2015; Tan et al., 2012) (Figure 1.4). The radial peripapillary capillary plexus (RPCP) is located in the RNFL, the SVP is located primarily in the GCL, the ICP is located above the INL and the DCP is located below the INL (Campbell et al., 2017; Chan et al., 2012). The RPCP, ICP and DCP are terminal capillary networks (Alterman & Henkind, 1968; Campbell et al., 2017; Chan et al., 2012; Henkind, 1967; Jia et al., 2014). Briefly, blood from branches of the CRA first arrives in the SVP, where it is shuttled either superiorly to the RPCP or inferiorly to the ICP and DCP via vertical pre-capillary arterial segments (Campbell et al., 2017; Henkind, 1967; Snodderly et al., 1992). Venous drainage within the inner retina consists of post-capillary vertical venules draining blood from the RPCP, ICP and DCP to the SVP, where branch veins collect the blood and eventually leave the eye through the CRV (Campbell et al., 2017).

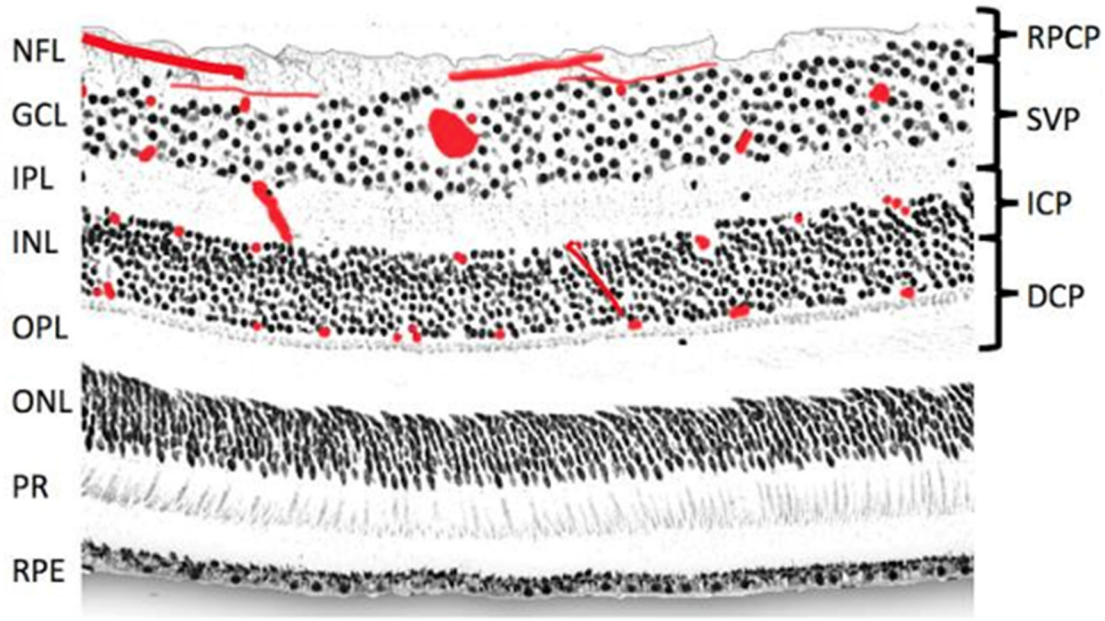

Figure 1.4. Localization of the four vascular plexuses in the human retina. Location of retinal capillary plexuses drawn in red (labelled on right) on top of a histological section of the human retina, which illustrates all anatomical layers (labelled on left). NFL= nerve fibre layer, GCL= ganglion cell layer, IPL= inner plexiform layer, INL= inner nuclear layer, OPL= outer plexiform layer, ONL= outer nuclear layer, PR= photoreceptor layers, RPE= retinal pigment epithelium, RPCP= radial peripapillary capillary plexus, SVP= superficial vascular plexus, ICP= intermediate capillary plexus and DCP= deep capillary plexus. Figure adapted from Campbell et al., 2017 and used under the non-commercial 4.0 international (CC BY- 4.0) creative commons license (https://creativecommons.org/licenses/by/4.0/).

1.2.3. Comparison of Human and Mouse Eye Vasculature

The mouse eye is an important experimental model system as the distribution and general pattern of the mouse eye vasculature is similar to that of humans (Ramos et al., 2013).

Blood distribution to the eye is similar between humans and mice (Hayreh, 1974; May & Lütjen-Drecoll, 2002; Olver et al., 1994). Blood supply to the outer and inner retina from the choriocapillaris and the CRA, respectively, is similar between humans and mice (Albrecht May, 2008; Germer et al., 1998; Ramos et al., 2013). One of the most characteristic differences is the contrast in CRA branching at the ONH (Figure 1.5). In humans, the CRA gives off four branches, the superior and inferior nasal arteries, as well as the superior and inferior temporal arteries, which supply blood to the four quadrants of the eye (Anand-Apte & Hollyfield, 2010; Wright et al., 2020). In contrast, the CRA in mice gives off four to eight branch arterioles running towards the periphery in a spoke-like pattern (Hawes et al., 1999). Another difference is the disparity in the number and location of the inner retinal capillary plexuses, with descriptions of four vascular plexuses in humans and three in mice (Campbell et al., 2017; Chan et al., 2012; Paques et al., 2003; Wright et al., 2020). Human retinas have a fovea, where the inner retina and thus, inner retinal vasculature is absent, whereas mice do not possess a fovea and inner retinal vasculature is found across the retina (Ramos et al., 2013). In humans, no arterio-venous shunts are found within the retina, however, both arterio-venous and arterio-arteriolar shunts have been found in mice and are proposed to protect the retina in hypoxic situations (Paques et al., 2003; Ramos et al., 2013). Venous drainage of the retina and eye are similar between humans and mice (Ramos et al., 2013).

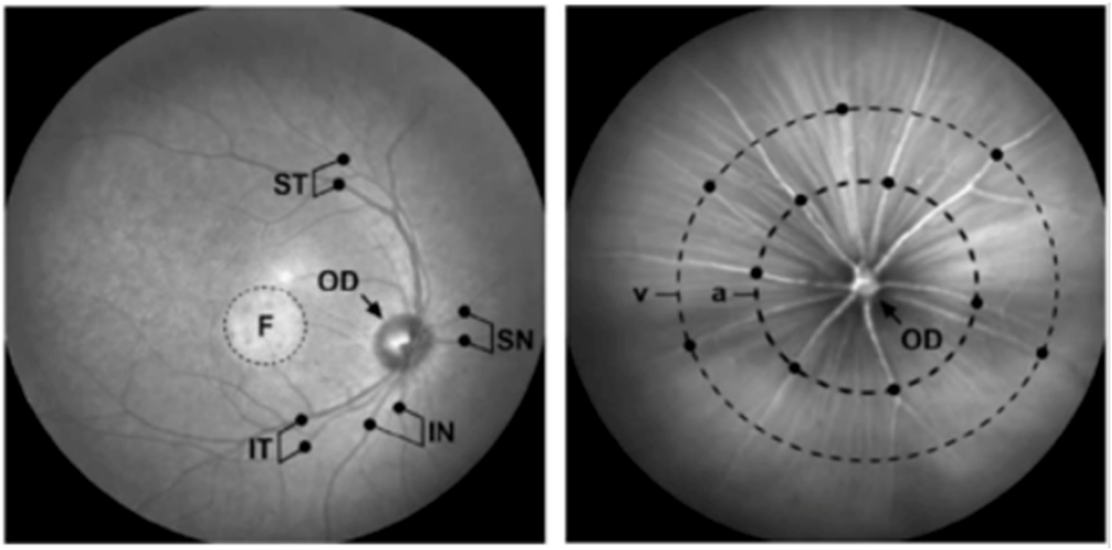

Figure 1.5. Comparison of vascular branching at the ONH in humans and mice. Fundus autofluorescence images illustrating the differing distributions of CRA and CRV branches in humans (left) and mice (right). F= fovea, ST= superotemporal arteries and veins, IT= inferotemporal arteries and veins, SN= superonasal arteries and veins, IN= inferotemporal arteries and veins, OD= optic disc, a= arteriole (indicated by solid black circles on inner dotted line), v= venule (indicated by solid black circles on outer dotted line). Figure used from Ramos et al., 2013, with permission.

1.3. Ischemia in the Retina

Retinal ischemia is a common pathology in many retinal diseases and is a main factor leading to visual impairment and blindness. A destructive two-phase ischemia-reperfusion (I/R) process leads to the death of retinal cells and breakdown of critical signalling pathways in the retina. The clinical significance of retinal ischemia has led researchers to find effective experimental animal models for knowledge translation.

1.3.1. Mechanisms of Retinal Ischemia

Retinal ischemia is indicated when a lack of blood supply results in the inability to meet metabolic demands of the retinal cells, such as the delivery of O_2, metabolic substrates and removal of metabolic by-products (Minhas et al., 2012; Osborne et al., 2004; Schmid et al., 2014). Ischemic retinal diseases include, central retinal artery occlusion (CRAO), branch retinal artery occlusion (BRAO), central retinal vein occlusion (CRVO), branch retinal vein occlusion (BRVO), age-related macular degeneration (AMD), diabetic retinopathy (DR) and glaucoma (Flammer, 1994; Kaur et al., 2008; Linsenmeier et al., 1998; Renner et al., 2017; Schmid et al., 2014).

The exact pathophysiological mechanisms underlying cell death during ischemia is still not completely understood. Some of the supported mechanisms of injury include: degeneration of plasma membrane function, glutamate excitotoxicity and increased intracellular calcium leading to reactive O_2 species (ROS) and nitric oxide (NO) production. The onset of ischemia decreases blood flow and therefore, O_2 and glucose to retinal tissues, reducing cellular metabolism and yielding less adenosine triphosphate (ATP), leading to the deterioration of cellular membrane function and ion homeostasis

(Lipton, 1999; Osborne et al., 2004). Notably, reduction in ATP decreases function of the sodium/potassium ATPase transporter, which further disrupts ion gradients, including the opening of voltage gated calcium channels (De Flora et al., 1998; Lipton, 1999). Stimulated via calcium dependent and independent means, the extracellular accumulation of glutamate during ischemia mediates pathogenesis of retinal degeneration via overstimulation of metabotropic glutamate receptors, as well as ionotropic amino-methyl-propionic-acid (AMPA) and N-methyl-D-aspartate (NMDA) glutamate receptors (Benveniste et al., 1984; Cao et al., 1994; Hartveit et al., 1995; Louzada-Junior et al., 1992; Vorwerk et al., 1996). Elevation of intracellular calcium due to the opening of voltage gated calcium channels and NMDA receptor overstimulation leads to the production of ROS and NO, which are critical to toxic cascades (Abdel-Hamid & Tymianski, 1997; Dugan et al., 1995; Siliprandi et al., 1992; Zipfel et al., 2000). The physical process of cell death during ischemia is due to either apoptosis or necrosis (Büchi, 1992; Dessi et al., 1993; Mehmet et al., 1994; Nakajima et al., 2000).

Retinal ischemia also induces inflammation and blood-retinal-barrier (BRB) dysfunction. During ischemia, leukocytes are recruited and produce proinflammatory cytokines such as interleukin-1 and tumor necrosis factor-α (TNF-α), that are implicated in cell death (Fontaine et al., 2002; Ju et al., 2003; Werns et al., 1985). Excess production of vascular endothelial growth factor and NO during ischemia results in disruption of the BRB, inducing fluid leakage and accumulation in both extracellular and intracellular spaces, leading to retinal degeneration via compression (Johnson, 1974; Marmor, 1999).

The inner and outer retina present differing responses to ischemia. The outer retina may be relatively protected from ischemic injury due to the photoreceptors' ability to

derive nutrition from anaerobic sources during ischemia (Osborne & Larsen, 1996; Stone et al., 1999; Winkler, 1972). Alternatively, the inner retina may be more sensitive to ischemic insult because inner retinal neurons have higher expressions of ionotropic glutamate receptors that are overstimulated during ischemia (Brandstätter et al., 1994). Also implicated is the dual nature of retinal circulation, since blood delivered to the outer and inner retina is derived from different sources and may contribute to the differing response to ischemia (Janáky et al., 2007; Tinjust et al., 2002). Cell degeneration and death is generally proportional to the length of ischemia, however, the threshold for irreversible damage varies between species and type (model) of injury (Faberowski et al., 1989; Lafuente et al., 2002; Smith & Baird, 1952; Zhu et al., 2002).

1.3.2. Reperfusion Injury

Reperfusion injury takes place following the reintroduction of blood flow to previously ischemic tissue. The retinal response to reperfusion depends on the magnitude and duration of the ischemic insult, as a certain period of ischemic time must elapse before reperfusion injury occurs, with threshold times varying across tissue types and species (Soares et al., 2019; Wang et al., 2001).

Mechanisms of injury after reperfusion revolve around oxidative and microcirculatory stress (Renner et al., 2017; Schmid et al., 2014; Soares et al., 2019). Upon reperfusion, reduced compounds accumulated during ischemia are re-oxidized, resulting in ROS formation and subsequent tissue damage (Belforte et al., 2011; Gilgun-Sherki et al., 2002; Nastos et al., 2014; Szabo et al., 1991). Reperfusion also mobilizes neutrophils in the vascular space, producing ROS, TNF-α, and inflammatory mediators

that contribute to tissue damage (Wu et al., 2018). Reperfusion additionally stimulates an extracellular accumulation of glutamate, as the two-fold increase in ischemia bloats to a five to ten-fold increase in reperfusion (Louzada-Junior et al., 1992).

1.3.3. Animal Models of Retinal Ischemia-Reperfusion Injury

In vivo animal models have been invaluable in understanding the pathophysiology of retinal I/R injuries. Common species in experimental models include primate, mouse, rabbit and the most used, rat (Osborne et al., 2004).

A variety of methods have been used to induce experimental retinal ischemia, such as the elevation of intraocular pressure (IOP), ligature of retinal vessels and photo-thrombosis of retinal vessels. The elevation of IOP above perfusion pressure in the eye results in the collapse of blood vessels, mimicking CRAO, acute primary angle closure glaucoma (PACG) and ophthalmic artery occlusion (Büchi et al., 1991; Smith & Baird, 1952). The most common technique to elevate IOP is cannulation of the anterior or vitreous chambers and pressure elevation via external reservoir. The elevation of IOP has many advantages including transiency, reversibility, reproducibility and requires minimally invasive techniques. A potential limitation is ocular and retinal damage due to the pressure elevation itself (Minhas et al., 2012). Ligature of the ON, or specifically the CRA and CRV, offers complete ischemia via constriction or collapse of vessels and resembles CRAO and ophthalmic artery occlusion (Otori et al., 1997; Stefánsson et al., 1988; Vidal-Sanz et al., 2001). A limitation of ON ligature is the potential mechanical damage to axons bundles, however, specific ligature of the CRA and CRV avoids this problem, but is more difficult to achieve technically (Osborne et al., 2004). Photo-

thrombosis of retinal vessels involves the injection of a photo-responsive dye, followed by exposure to a laser of a specific wavelength. This method results in incomplete ischemia, most closely resembling BRAO (Daugeliene et al., 2000; Mosinger & Olney, 1989; Romano et al., 1993). Advantages include simplicity and being relatively non-invasive, while limitations include variable injury and potential phototoxic damage to the retina (Osborne et al., 2004).

1.4. Visualizing Retinal Structure and Perfusion In Vivo

Technological advances have revolutionized the way we image retinal structures. Information on retinal structure and vasculature previously available only through histological analyses can now be available with *in vivo* imaging. The application of *in vivo* imaging modalities has enhanced our knowledge of retinal disease pathophysiology and will continue to be invaluable as we expand our understanding in both experimental and clinical settings.

1.4.1. Confocal Scanning Laser Ophthalmoscopy

Confocal scanning laser ophthalmoscopy (CSLO) is an imaging technique that enables the *in vivo* visualization of retinal and vascular structures with an *en face* view (Manivannan et al., 1993; Webb et al., 1987). CSLO works via the projection of specific wavelengths of laser light, pinhole apertures arranged in confocal positions and a beam splitter that directs backscattered light from the retina on to a detector (Webb et al., 1987). CSLO is commonly used to image gross changes in retinal and vascular structures and recent examples include *en face* visualization and characterization of retinal

degeneration following disease progression in experimental murine models (Huber et al., 2009; Pinilla et al., 2016; Yang et al., 2014). CSLO can also be used for fluorescence imaging of single cells. This has been shown previously in mice, where fluorescent proteins specific to retinal cells are excited by CSLO, permitting subsequent *in vivo* visualization and image acquisition (Beck et al., 2009; Chauhan et al., 2012; Leung et al., 2008). Strengths of CSLO include high lateral resolution and scanning efficiency, while a limitation of conventional CSLO is poor axial resolution (Balendra et al., 2015; Sher et al., 2020).

1.4.2. Optical Coherence Tomography

Optical coherence tomography (OCT) is an *in vivo* imaging technique that provides high resolution cross-sectional images of the retinal layers (Alex et al., 2019; Sher et al., 2020). The principles of OCT imaging have been described elsewhere (Wojtkowski et al., 2005). Briefly, the OCT device generates a beam of low-coherence light which is split, diverting one half to the retina and the other half to the reference mirror. Backscattered light from the retina and reference mirror converge to produce an interference pattern that is sent to an interferometer for A-scan processing (Drexler & Fujimoto, 2008; Fujimoto et al., 2000; Jaffe & Caprioli, 2004).

The applications of OCT imaging are diverse. Several types of OCT devices exist with different properties, such as: time-domain OCT, spectral-domain OCT, swept-source OCT and long-wavelength OCT (Keane & Sadda, 2014). Recently, OCT has been utilized by clinicians to measure retinal layer and choroidal thickness, evaluate retinal lesions, visualize retinal atrophy and evaluate macular ischemia due to DR or retinal vein

obstruction (Bakhoum et al., 2018; Corradetti et al., 2019; Govetto et al., 2020; Shi et al., 2021; Virgili et al., 2015). Experimental OCT imaging has been widely used in various animal models of disease, for example, the longitudinal characterization and evaluation of retinal structure at different stages of DR disease progression (Allingham et al., 2018; Bubis et al., 2019; Groh et al., 2014; Shirai et al., 2016). Limitations for OCT imaging include poor imaging of retinal blood vessels, inability to display single cells and limited field of view (Drexler et al., 2014; Leitgeb et al., 2014; McNabb et al., 2019).

1.4.3. Optical Coherence Tomography Angiography

Optical coherence tomography angiography (OCTA) is a relatively new, non-invasive imaging technique that provides images of retinal and choroidal microvasculature with enhanced depth resolution (Keane & Sadda, 2014; Rocholz et al., 2018; Spaide, 2015). Prior to OCTA, the gold-standard of retinal vascular imaging was fluorescein angiography (FA) and indocyanine green angiography (ICGA), however, both require invasive injections of dyes and have comparatively poor depth resolution of the inner retinal microvasculature and choroidal circulation (Gao et al., 2016; Spaide et al., 2015). OCTA analyzes the intensity of reflected light as it changes over time by repeatedly capturing OCT B-scans at a single point in the retina to generate motion contrast between the blood vessels (with moving erythrocytes) and the static surrounding tissue (Fogel-Levin et al., 2022; Rocholz et al., 2018). OCTA image generation employs algorithms to assess the variations between repeated OCT B-scans. The Spectralis program used in this thesis (Spectralis Multiline, Heidelberg Engineering GmbH, Heidelberg, Germany) employs a probabilistic algorithm that calculates the probability of

whether a pixel is in a location of perfused or non-perfused structure, based on pre-existing OCT signal distributions (Rocholz et al., 2018). Algorithms can be different between manufacturers and dependent on acquisition protocols (Zhang et al., 2015).

The use of OCTA has recently become more widespread in clinical and experimental settings. It has been used in the detection of microvascular changes, microaneurysms and choroidal or retinal ischemia following vascular diseases such as DR and retinal vein occlusion (Balaratnasingam et al., 2016; Greig et al., 2020; Salz et al., 2016; Soares et al., 2017). It has also been used to evaluate ischemic optic neuropathies and even proposed as a diagnostic indicator of choroidal neovascularization and AMD (Sharma et al., 2017; Sulzbacher et al., 2017). Limitations of OCTA imaging include the inability to visualize vascular leakage and provide information on blood velocity and flow (Ang et al., 2018; Fogel-Levin et al., 2022). Other limitations include potential segmentation errors in the case of retinal layer alteration, restricted field of vision and the lack of a standardized segmentation method (Chen et al., 2016; Rocholz et al., 2018; Sher et al., 2020).

1.5. Objectives and Hypothesis

Previous experimental research, including work from our own laboratory, has used OCTA imaging to assess the impact of acute I/R injury at limited time points, or neuronal damage at longitudinal time points, on rodent retinal microvasculature, though the impact of acute I/R injury at longitudinal time points has yet to be fully explored. (Choi et al., 2021; Jiang et al., 2018; Park et al., 2016; Smith et al., 2019; Zhao et al., 2020). The overall goal of this research was to explore the time course of perfusion

changes and the longitudinal relationship between retinal perfusion, retinal thickness and RGC loss using a model of acute retinal ischemia in mice.

The specific objectives of this thesis were to:

1. Track inner retinal perfusion and GCC thickness longitudinally with OCTA and OCT, respectively, following acute I/R injury
2. Evaluate longitudinal changes in retinal perfusion and GCC thickness, as well as cumulative changes in RGC density, by comparing groups with differing durations of ischemia
3. Evaluate retinal perfusion longitudinally, by comparing changes in perfusion between the vascular plexuses

We hypothesized that:

1. We would be able to track retinal perfusion and GCC thickness longitudinally *in vivo*.
2. We would record retinal perfusion and GCC thickness loss over time following acute I/R injury, as well as cumulative RGC loss, all increasing with duration of ischemia.
3. We would record no difference in perfusion changes between vascular plexuses following acute I/R injury.

CHAPTER 2. Materials and Methods

2.1. Animals

2.1.1. Ethics, Housing and Usage

All animal procedures were conducted in accordance with the Canadian Council of Animal Care (CCAC). Ethics approval was obtained from the Animal Ethics Committee at Dalhousie University. Adult female C57Bl/6 mice (JAX™ Mice Stock Number: 027, Charles River Laboratories, Wilmington, MA, USA) were used in this study. The mice were housed in a 12-hour light-dark cycle environment and had access to water and food *ad libitum*. Twenty-four mice underwent retrograde labelling of the superior colliculus (RCL) and subsequent experimental elevation of IOP. The mice were split into three experimental groups with eight mice used for each of the 15- , 30-, and 45-minute elevated IOP timepoints. A separate group of four mice was used for repeatability testing. All twenty-eight mice were used to quantify ganglion cell complex (GCC) thickness and retinal perfusion density (PD) with longitudinal *in vivo* imaging over 10 days. 47 retinas from the 15-, 30-, and 45-minute elevated IOP groups (15, 16 and 16, respectively) were used to quantify RGC density with immunohistochemistry (IHC).

2.1.2. Anaesthesia

For the RCL, elevated IOP and longitudinal *in vivo* imaging procedures, mice were initially anaesthetized with 2% isoflurane (Baxter Corporation, Mississauga, ON, Canada) and 1% O_2, administered at a flow rate of 1.5 l/min. Following initial induction,

mice were maintained at 1.5% isoflurane and 1% O_2, with 1.5 l/min O_2 flow via nose cone for the duration of the procedure.

2.2. Retrograde Labelling of the Superior Colliculus

2.2.1. Retrograde Labelling Procedure

Prior to the surgery, mice were injected subcutaneously with buprenorphine and meloxicam at dosages of 0.1mg/kg and 5mg/kg body weight, respectively, for analgesia. Following anaesthesia (see 2.1.2.), the depth of anaesthesia was confirmed by the pedal reflex and breathing rate. Mice were placed in a stereotaxic frame and on a heating pad to maintain body temperature for the duration of the procedure. Prior to incision, the skin was shaved, cleaned and sterilized with povidone-iodine (Betadine, Purdue Pharma, Pickering, ON, Canada). Using anatomical skull markings, a 2-3cm incision was made in the skin from bregma to just posterior to lambda. To remove a small portion of the skull, bilateral 0.5 cm square-shaped holes were drilled into the skull beginning midway between bregma and lambda, extending posteriorly to lambda. Once the brain matter was exposed, suction apparatus (Allied Healthcare Products Inc., St. Louis, MO, USA) with tubing attached to a glass needle was used to suction the white and grey matter, uncovering the SC. Absorbable gelatin sponges (Ethicon, Bridgewater, NJ, USA) soaked with 4% Fluoro-Gold (FG; Fluorochrome LLC., Denver, CO, USA) were placed bilaterally above the SC, filling the space left by suctioned matter. With the sponges in place, the skin was sutured with 5-0 monofilament suture. Ophthalmic gel was applied to the eyes for recovery and saline was administered subcutaneously to replenish fluid lost during surgery. Mice were recovered on heat overnight. Subcutaneous meloxicam

(5mg/kg body weight) was administered the following morning and mice were recovered for 7 days. All surgical instruments were autoclaved and bead sterilized between surgeries.

2.2.2. In vivo CSLO Fluorescence Imaging

CSLO was centred on the ONH and fluorescence images of FG labelled RGCs were acquired at baseline and 1-, 3-, 5-, 7- and 10-days post-ischemic insult, for the purposes of quantifying *in vivo* RGC density. Images were focused axially where fluorescence signal was strongest and fluorescently labelled cells within a 30° scan angle were imaged. Fluorescence images were acquired with an 448nm excitation bandpass and barrier filter of 460-490nm (Chauhan et al., 2012).

2.2.3. Difficulties Encountered

We dedicated several months optimizing the technique for labeling the SC in mouse. While we use this technique routinely in rats it was considerably more challenging in mice. Initially, the RCL procedures appeared successful and baseline *in vivo* imaging showed that fluorescently labelled RGCs could be visualized and imaged. However, the axial depth at which the fluorescence signal was strongest (and thus, presence of labelled cells) was largely variable between mice. Furthermore, labelling location across the retina was unreliable, wherein some mice showed labelling across the whole retina, while others had labelling in only one quarter of the retina.

Further difficulties were encountered during follow-up imaging sessions in tracking RGC density. Because of acute edema and inflammation that occurred

immediately post-IOP elevation, follow-up images were difficult to register to baseline and were of sub-optimal quality. Furthermore, image quality at later follow-up imaging timepoints was often poor (Figure 2.1). These factors made it impossible to use *in vivo* RGC as a longitudinal measure of RGC viability

Due to the difficulties outlined above, it was not feasible to quantify *in vivo* RGC density accurately and consistently using the *in vivo* fluorescence images. As an alternative to *in vivo* RGC density quantification, we elected to quantify *in vivo* GCC thickness as a proxy assessment of inner retinal health. This technique has been used frequently and published by our lab before (Di Pierdomenico et al., 2022).

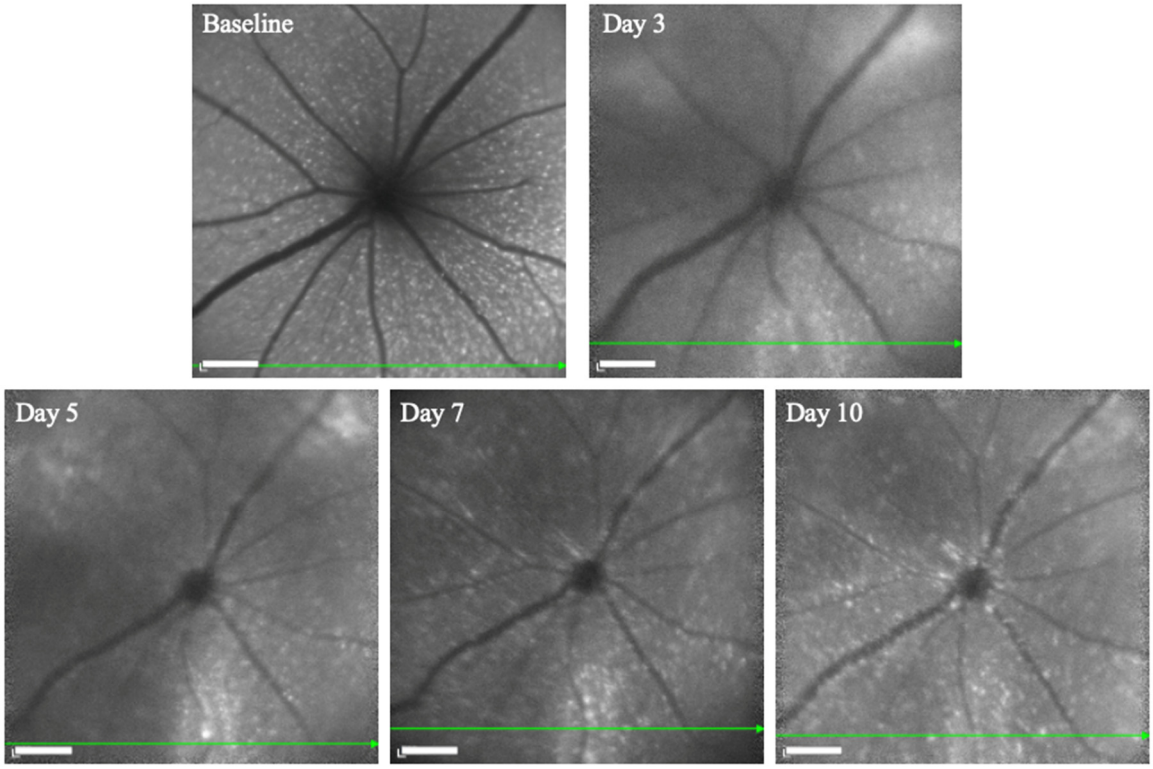

Figure 2.1. Longitudinal *in vivo* CSLO imaging of a mouse that received 45 minutes of retinal ischemia. The same mouse was imaged at baseline (prior to elevated IOP procedure) and over a period of 10 days post-elevated IOP procedure. Follow-up images representative of the 45-minute elevated IOP group demonstrate poor image quality of FG labelled RGCs. Green line indicates OCT B-scan location. Follow-up images were unable to be registered to baseline. White scale bars represent 200μm.

2.3. In vivo Longitudinal Imaging

2.3.1. Set-Up and Animal Preparation

In vivo longitudinal imaging procedures were performed with CSLO and spectral domain OCT device, modified for use in mice (Heidelberg Engineering GmbH) (Chauhan et al., 2012). OCT imaging was used to acquire cross-sectional B-scans of the retina at baseline and over a period of 10 days post-elevated IOP procedure, to quantify GCC thickness. OCTA imaging was used to acquire images of the vascular plexuses at various retinal depths at baseline and over a period of 10 days post-elevated IOP procedure, to quantify retinal PD. To protect the integrity and quality of longitudinal imaging, the software minimizes motion artifacts by using real time eye tracking (Chauhan et al., 2012). Additionally, the software is set to register all follow-up images to baseline, granting serial analysis at the exact same retinal location for each time point.

Following anaesthesia (see 2.1.2.), all mice were placed on a heating pad and the left pupil was dilated with 1% tropicamide (Alcon, Mississauga, ON, Canada) and 2.5% phenylephrine hydrochloride (Alcon). Ophthalmic gel and a polymethyl methacrylate contact lens (Cantor and Nissel Limited, Brackley, UK) were placed on the cornea for maintenance of corneal hydration and image quality.

2.3.2. In vivo Imaging Timeline

For each of the 15-, 30- and 45-minute elevated IOP groups, follow-up imaging sessions were performed at 1-, 3-, 5-, 7- and 10-days post-elevated IOP procedure. As the repeatability group did not undergo the elevated IOP procedure, follow-up imaging sessions were performed at 1-, 3-, 5-, 7- and 10-days post-baseline imaging (Figure 2.2).

Along with the imaging set-up and animal preparation outlined above, each baseline and follow-up imaging session included: i) One circular peripapillary OCT B-scan; ii) one OCTA volume acquired both nasal and temporal to the ONH; and iii) CSLO fluorescence imaging of RGCs at various retinal depths. Additionally, at each timepoint one infrared light (IR; 820nm) image and one 19-line raster pattern OCT B-scan were acquired to monitor retinal integrity.

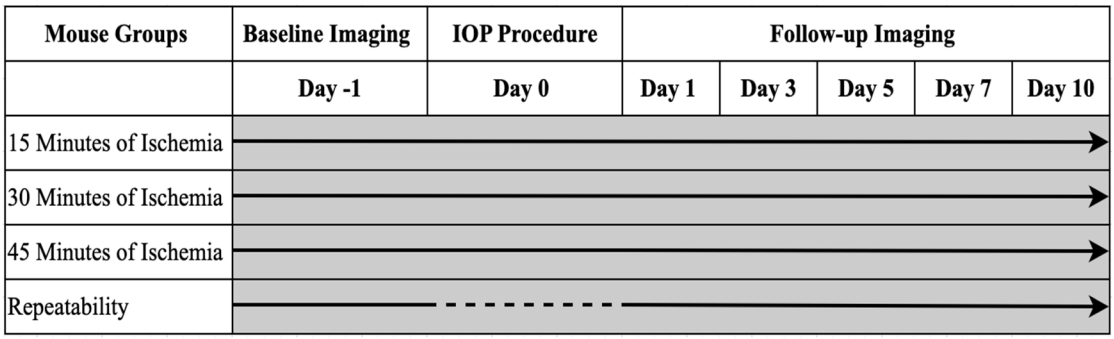

Figure 2.2. Timeline for *in vivo* imaging sessions performed on each group of mice. Mice in the 15-, 30- and 45-minute elevated IOP groups were imaged at baseline and for a period of 10-days following the elevated IOP procedure. Mice in the repeatability group underwent baseline, then follow-up imaging beginning 1-day post-baseline imaging. All imaging sessions consisted of OCT and OCTA imaging.

2.3.3. In vivo OCT Imaging

Beginning by centering OCT on the ONH and focusing into the RNFL, one circular peripapillary B-scan subtending 12° was acquired for the purposes of quantifying GCC thickness over time. For OCT imaging, the scanning speed was 40,000 A-scans per second and each B-scan was comprised of 1536 A-scans. The B-scans were averaged 100 times.

2.3.4. In vivo OCTA Imaging

One OCTA image volume was acquired both temporal and nasal to the ONH for the purposes of quantifying retinal PD. The OCTA image was focused on the RNFL and OCT B-scan image quality was maximized. Each OCTA volume was 512 A-scans by 512 B-scans (20° x 20° in high-speed mode), each an average of four B-scans. Compared to smaller (10° x 10°), slower options, the larger high-speed scan pattern was the ideal choice for detection of large vascular abnormalities and perfusion drop out resulting from retinal conditions (Rocholz et al., 2018).

2.4. Experimental Elevation of Intraocular Pressure

All mice used in this project underwent the elevated IOP procedure, excluding four in the repeatability group.

2.4.1. Pressure Column Set-Up

The pressure column utilized to increase IOP in this project has been described previously (Nuschke, 2017) and later adapted for this project. Briefly, a 60ml syringe

reservoir was filled with Hanks' Balanced Salt Solution (HBSS; GIBCO, Grand Island, NY, USA) and connected to a wall-mounted track. A pulley system was fitted to the reservoir, permitting vertical translation along the track and subsequent generation of hydraulic pressure. The HBSS reservoir was connected to a three-way stopcock via plastic tubing. The stopcock directed HBSS flow to both a sphygmomanometer, for the purposes of monitoring pressure within the system and polyethylene PE10 tubing, connected to a 32-gauge needle (TSK Laboratory, Tochigi, Japan) at the distal endpoint.

2.4.2. Cannulation Procedure

Following anaesthesia (see 2.1.2.), mice were placed on a heating pad to maintain body temperature throughout the procedure and the left eye was dilated with 1% tropicamide (Alcon) and 2.5% phenylephrine hydrochloride (Alcon).

The cannulation technique used for the elevated IOP procedure was adapted from a mouse anterior chamber cannulation protocol described previously (Hartsock et al., 2016). The modifications included the use of the pressure column (see 2.4.1.), tubing and needle for a single mouse and the use of a 32-gauge needle.

Following dilation of the left eye, the pressure column was raised until the sphygmomanometer read 90 mmHg. This pressure level was chosen as it appeared to be the lowest value at which retinal ischemia was observed by fundoscopic examination. The stopcock was then opened and HBSS was allowed to flow through the needle tip. Visualizing the left cornea through a surgical microscope (Carl Zeiss AG, Oberkochen, Germany) two forceps were used simultaneously: the first was used to gently proptose the left eye, while the second was used to guide the needle into the anterior chamber with

the needle bevel facing up. The anterior chamber was cannulated midway between the corneal apex and the zonular fibres, angling the needle anteriorly towards the corneal apex, away from the crystalline lens. Special care was taken to avoid scratching the lens or pushing the needle through the opposite side of the cornea, both of which would classify a failed experiment.

Following successful cannulation, the needle and connected tubing was secured so that it did not move for the remainder of the experiment. The eye was then checked to confirm there were no leaks and balanced salt solution (Alcon Laboratories, Fort Worth, TX, USA) was applied to the eye to maintain corneal hydration. Retinal ischemia was confirmed by cessation of blood flow at the optic disc visualized with the surgical microscope. Every 15 minutes for the duration of the procedure, the eye was checked for any signs of leakage and to confirm the retina was still ischemic. Balanced salt solution was reapplied for maintenance of corneal hydration. Following completion of the ischemic timepoint, the needle was carefully removed and the stopcock was closed to halt the flow of HBSS. Reperfusion within the retina was confirmed via the return of blood flow at the optic disc. Ophthalmic gel was applied to maintain corneal hydration during recovery and the mice were given a subcutaneous injection of buprenorphine hydrochloride (0.02 mg/kg body weight) for analgesia. The mice were then returned to cage and left on a heat pad overnight for recovery.

2.4.3. Ischemia Groups

The three elevated IOP groups chosen for this project all received the same degree of IOP elevation (90mmHg) to induce retinal ischemia, however the duration of elevated

IOP in the three groups differed at 15-, 30- and 45-minutes. A fourth group for repeatability did not undergo the elevated IOP procedure and thus, did not receive retinal ischemia.

The selection of ischemic timepoints was based on information gained from previous work done in the laboratory and preliminary testing. The 15-, 30- and 45-minute ischemic timepoints were ultimately selected to induce mild, moderate and severe damage, respectively.

2.5. Immunohistochemistry and Tissue Preparation

Upon completion of the last *in vivo* imaging timepoint, all mice (excluding the repeatability group) were sacrificed using an overdose of sodium pentobarbital (Dorminal, Rafter 8 Products, Calgary, AB, Canada) via intraperitoneal injection. Experimental and fellow eyes were enucleated and the corneas incised to remove the lenses. They were then fixed in 4% paraformaldehyde (PFA; Fisher Scientific, Ottawa, ON, Canada) for 24 hours. The retinas were dissected and prepared for IHC by blocking in 10% normal donkey serum (NDS; Sigma- Aldrich Co., St. Louis, MO, USA) in phosphate buffered solution (PBS) with 0.5% Triton-X overnight at 4°C. After blocking, the retinas were incubated in primary antibodies against RNA-binding protein with multiple splicing (RBPMS; 1:1000 guinea pig anti-RBPMS, PhosphoSolutions #1832, Aurora, CO, USA) in PBS with 0.5% Triton-X for 5 days at 4°C to stain the RGCs. Retinas were then washed 3 x 20 minutes in PBS and incubated in the secondary antibody Cy3 (1:500 Cy3-conjugated donkey anti-guinea pig, Jackson ImmunoResearch Laboratories Inc., West Grove, PA, USA) in PBS with 0.5% Triton-X overnight at 4°C.

The retinas were washed 3 x 20 minutes in PBS and mounted on microscope slides. Fluorescence mounting medium (Vectashield, Vector Laboratories Inc., Burlingame, CA, USA) was applied for anti-fading purposes and the retinal wholemounts were cover-slipped for subsequent epifluorescence imaging.

2.6. Epifluorescence Imaging

Following IHC, a fluorescence microscope (Axio Imager M2, Carl Zeiss AG, Oberkochen, Germany) with a 20x objective (Plan-Apochromat 0.8 numerical aperture; Carl Zeiss) was used to acquire tiled images of wholemounted retinas. With device software (Zen, Carl Zeiss), the retinal wholemounts were viewed under a rhodamine filter channel and fluorescence images of cells expressing RBPMS were captured.

2.7. Data Analysis

2.7.1. Image Analysis, Data Management and Statistics

For analysis, OCT and OCTA images were segmented using device software (Heidelberg Engineering GmbH). OCTA images were batch-cropped using ImageJ (version 2.9 for macOS, open-source) and binarized using MATLAB (The Mathworks, Natick, MA, USA). Data was managed using Microsoft Excel (version 16.66.1 for Macintosh, Microsoft, Redmond, WA, USA). Statistics were performed using Prism (version 9.4.1 for MacOS, GraphPad Software, San Diego, CA, USA). Statistical significance was assumed when the p value was less than 0.05.

2.7.2. OCT Imaging

Circular peripapillary OCT B-scans acquired longitudinally following ischemic insult were manually segmented using the segmentation editor within the device software (Heidelberg Engineering GmbH). GCC thickness was measured from the inner limiting membrane (ILM) to the outer border of the IPL, after these borders were segmented. GCC thickness (in μm), averaged across the retina was calculated by the device software. GCC thickness change relative to baseline for each timepoint was computed and reported as a percentage change from baseline. Ordinary one-way ANOVAs with Tukey's multiple comparisons test were performed to determine statistical significance by comparing the differences between group means at each timepoint.

2.7.3. OCTA Imaging

OCTA scans acquired longitudinally following ischemic insult were automatically segmented by the device software (Heidelberg Engineering GmbH). Derived from the automatic segmentations, 2D transverse projection images of various vascular volumes were created by the software. For the 15- and 30-minute elevated IOP groups, transverse projection images of the SVP (segmented from the RNFL to the inner border of the IPL), ICP (segmented from the inner border of the IPL to the outer border of the IPL) and DCP (segmented from the outer border of the IPL to the OPL) were used for analysis. For the 45-minute elevated IOP group, transverse projection images of a custom vascular volume (CCV; segmented from the RNFL to the OPL) combining the SVP, ICP and DCP were used for analysis. The CCV images were used because 45-minutes of ischemia resulted in significant thinning of retinal layers, therefore the device software was ineffective in segmenting all retinal layers and produced poor transverse projections that artifactually

influenced retinal PD quantification. Transverse projection images of the SVP, ICP and DCP, as well as CCV projections, were used for repeatability group analysis, which served as a comparison for the 15-, 30- and 45-minute elevated IOP groups. OCTA images at one-day post-ischemic insult were not included in analysis or statistics. This was implemented due to the presence of vitreous haze artifactually lowering retinal PD quantification, which resolved in all cases by the 3-day time point. All images were exported as tiff files.

All transverse projection images were imported into Image J (open-source) as image sequences and batch-cropped to 600 x 600-pixel region of interests (ROI) representing the best image quality across all timepoints and vascular volumes within the same mouse. The batch-cropping was implemented to mitigate the artifactual impact of poor image quality areas within projection images, on retinal PD quantification. For each mouse, batch-cropping was done at the same location within the image across all timepoints and vascular volumes, to maintain longitudinal and comparative integrity

Following batch-cropping, the transverse projection images were imported into MATLAB (The Mathworks) and analyzed with a customized OCTA binary threshold analysis. The analysis algorithm has been published in detail elsewhere (Smith et al., 2019), however, in brief, the transverse projection images were first converted to greyscale and a gaussian filter ($\sigma = 1$, $h = 7$) was applied for noise removal and contrast enhancement. A locally adaptive image-thresholding algorithm was then employed to binarize the projection images coding each pixel within the image to either white (areas of blood flow), or black (areas with no blood flow; Figure 2.3). Following thresholding, mask-subtraction, where large vessels identified in the SVP were removed from the

deeper ICP and DCP vascular volumes, was implemented to avoid shadow artifacts. Finally, PD was calculated as the ratio of white pixels over total binarized image area.

PD change respective to baseline was computed for all PD values and reported as a percent change from baseline. Ordinary one-way ANOVAs with Tukey's multiple comparison test were used to determine statistical significance by comparing means between groups at each timepoint for the repeatability, 15- and 30-minute elevated IOP groups. Unpaired t-tests with Welch's correction for groups with unequal variance were used to determine statistical significance by comparing group means at each timepoint for the repeatability and 45- minute elevated IOP groups. Pearson correlation with two-tailed significance tests were also used to correlate day 10 PD values with RBPMS density values for the 15-, 30- and 45-minute elevated IOP groups.

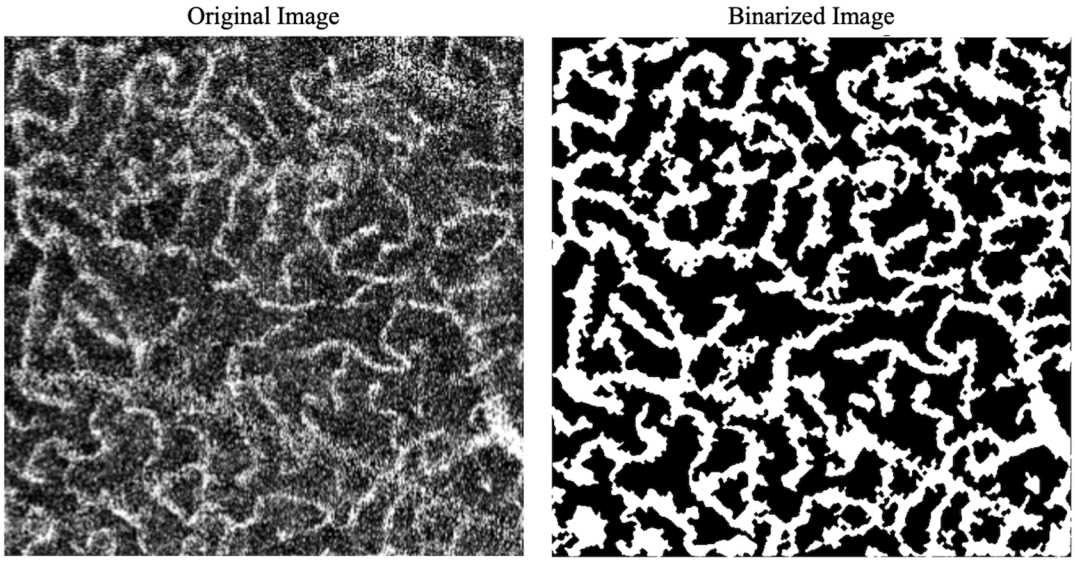

Figure 2.3. *In vivo* OCTA image binarization of the ICP in a mouse at baseline during binary threshold analysis. A transverse projection image of the ICP vascular volume was acquired via *in vivo* OCTA imaging. A locally adaptive image-thresholding algorithm was used to produce a binary version of the original image.

2.7.4. Immunohistochemistry

Tiled images of wholemounted retinas expressing fluorescently labelled RBPMS cells were analyzed using Zen software (Carl Zeiss AG, Oberkochen, Germany). For each wholemounted retina, 318µm x 318µm ROIs were acquired. For each retinal quadrant, ROIs from the central, middle and peripheral retina were collected for a total of 12 ROIs. All 12 ROIs for each retina were exported as tiff files.

Each ROI was imported into Image J (open-source) and cells expressing RBPMS were manually counted using the cell counter plug-in. RBPMS cell counts were manually imported into Excel (Microsoft) for management. Cell counts from the non-experimental fellow eyes from all mice in the 15-, 30- and 45-minute elevated IOP groups were accumulated to create a control group for comparison. RBPMS density was computed and reported as mean RBPMS density (standard deviation [SD]). A Brown-Forsythe and Welch ANOVA test with Dunnett's T3 multiple comparisons test was used to determine statistical significance by comparing means between groups with unequal variance. Pearson correlation with two-tailed significance tests were used to correlate RBPMS density values with day 10 PD values for the 15-, 30- and 45-minute elevated IOP groups.

CHAPTER 3. Results

3.1. Longitudinal Evaluation of Perfusion and Structure in the Repeatability Group

All four mice in the repeatability group were imaged *in vivo* with OCTA and OCT at all time points post-baseline imaging.

3.1.1. Evaluating the Time Course of Changes in Retinal Perfusion Density

We tracked the time course of *in vivo* changes in retinal PD for the repeatability group, which received no ischemic injury. Vascular volumes from the SVP, ICP, DCP and CCV were acquired, then used to quantify retinal PD and subsequently reported as a percent change respective to baseline. Statistics were reported elsewhere.

Vascular volumes of the SVP, ICP, DCP and CCV from a representative mouse are shown (Figures 3.1A, 3.2A, 3.3A and 3.4A, respectively). Compared to baseline, mean PD remained relatively consistent across all time points and plexuses. Mean PD in all vascular volumes were at approximately baseline values at the 10-day imaging endpoint, when mean change from baseline (SD) was -0.4% (5.4), -2.4% (5.3), -1.1% (3.3) and -0.1% (3.4) for the SVP, ICP, DCP and CCV (Figures 3.1B, 3.2B, 3.3B and 3.4B, respectively).

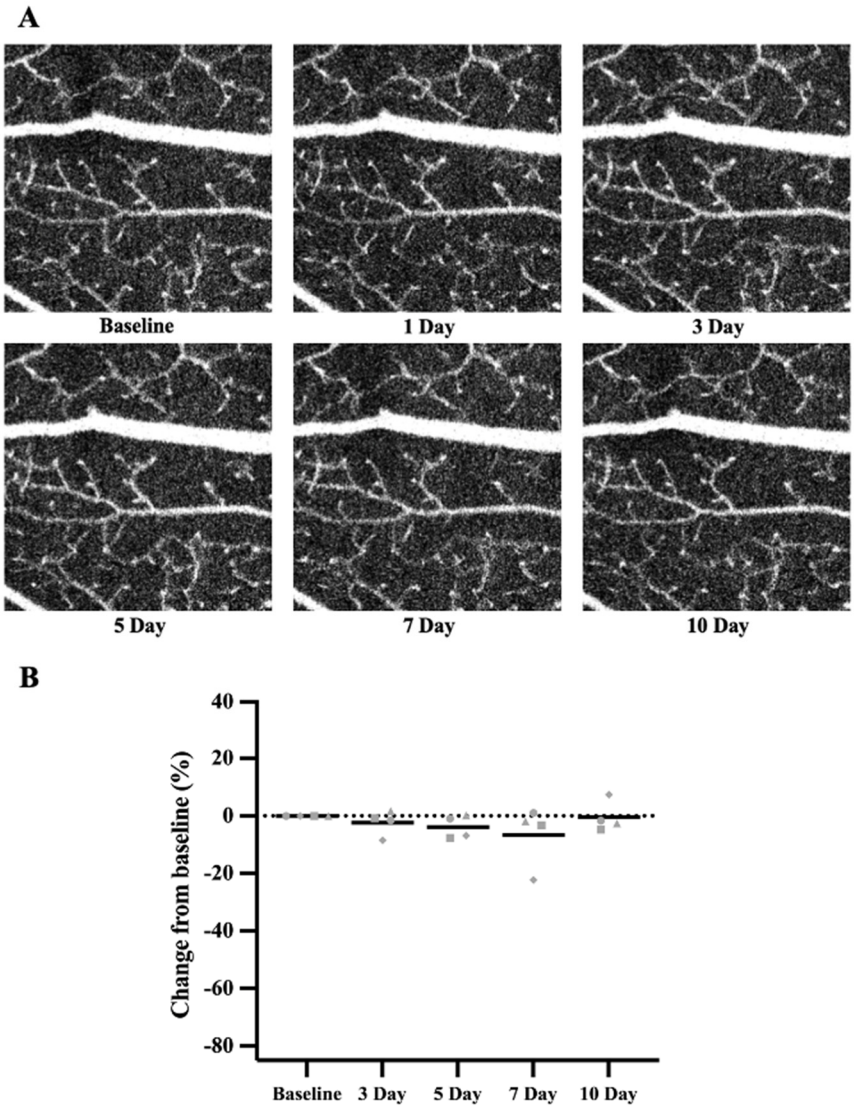

Figure 3.1. Time course of PD in the repeatability group SVP. A) *In vivo* OCTA images were acquired at baseline and over a period of 10-days post-baseline imaging in a mouse that received no elevation of IOP. Images were acquired in the same mouse and retinal location at each time point. B) *In vivo* quantification of PD in the SVP vascular volume. At each time point, PD was computed from the *in vivo* images and reported as change respective to baseline. Figure illustrates minimal change in mean PD at all time points post-baseline imaging in the SVP of the repeatability group. Black bars indicate group mean and grey symbols indicate individual values; n=4.

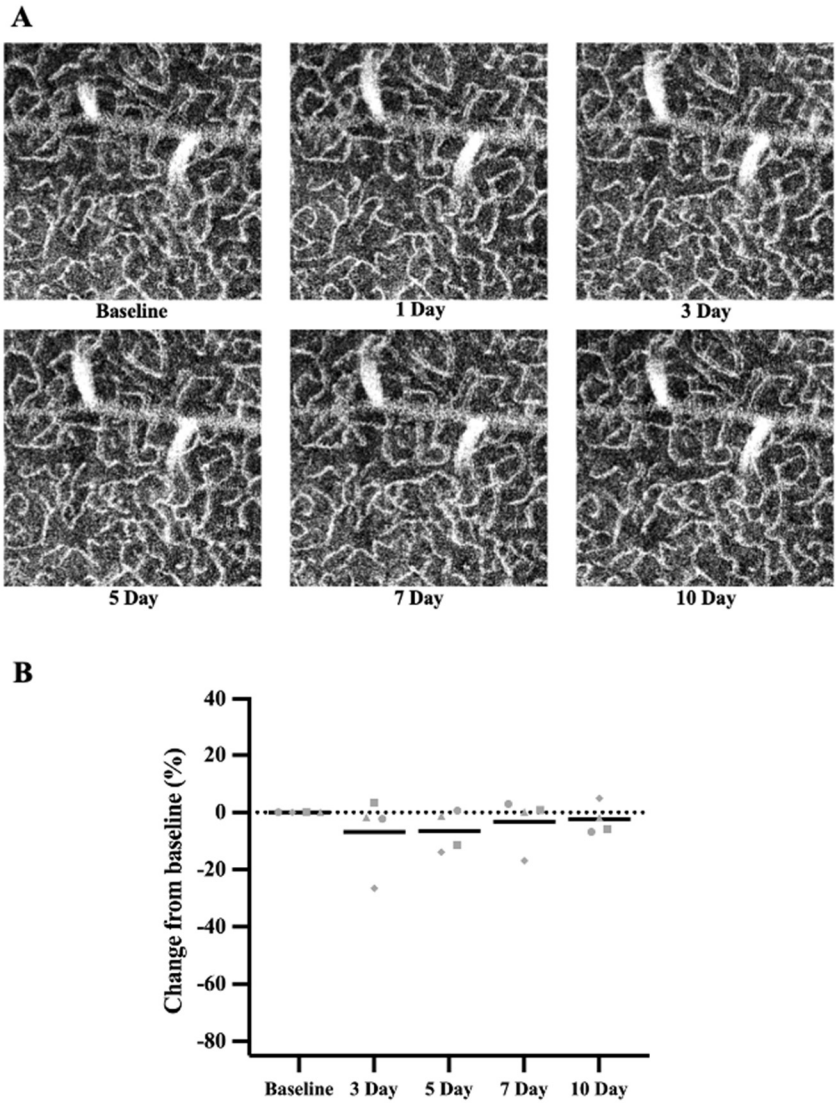

Figure 3.2. Time course of PD in the repeatability group ICP. A) *In vivo OCTA* images were acquired at baseline and over a period of 10 days post-baseline imaging in a mouse that received no elevation of IOP. Images were acquired in the same mouse and retinal location at each time point. B) *In vivo* quantification of PD in the ICP vascular volume. At each time point, PD was computed from the *in vivo* images and reported as change respective to baseline. Figure illustrates a slight decrease in mean PD, followed by an approximate return to baseline values at the 10-day imaging endpoint. Black bars indicate group mean and grey symbols indicate individual values; n=4.

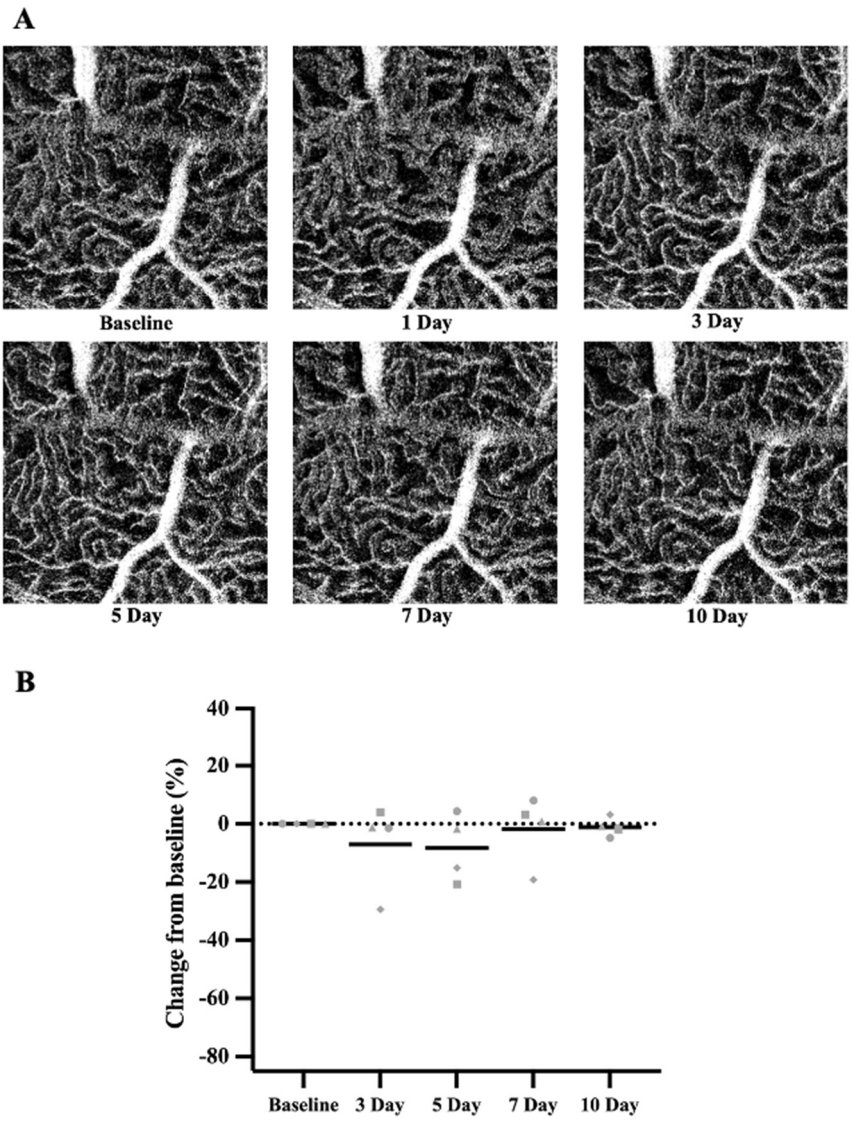

Figure 3.3. Time course of PD in the repeatability group DCP. A) *In vivo* OCTA images were acquired at baseline and over a period of 10 days post-baseline imaging in a mouse that received no elevation of IOP. Images were acquired in the same mouse and retinal location at each time point. B) *In vivo* quantification of PD in the DCP vascular volume. At each time point, PD was computed from the *in vivo* images and reported as change respective to baseline. Figure illustrates a slight decrease in mean PD, followed by an approximate return to baseline values at the 10-day imaging endpoint. Black bars indicate group mean and grey symbols indicate individual values; n=4.

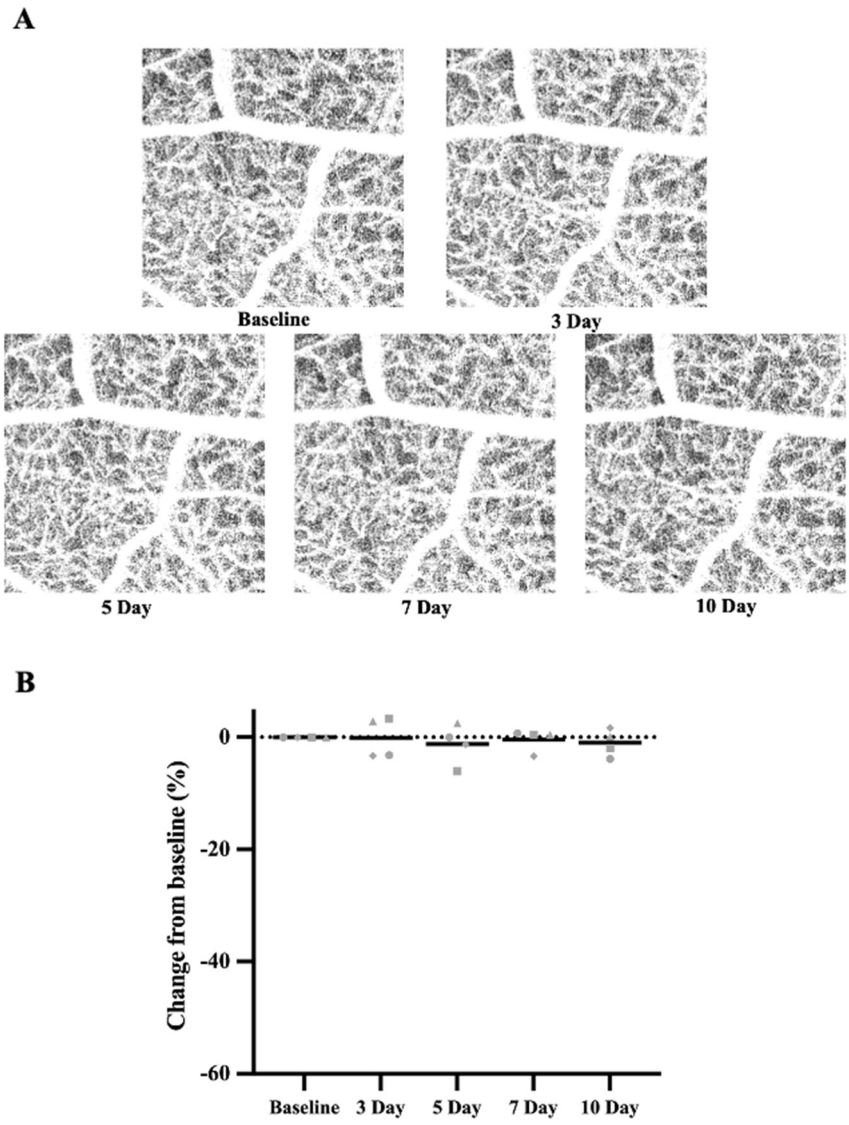

Figure 3.4. Time course of PD in the repeatability group CCV. A) *In vivo* OCTA images were acquired at baseline and over a period of 10 days post-baseline imaging in a mouse that received no elevation of IOP. Images were acquired in the same mouse and retinal location at each time point. B) *In vivo* quantification of PD in the CCV. At each time point, PD was computed from the *in vivo* images and reported as change respective to baseline. Figure illustrates minimal change in PD at all time points post-baseline imaging. Black bars indicate group mean and grey symbols indicate individual values; n=4.

3.1.2. Evaluating the Time Course of Changes in Retinal Thickness

We tracked the time course of *in vivo* changes in GCC thickness for the repeatability group, which received no ischemic injury. Circular peripapillary OCT B-scans were acquired, then used to compute *in vivo* GCC thickness and subsequently reported as percent change respective to baseline. Statistics were run elsewhere.

Circular peripapillary OCT B-scans from a representative mouse are shown (Figure 3.5A). Compared to baseline values, mean GCC thickness in the repeatability group was relatively consistent across all time points, as mean change from baseline (SD) never exceeded more than 0.6% (0.7), or less than -1.2% (1.0) at any time point (Figure 3.5B).

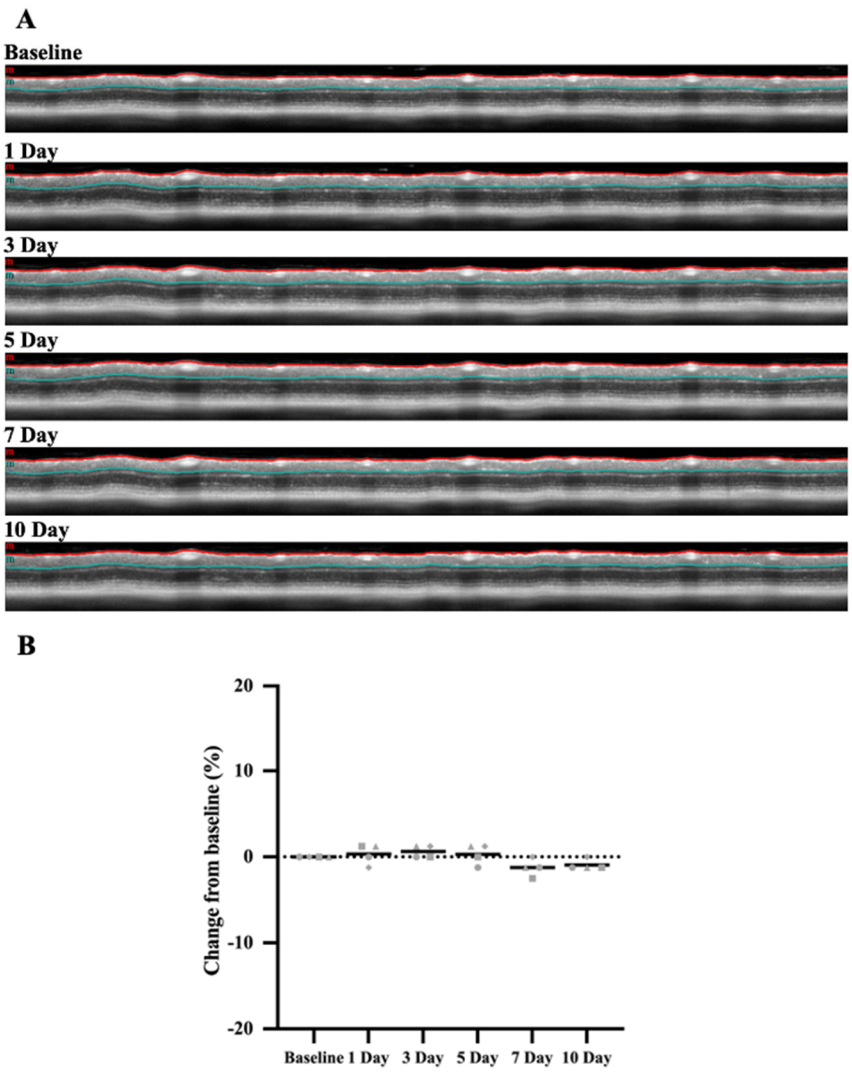

Figure 3.5. Time course of GCC thickness in the repeatability group. A) *In vivo* OCT B-scans were acquired at baseline and over a period of 10 days post-baseline imaging in a mouse that received no elevation of IOP. Depicted images were acquired in the same mouse and retinal location, at each time point. Coloured lines demarcate the GCC, with the red and blue lines indicating segmentation of the ILM and outer border of the IPL, respectively. B) *In vivo* quantification of mean GCC thickness in mice that underwent no elevation of IOP. At each time point, GCC thickness was computed and reported as change respective to baseline. Figure illustrates minimal change in mean GCC thickness at all imaging time points. Black bars indicate group mean and grey symbols indicate individual values; n=4.

3.2. Longitudinal Evaluation of Perfusion and Structure Following Acute Ischemia

3.2.1. Evaluating the Time Course of Changes in Retinal Perfusion Density

Eight mice in each of the 15-, 30- and 45-minute elevated IOP groups were imaged *in vivo* with OCTA at all time points post-I/R injury. We tracked the time course of changes in retinal PD for groups with differing durations of acute retinal ischemia by acquiring vascular volumes of the SVP, ICP, DCP and CCV and quantifying retinal PD, which was then subsequently reported as a percent change respective to baseline. Statistics were reported elsewhere.

In the 15-minute elevated IOP group, vascular volumes of the SVP, ICP and DCP from a representative mouse are shown (Figures 3.6A, 3.7A and 3.8A, respectively). Compared to baseline, mean PD in each vascular volume was decreased at 3-days, which persisted to the 10-day imaging endpoint when mean change from baseline (SD) was -10.4% (16.5), -9.1% (19.1) and -13.4% (25.5) for the SVP, ICP and DCP (Figures 3.6B, 3.7B and 3.8B, respectively).

In the 30-minute elevated IOP group, examples of the vascular volumes from a representative mouse are shown (Figures 3.9A, 3.10A and 3.11A, respectively). Compared to baseline, mean PD was decreased in each volume at the 3-day imaging time point, which persisted over all time points post-I/R injury. Mean change from baseline (SD) at the 10-day imaging endpoint was -11.8% (9.2), -7.6% (17.4) and -14.4% (20.7) for the SVP, ICP and DCP (Figures 3.9B, 3.10B and 3.11B, respectively).

In the 45-minute elevated IOP group, vascular volumes of the CCV from a representative mouse are shown (Figure 3.12A). Compared to baseline, mean PD was decreased at 3-days post-ischemic insult, which persisted to the 5-day imaging time point

and further decreased at subsequent imaging sessions until the 10-day imaging endpoint, when mean change from baseline (SD) was -19.8% (15.3) (Figure 3.12B).

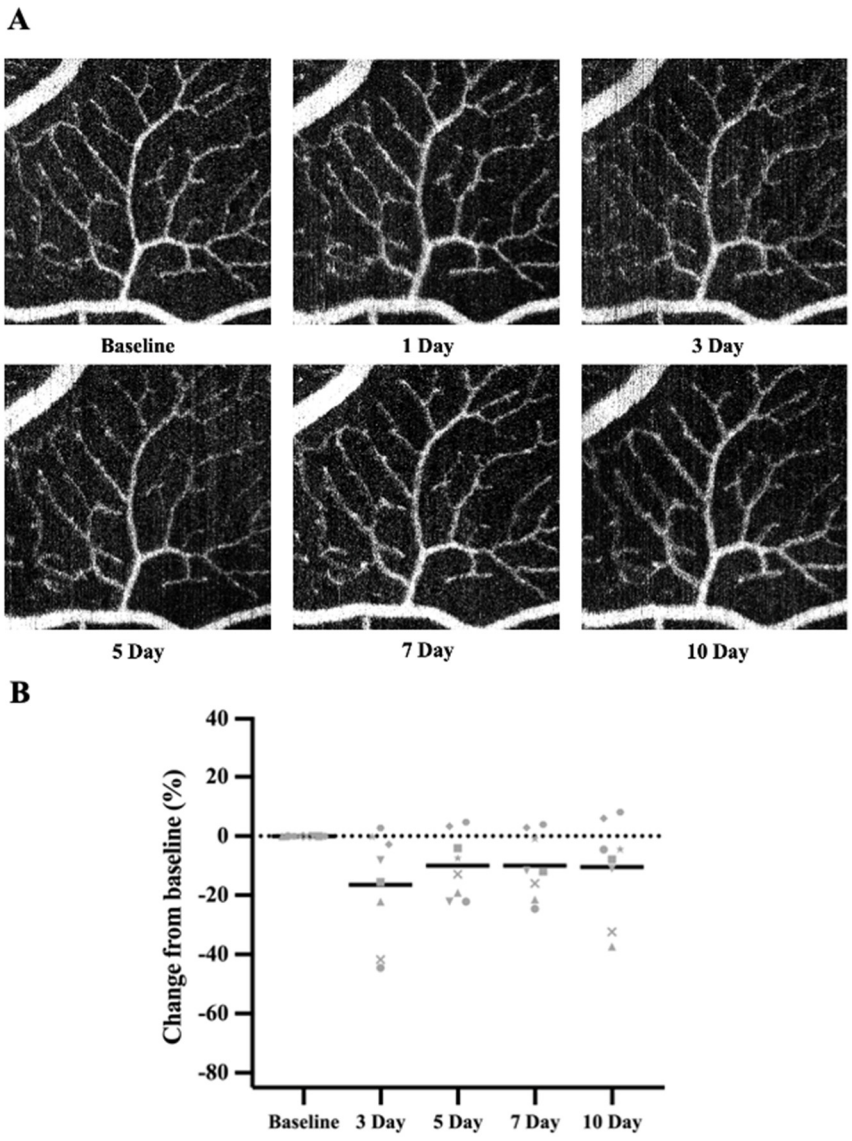

Figure 3.6. Time course of PD in the 15-minute elevated IOP group SVP. A) *In vivo* OCTA images were acquired at baseline and over a period of 10 days post-I/R injury in a mouse that received 15 minutes of ischemia. Images were acquired in the same mouse and retinal location at each time point. B) *In vivo* quantification of PD in the SVP vascular volume. At each time point, PD was computed from the *in vivo* images and reported as change respective to baseline. Figure illustrates a decrease in mean PD at all time points post-I/R injury. Black bars indicate group mean and grey symbols indicate individual values; n=8.

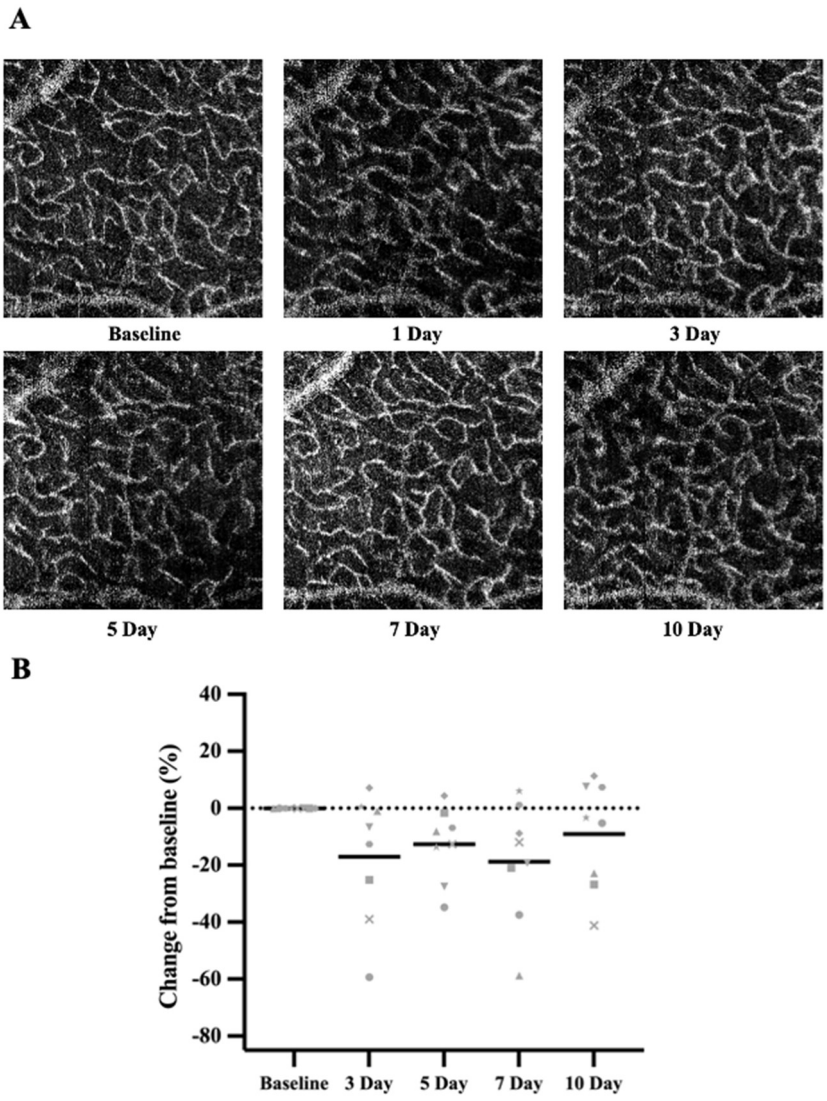

Figure 3.7. Time course of PD in the 15-minute elevated IOP group ICP. A) *In vivo* OCTA images were acquired at baseline and over a period of 10 days post-I/R injury in a mouse that received 15 minutes of ischemia. Images were acquired in the same mouse and retinal location at each time point. B) *In vivo* quantification of PD in the ICP vascular volume. At each time point, PD was computed from the *in vivo* images and reported as change respective to baseline. Figure illustrates a decrease in mean PD at all time points post-I/R injury, as well as a wide variability in PD values. Black bars indicate group mean and grey symbols indicate individual values; n=8.

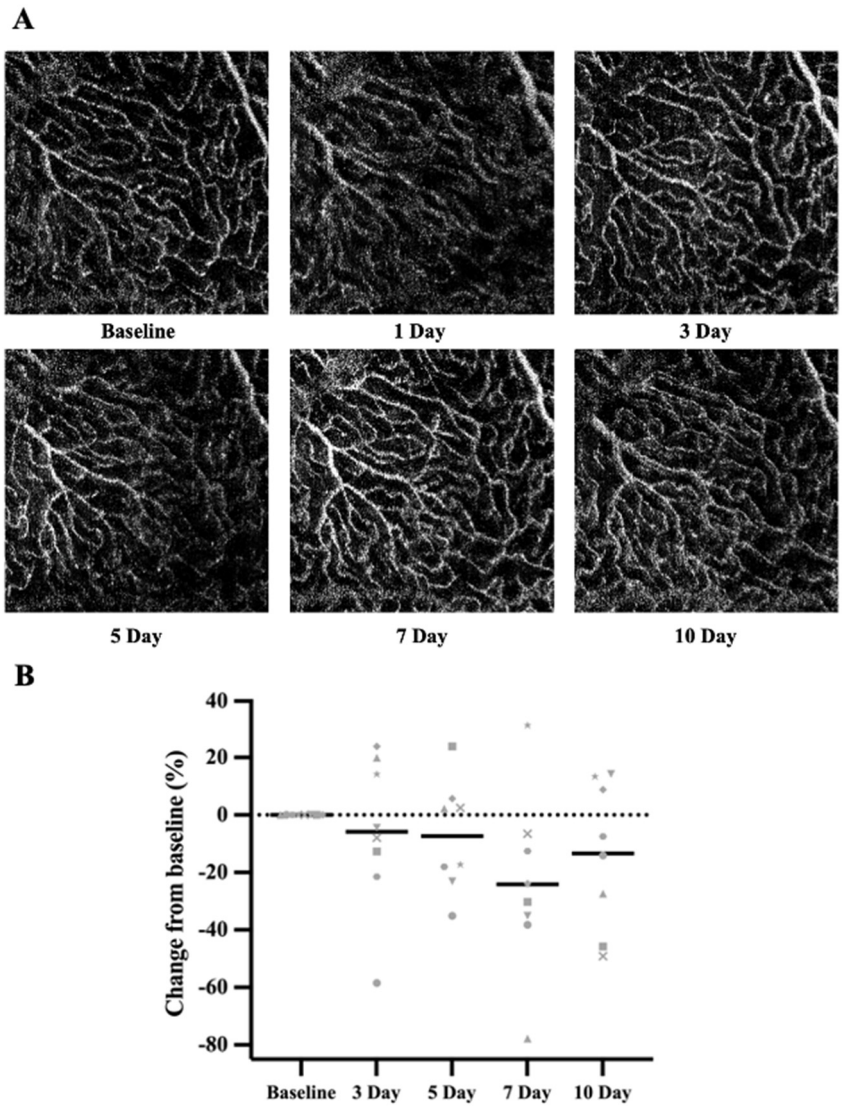

Figure 3.8. Time course of PD in the 15-minute elevated IOP group DCP. A) *In vivo* OCTA images were acquired at baseline and over a period of 10 days post-I/R injury in a mouse that received 15 minutes of ischemia. Images were acquired in the same mouse and retinal location at each time point. B) *In vivo* quantification of PD in the DCP vascular volume. At each time point, PD was computed from the *in vivo* images and reported as change respective to baseline. Figure illustrates a decrease in mean PD at all time points post-I/R injury, as well as a wide variability in PD values. Black bars indicate group mean and grey symbols indicate individual values; n=8.

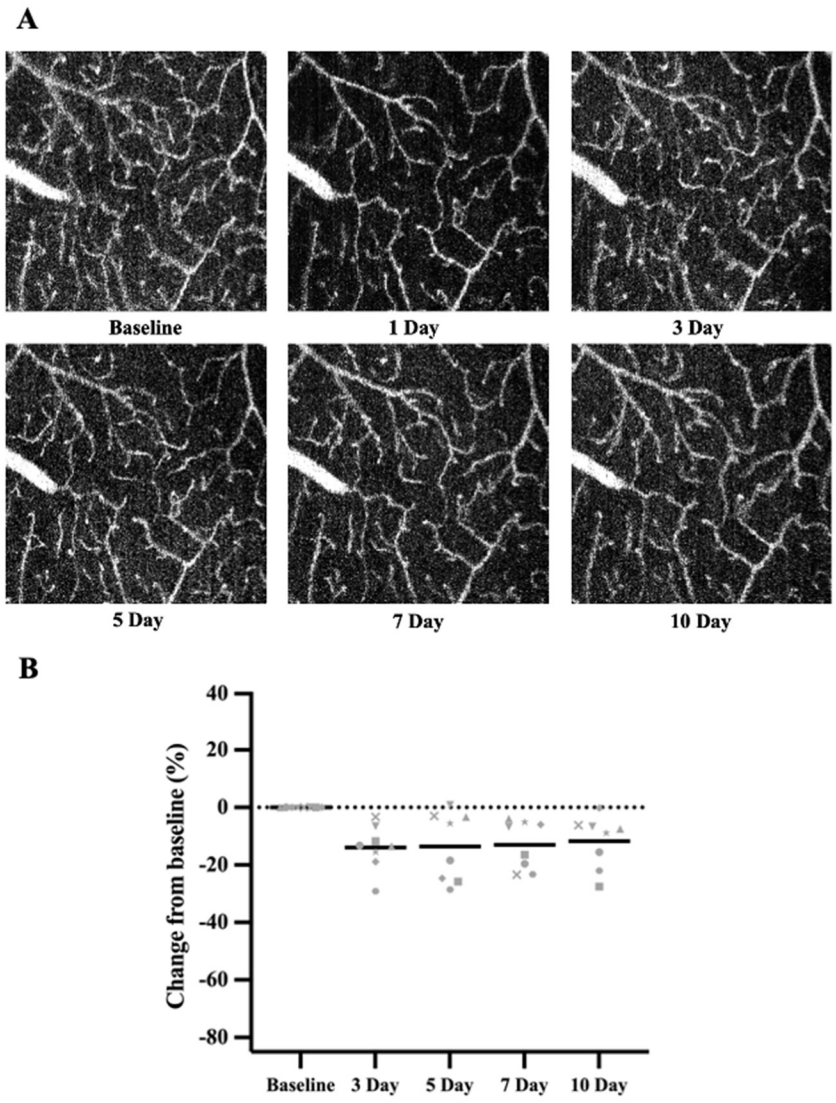

Figure 3.9. Time course of PD in the 30-minute elevated IOP group SVP. A) *In vivo* OCTA images were acquired at baseline and over a period of 10 days post-I/R injury in a mouse that received 30 minutes of ischemia. Images were acquired in the same mouse and retinal location at each time point. B) *In vivo* quantification of PD in the SVP vascular volume. At each time point, PD was computed from the *in vivo* images and reported as change respective to baseline. Figure illustrates a decrease in mean PD at all time points post-I/R injury. Black bars indicate group mean and grey symbols indicate individual values; n=8.

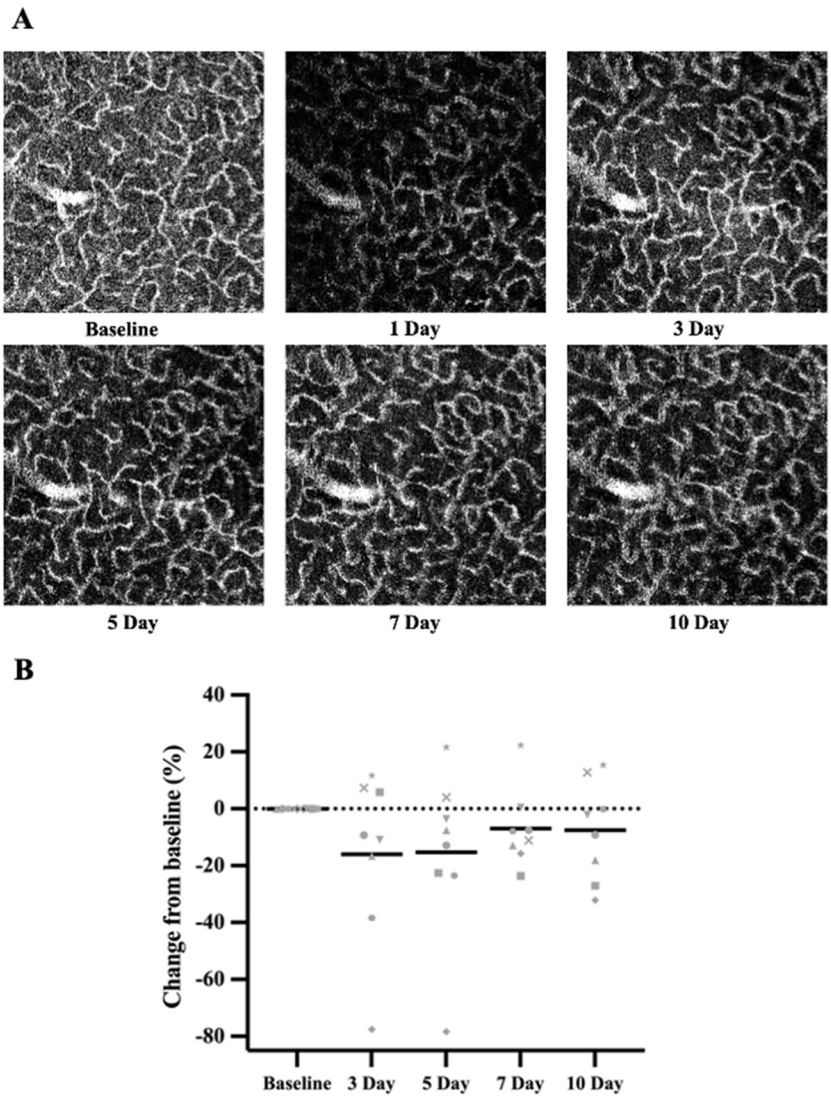

Figure 3.10. Time course of PD in the 30-minute elevated IOP group ICP. A) *In vivo* OCTA images were acquired at baseline and over a period of 10 days post-I/R injury in a mouse that received 30 minutes of ischemia. Images were acquired in the same mouse and retinal location at each time point. B) *In vivo* quantification of PD in the ICP vascular volume. At each time point, PD was computed from the *in vivo* images and reported as change respective to baseline. Figure illustrates a decrease in mean PD at all time points post-I/R injury, as well as a wide variability in PD values. Black bars indicate group mean and grey symbols indicate individual values; n=8.

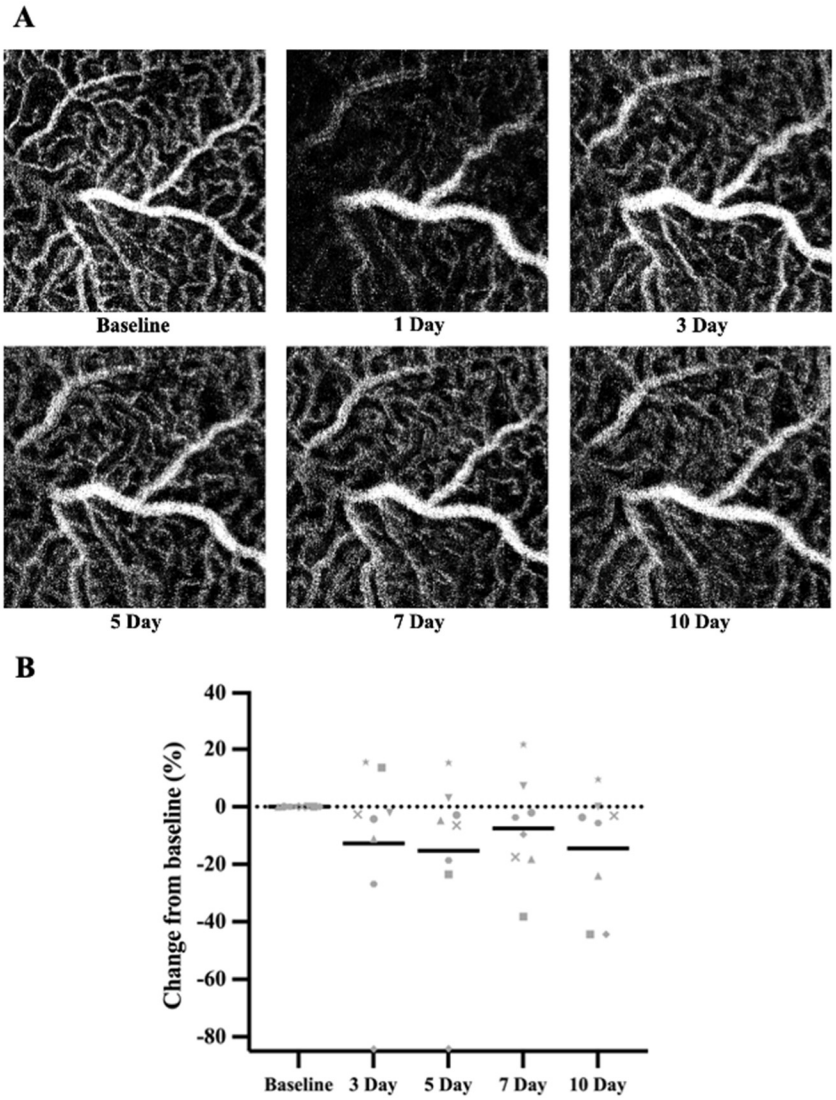

Figure 3.11. Time course of PD in the 30-minute elevated IOP group DCP. A) *In vivo* OCTA images were acquired at baseline and over a period of 10 days post-I/R injury in a mouse that received 30 minutes of ischemia. Images were acquired in the same mouse and retinal location at each time point. B) *In vivo* quantification of PD in the DCP vascular volume. At each time point, PD was computed from the *in vivo* images and reported as change respective to baseline. Figure illustrates a decrease in mean PD at all time points post-I/R injury, as well as a wide variability in PD values. Black bars indicate group mean and grey symbols indicate individual values; n=8.

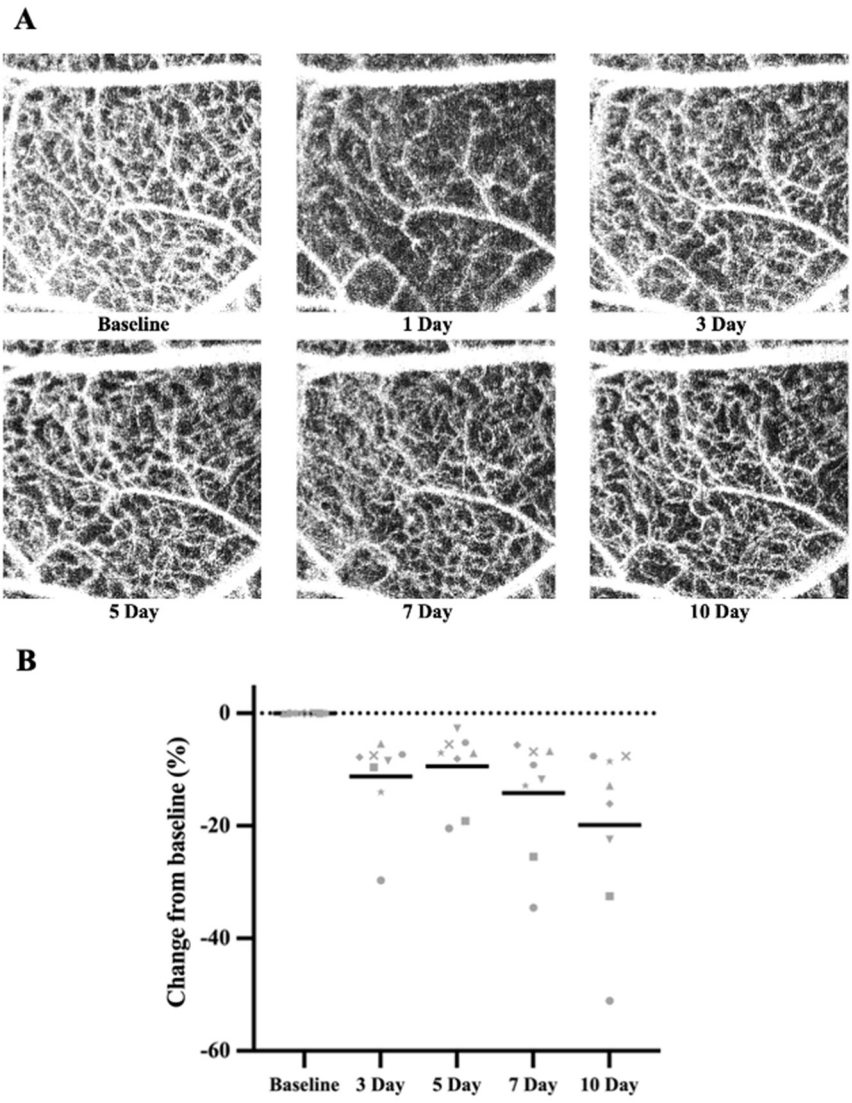

Figure 3.12. Time course of PD in the 45-minute elevated IOP group CCV. A) *In vivo* OCTA images were acquired at baseline and over a period of 10 days post-I/R injury in a mouse that received 45 minutes of ischemia. Images were acquired in the same mouse and retinal location at each time point. B) *In vivo* quantification of PD in the CCV. At each time point, PD was computed from the *in vivo* images and reported as change respective to baseline. Figure illustrates a decrease in mean PD at all time points post-I/R injury. Black bars indicate group mean and grey symbols indicate individual values; n=8.

3.2.2. Evaluating the Time Course of Changes in Retinal Thickness

Eight mice in each of the 15-, 30- and 45-minute elevated IOP groups were imaged *in vivo* with OCT at all time points post-I/R injury. We tracked the time course of changes in GCC thickness for groups with differing durations of acute retinal ischemia by acquiring circular peripapillary OCT B-scans and computing *in vivo* GCC thickness, which was then reported as percent change respective to baseline. Statistics were reported elsewhere.

In the 15-minute elevated IOP group, circular peripapillary OCT B-scans from a representative mouse are shown (Figure 3.13A). Mean GCC thickness in the 15-minute elevated IOP group was increased compared to baseline at 1-day post-I/R injury, which extended to the 10-day imaging endpoint. Mean change from baseline (SD) peaked at 6.4% (2.4) 3-days post-I/R injury, then continuously declined over each timepoint until the 10-day imaging endpoint, where mean change from baseline was 0.5% (0.9) (Figure 3.13B).

In the 30-minute elevated IOP group, circular peripapillary OCT B-scans from a representative mouse are shown (Figure 3.14A). Mean GCC thickness in the 30-minute elevated IOP group was first increased at 1-, 3- and 5-days post-I/R injury, then decreased at 7- and 10-days post-I/R injury. Mean change from baseline (SD) peaked at 5.2% (2.1) 1-day post-I/R injury, remained elevated at 3-days, then continuously declined at each timepoint thereafter until the 10-day imaging endpoint when mean change from baseline was -4.3% (5.1) (Figure 3.14B).

In the 45-minute elevated IOP group, circular peripapillary OCT B-scans from a representative mouse are shown (Figure 3.15A). Mean GCC thickness was increased at 1-

day post-I/R injury and decreased at all subsequent time points. Mean change from baseline (SD) spiked to 44.3% (33.6) 1-day post-I/R injury, then rapidly declined at 3-days post-I/R injury to -4.8% (18.5), continuing to decline to the 10-day imaging endpoint when mean change from baseline was -46.7% (5.1) (Figure 3.15B).

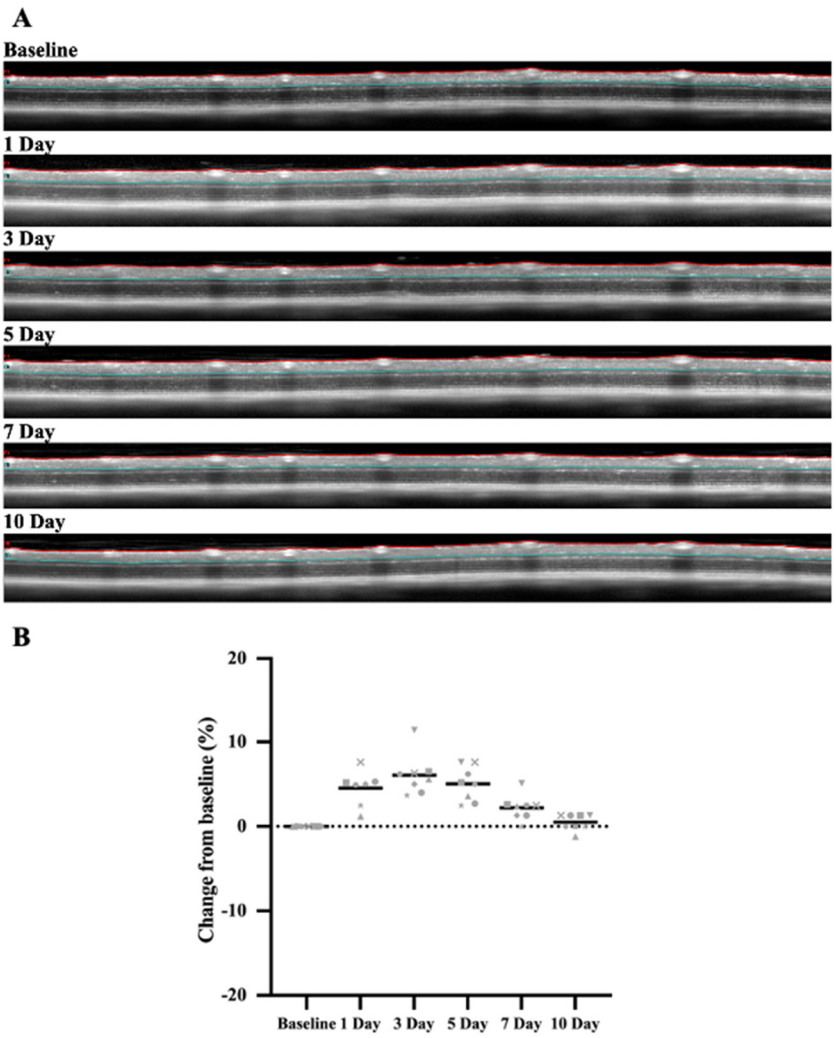

Figure 3.13. Time course of GCC thickness in the 15-minute elevated IOP group. A) *In vivo* OCT B-scans were acquired at baseline and over a period of 10 days post-I/R injury in a mouse that received 15-minutes of ischemia. Depicted images were acquired in the same mouse and retinal location, at each time point. Coloured lines demarcate the GCC, with the red and blue lines indicating segmentation of the ILM and outer border of the IPL, respectively. B) *In vivo* quantification of mean GCC thickness in mice that received 15-minutes of ischemia. At each time point, GCC thickness was computed and reported as change respective to baseline. Figure illustrates an increase in mean GCC thickness, followed by an approximate return to baseline values by the 10-day imaging endpoint. Black bars indicate group mean and grey symbols indicate individual values; n=8.

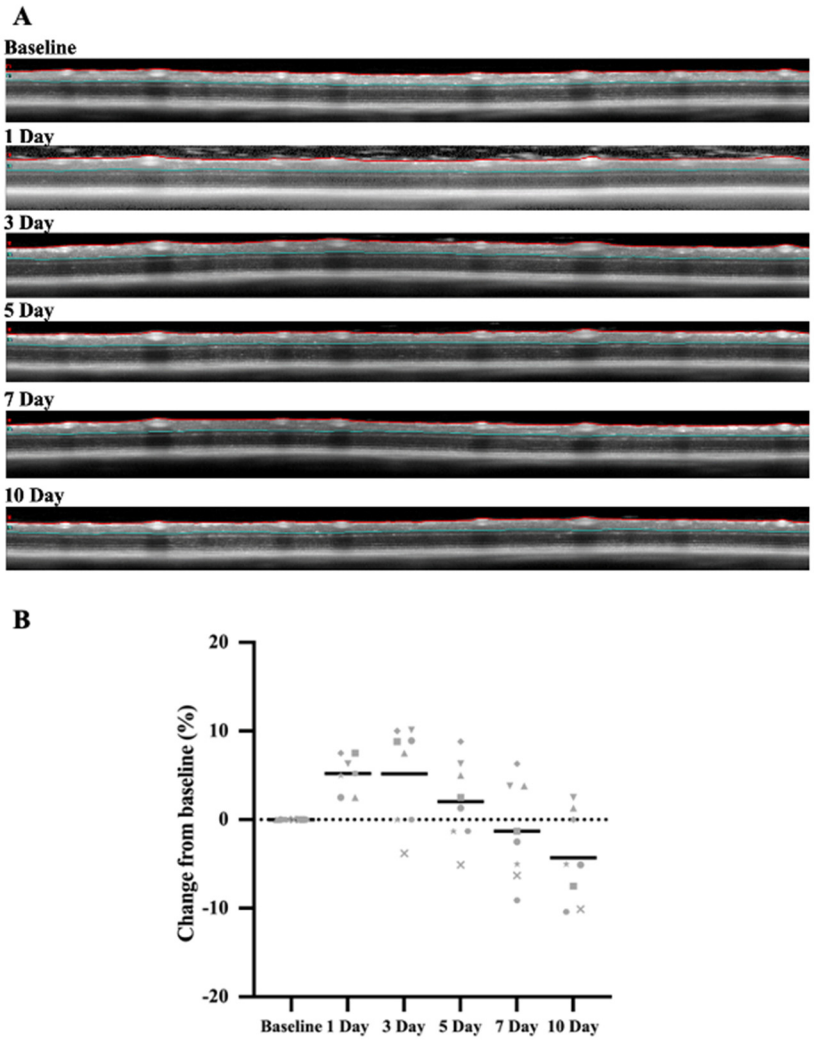

Figure 3.14. Time course of GCC thickness in the 30-minute elevated IOP group. A) *In vivo* OCT B-scans were acquired at baseline and over a period of 10 days post-I/R injury in a mouse that received 30-minutes of ischemia. Depicted images were acquired in the same mouse and retinal location, at each time point. Coloured lines demarcate the GCC, with the red and blue lines indicating segmentation of the ILM and outer border of the IPL, respectively. B) *In vivo* quantification of mean GCC thickness in mice that received 30-minutes of ischemia. At each time point, GCC thickness was computed and reported as change respective to baseline. Figure illustrates an initial increase in mean GCC thickness, followed by a gradual decrease up to the 10-day imaging endpoint. The figure also illustrates a wide variability of individual GCC thickness results. Black bars indicate group mean and grey symbols indicate individual values; n=8.

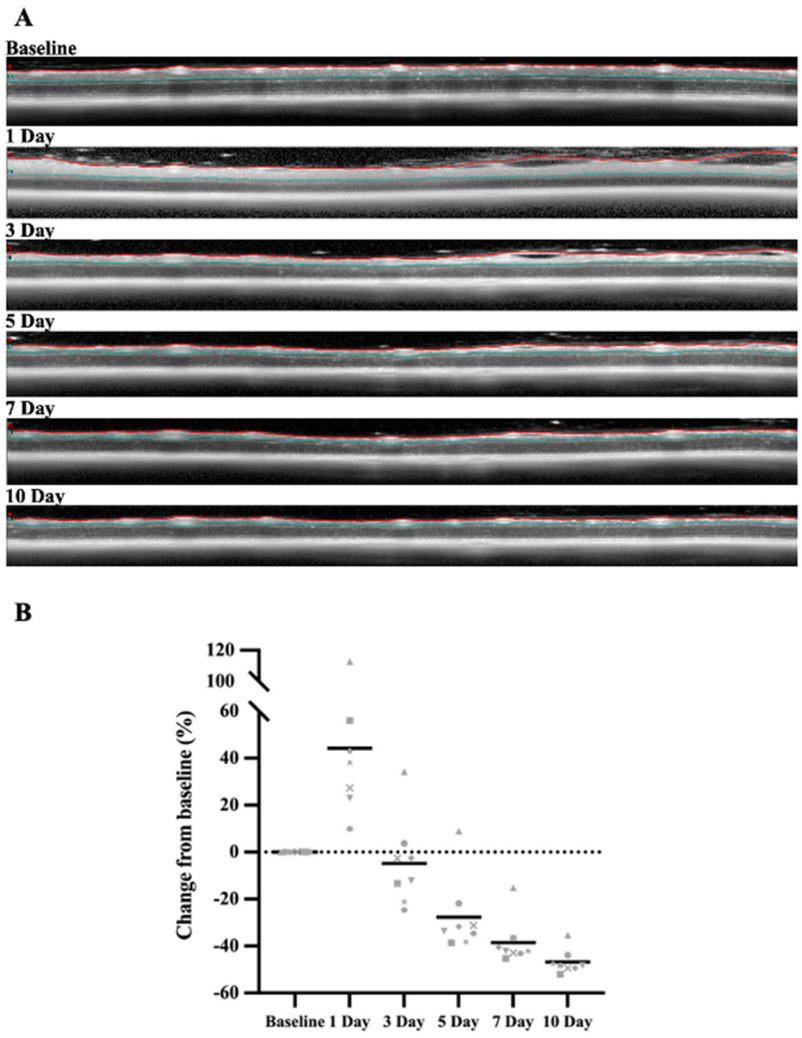

Figure 3.15. Time course of GCC thickness in the 45-minute elevated IOP group. A) *In vivo* OCT B-scans were acquired at baseline and over a period of 10 days post-I/R injury in a mouse that received 45-minutes of ischemia. Depicted images were acquired in the same mouse and retinal location, at each time point. Coloured lines demarcate the GCC, with the red and blue lines indicating segmentation of the ILM and outer border of the IPL, respectively. B) *In vivo* quantification of mean GCC thickness in mice that received 45-minutes of ischemia. At each time point, GCC thickness was computed and reported as change respective to baseline. Figure illustrates a sharp initial increase in mean GCC thickness, followed by a large decrease up to the 10-day imaging endpoint, when compared to baseline. Black bars indicate group mean and grey symbols indicate individual values; n=8.

3.3. Comparison of Changes in Retinal Perfusion, Structure and RGCs Between Groups with Varying Ischemic Durations

3.3.1. Longitudinal Comparison of Changes in Perfusion Density Between Groups

Vascular volumes of the SVP, ICP, DCP and CCV were used to quantify *in vivo* retinal PD. At each time point, retinal PD (reported as percent change respective to baseline) was statistically compared between the repeatability group and the 15- and 30-minute elevated IOP groups in the SVP, ICP and DCP volumes, then between the repeatability group and the 45-minute elevated IOP group in the CCV.

In the SVP, there was no significant difference in mean PD between the repeatability group and the 15- and 30-minute elevated IOP groups at any time point (Figure 3.16). Although non-significant, the 15- and 30-minute elevated IOP groups had a lower mean change from baseline than the repeatability group at all time points. Further, mean change from baseline in the 30-minute elevated IOP group was lower than the 15-minute elevated IOP group at all time points except 3-days post-I/R injury, though differences were non-significant.

In the ICP, mean PD was not significantly different between the repeatability group and the 15- and 30-minute elevated IOP groups, across all time points (Figure 3.17). Like the SVP, mean change from baseline in both the 15- and 30-minute elevated IOP groups were non-significantly lower than the repeatability group at all time points. Further, mean change from baseline in the 15-minute elevated IOP group was lower than the 30-minute elevated IOP group at all time points except 5-days post-I/R injury, however, differences were non-significant.

In the DCP, there was no significant difference in mean PD between the

repeatability group and the 15- and 30-minute elevated IOP groups, at any time point (Figure 3.18). When compared to the repeatability group, mean change from baseline in the 15-minute elevated IOP was slightly higher at 3- and 5-days post-I/R injury, then lower at 7- and 10-days post-I/R injury, although all differences were non-significant. Mean change from baseline in the 30-minute elevated IOP group was lower than the repeatability group and the 15-minute elevated IOP group at all time points except for at 7-days post-I/R injury, when the 15-minute elevated IOP group was higher, however, differences were non-significant.

Variability was higher in both elevated IOP groups across almost all time points when compared to the repeatability group. Group SDs were higher in both elevated IOP groups for each of the SVP, ICP and DCP at all time points (except 7-days in the SVP, when group SD in the repeatability group exceeded that of the 30-minute elevated IOP group). This is shown by the larger dispersion of change from baseline values around the mean, at each time point in the SVP, ICP and DCP (Figures. 3.16, 3.17 and 3.18, respectively).

In the CCV, mean change from baseline (and thus, mean PD) in the 45-minute elevated IOP group was significantly lower than the repeatability group at all time points (Figure 3.19). Further, variability in the 45-minute elevated IOP group was higher, as group SDs were higher when compared to those of the repeatability group, shown by the larger dispersion of change from baseline values around the mean (Figure 3.19).

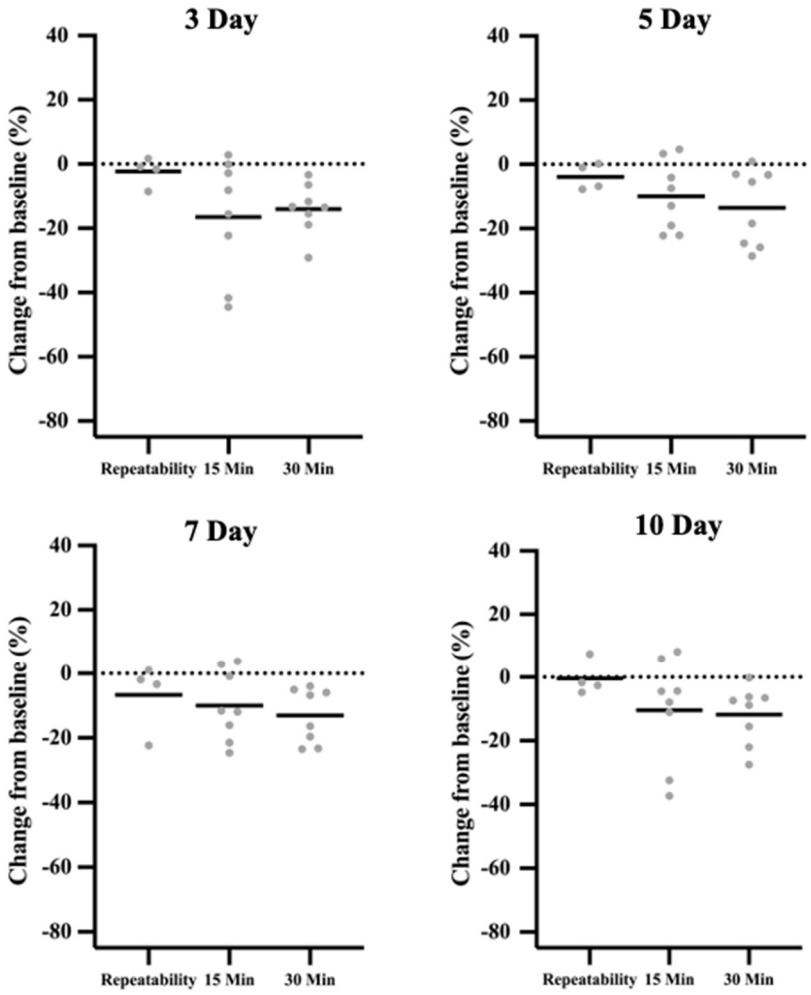

Figure 3.16. Longitudinal inter-group comparison of PD in the SVP. *In vivo* quantification of PD was computed from OCTA images of the SVP vascular volume, for the repeatability, 15- and 30-minute elevated IOP groups. At all time points, mean change from baseline for both elevated IOP groups and repeatability group were compared for significance using an ordinary one-way ANOVA with multiple comparisons. There was no significant difference in mean change from baseline between the repeatability, 15- and 30-minute elevated IOP groups at any time point in the SVP; n= 4, 8, 8 for the repeatability and 15- and 30-minute elevated IOP groups, respectively. Assume non-significance unless otherwise stated. Black bars indicate group mean and grey symbols indicate individual values.

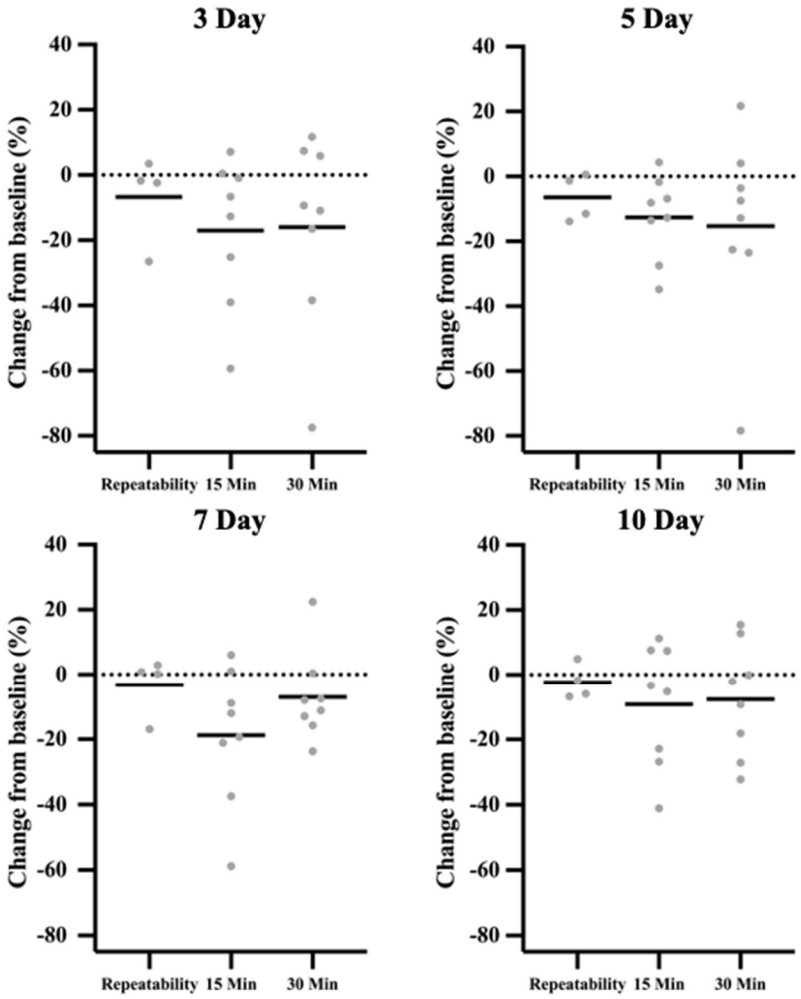

Figure 3.17. Longitudinal inter-group comparison of PD in the ICP. *In vivo* quantification of PD was computed from OCTA images of the ICP vascular volume, for the repeatability, 15- and 30-minute elevated IOP groups. At all time points, mean change from baseline for both elevated IOP groups and repeatability group were compared for significance using an ordinary one-way ANOVA with multiple comparisons. There was no significant difference in mean change from baseline between the repeatability, 15- and 30-minute elevated IOP groups at any time point in the ICP; n= 4, 8, 8 for the repeatability and 15- and 30-minute elevated IOP groups, respectively. Assume non-significance unless otherwise stated. Black bars indicate group mean and grey symbols indicate individual values.

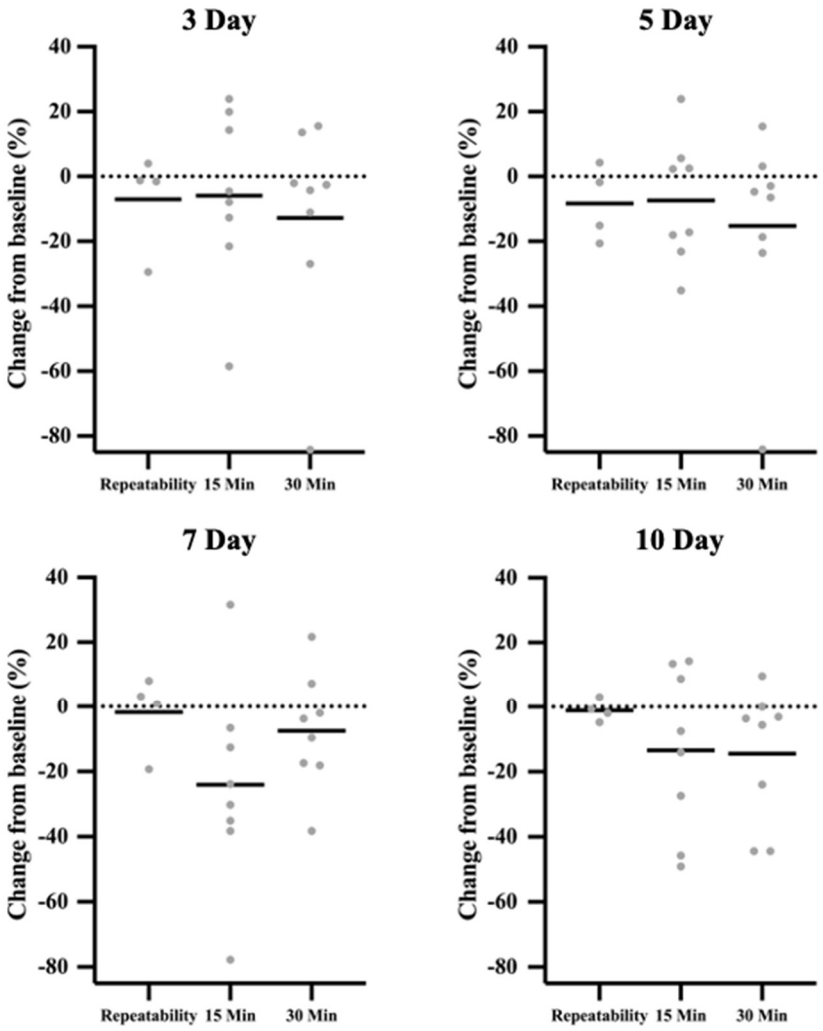

Figure 3.18. Longitudinal inter-group comparison of PD in the DCP. *In vivo* quantification of PD was computed from OCTA images of the DCP vascular volume, for the repeatability, 15- and 30-minute elevated IOP groups. At all time points, mean change from baseline for both elevated IOP groups and repeatability group were compared for significance, using an ordinary one-way ANOVA with multiple comparisons. There was no significant difference in mean change from baseline between the repeatability, 15- and 30-minute elevated IOP groups at any time point in the DCP; n= 4, 8, 8 for the repeatability and 15- and 30-minute elevated IOP groups, respectively. Assume non-significance unless otherwise stated. Black bars indicate group mean and grey symbols indicate individual values.

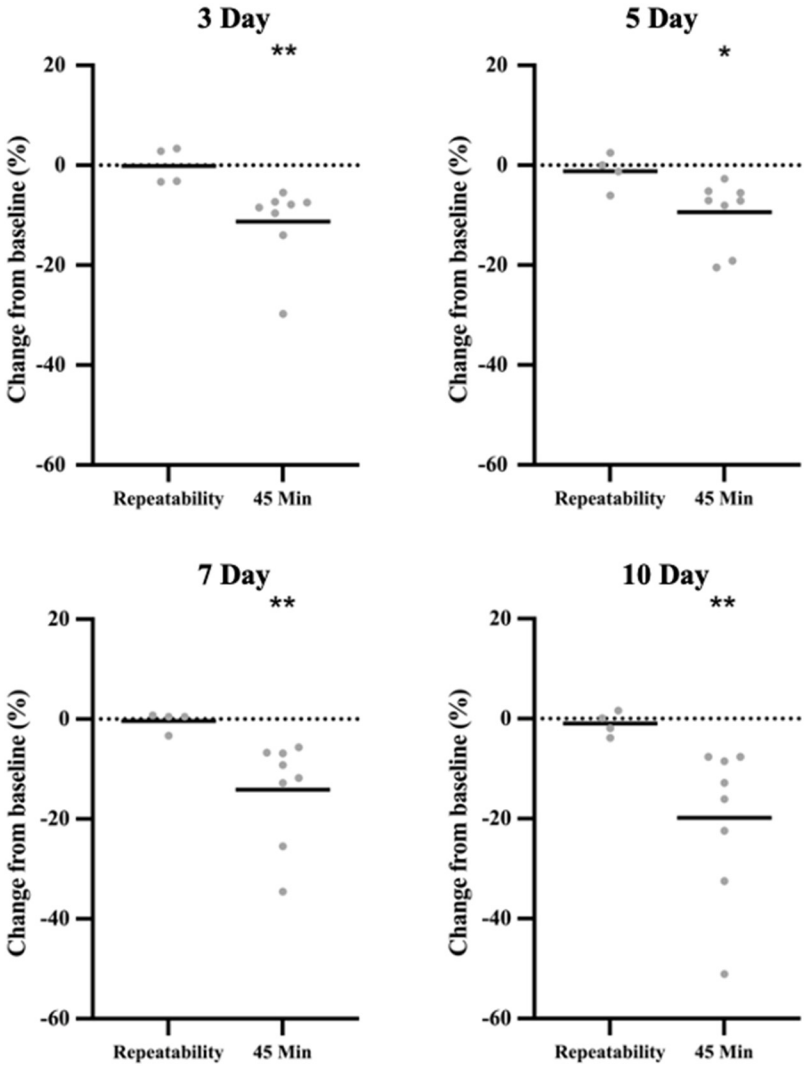

Figure 3.19. Longitudinal inter-group comparison of PD in the CCV. *In vivo* quantification of PD was computed from OCTA images of the CCV in the repeatability and 45-minute elevated IOP groups, across all time points. Group mean change respective to baseline at each time point was compared for significance using an unpaired t-test with Welch's correction for unequal variances. When compared to the repeatability group, mean change from baseline in the 45-minute elevated IOP group was significantly decreased at all time points post-I/R injury; n= 4 and 8 for the repeatability and 45-minute elevated IOP group, respectively. Assume non-significance unless otherwise stated for *= $p < 0.05$ and **= $p < 0.01$. Black bars indicate group mean and grey symbols indicate individual values.

3.3.2. Longitudinal Comparison of Changes in Retinal Thickness Between Groups

Circular peripapillary OCT B-scans were used to compute *in vivo* GCC thickness. At each time point, GCC thickness (reported as percent change respective to baseline) was statistically compared between the repeatability group and the 15-, 30- and 45-minute elevated IOP groups.

Although mean change from baseline was higher at all time points in the 15-minute elevated IOP group, there was no significant difference in mean GCC thickness when compared to the repeatability group across all time points (Figure 3.20). Similarly, there was no significant difference in mean GCC thickness between the repeatability group and the 30-minute elevated IOP group across all time points, even though mean change from baseline in the 30-minute elevated IOP group was higher than the repeatability group at 1-, 3- and 5-days post-ischemic insult, then subsequently lower at 7- and 10-days post-ischemic insult (Figure 3.20). Additionally, there was no significant difference in mean GCC thickness between the 15- and 30-minute elevated IOP groups at all time points, even though mean change from baseline in the 30-minute elevated IOP group was lower at the 5-, 7- and 10-day imaging time points (Figure 3.20). Compared to the repeatability, 15- and 30-minute elevated IOP groups, mean GCC thickness in the 45-minute elevated IOP group was significantly higher at 1-day post-I/R injury, then significantly lower at all subsequent imaging time points, except the 3-day imaging time point, where differences between the groups were non-significant (Figure 3.20).

Variability tended to increase with duration of ischemia across all time points, as the 45-minute elevated IOP group had the largest SD amongst all groups. This is shown

by the larger dispersion of change from baseline values around the mean at all time points (Figure 3.20).

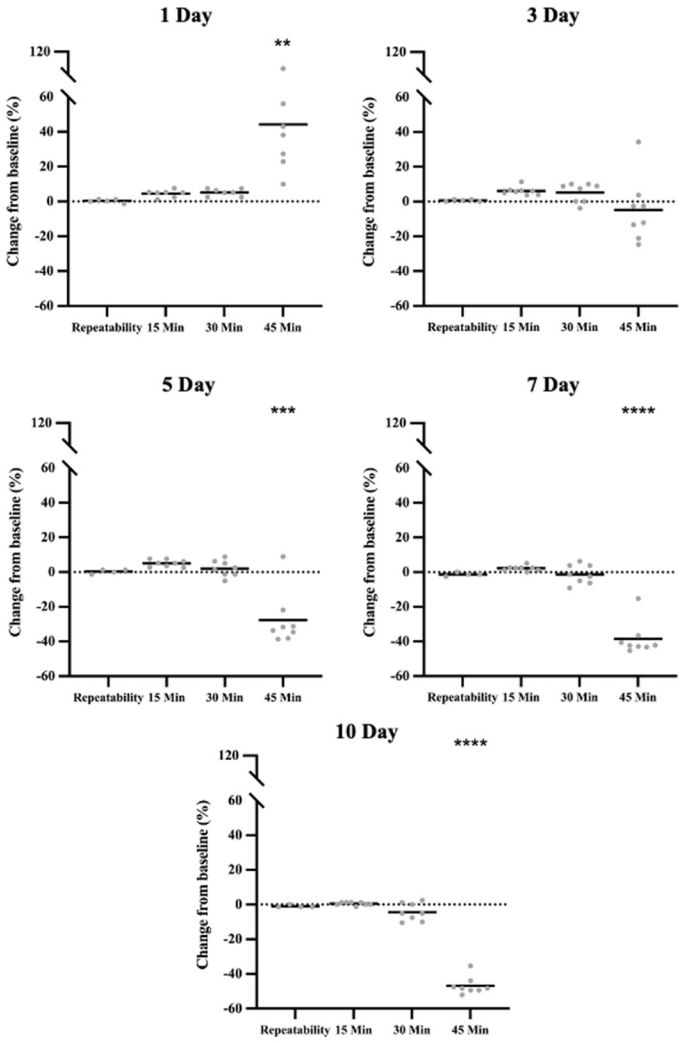

Figure 3.20. Longitudinal inter-group comparison of GCC thickness. *In vivo* quantification of GCC thickness was computed from OCT B-scans for the repeatability, 15-, 30- and 45-minute elevated IOP groups. At all time points, mean change from baseline for the repeatability group and all elevated IOP groups were compared for significance, using an ordinary one-way ANOVA with multiple comparisons. There was no significant difference between the repeatability, 15- and 30-minute elevated IOP groups at any timepoint, however, the 45-minute group was significantly increased at 1 day and significantly decreased at days 5, 7 and 10, when compared to all other groups; n= 4, 8, 8, 8 for the repeatability, 15-, 30- and 45-minute elevated IOP groups, respectively. Significance indicated in reference to repeatability group. Assume non-significance unless otherwise stated for **= $p < 0.01$, ***= $p < 0.001$ and ****= $p < 0.0001$. Black bars indicate group mean and grey symbols indicate individual values.

3.3.3. Cumulative Comparison of Changes in RGC Density Between Groups

We statistically compared changes in RGC density between the non-experimental control retinas and retinas with differing durations of acute I/R injury. Following the last imaging time point, retinal wholemounts with fluorescently labelled RBPMS cells were used to quantify RGC density, which was reported as mean RBPMS density.

Mean RBPMS density (in cells/mm^2) (SD) at 10-days post-I/R injury was 3009.9 (812.6), 3021.3 (795.0), 2651.5 (678.1) and 1157.1 (591.1) for the control, 15-, 30- and 45-minute elevated IOP groups, respectively (Figure 3.21). There was no significant difference between the control and 15-minute elevated IOP groups. Although the 30-minute group mean RBPMS density was lower than the control and 15-minute elevated IOP groups, the difference between them was non-significant. The 45-minute elevated IOP groups had a significantly lower mean RBPMS density when compared to all other groups. Variability was highest in the control group and decreased as the duration of IOP elevation increased, as shown in figure 3.21.

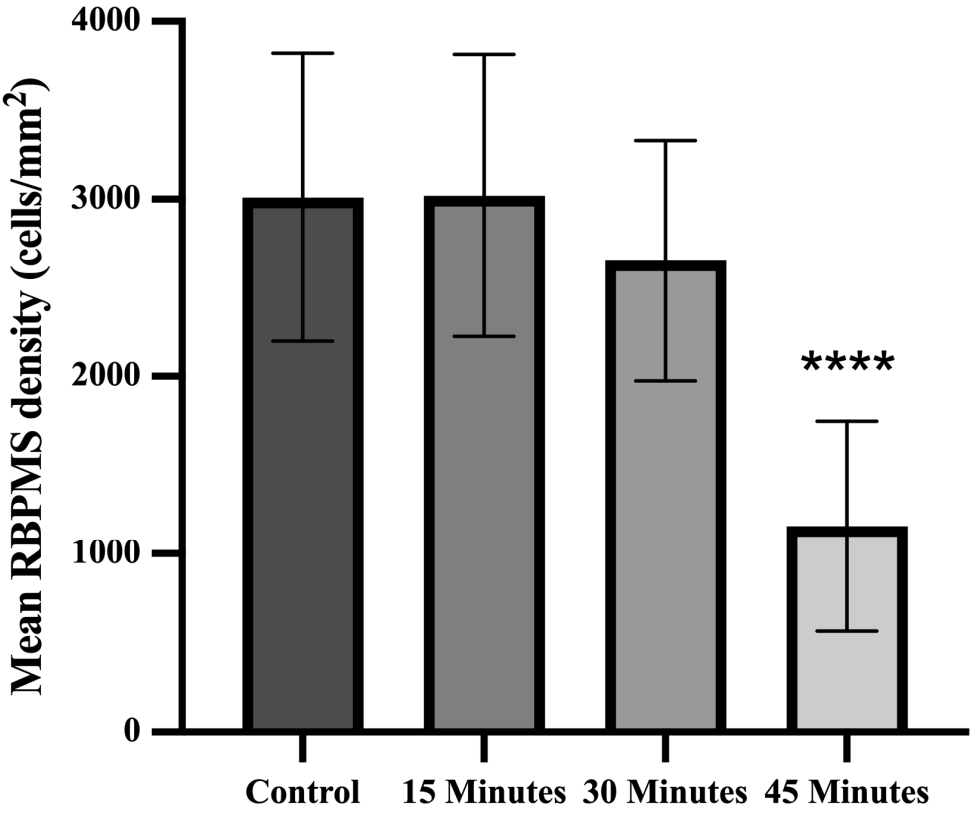

Figure 3.21. Inter-group comparison of cumulative RGC density loss. Cells fluorescently labelled with RBPMS were quantified in tiled images of retinal wholemounts from the control, 15-, 30- and 45-minute elevated IOP groups. Mean RBPMS density in the control group and all elevated IOP groups were compared for significance, using a Brown-Forsythe and Welch ANOVA test with Dunnett's T3 multiple comparisons test (for unequal variance). There was no significant difference in mean RBPMS density found between the control, 15- and 30-minute elevated IOP groups, however, mean RBPMS density in the 45-minute elevated IOP group was significantly decreased when compared to all other groups; n= 24, 7, 8, 8 for the control, 15-, 30- and 45-minute elevated IOP groups, respectively. Retinas in the control group were from the non-experimental right eyes of mice in the elevated IOP groups. Retinas in the 15-, 30- and 45-minute elevated IOP groups were from the experimental left eye. Significance indicated in reference to repeatability group. Assume non-significance unless otherwise stated for ****= $p < 0.0001$. Shaded bars indicate group mean and error bars represent SD.

3.3.4. Correlation Between Perfusion Density and RGC Density

We correlated PD at the last time point with RGC density. For each mouse in the 15- and 30-minute elevated IOP groups, PD values (reported as percent change respective to baseline) in the SVP, ICP and DCP were correlated to the corresponding RGC density values (reported as mean RBPMS density). For each mouse in the 45-minute elevated IOP group, PD values in the CCV were correlated to the corresponding RGC density values.

In the 15-minute elevated IOP group, all Pearson correlation coefficient (r) values were positive: 0.63, 0.46 and 0.55 for the SVP, ICP and DCP, respectively (Figure 3.22A). However, all correlations were found to be non-significant, with two-tailed P-values of 0.13, 0.30 and 0.20 for the SVP, ICP and DCP, respectively.

In the 30-minute elevated IOP group, all r values were positive: 0.39, 0.67 and 0.54 for the SVP, ICP and DCP, respectively (Figure 3.22B). Similar to the 15-minute elevated IOP group, all correlations were found to be non-significant, with two-tailed P-values of 0.34, 0.07 and 0.17 for the SVP, ICP and DCP, respectively.

In the 45-minute elevated IOP group, PD in the CCV correlated to RGC density yielded an r value of -0.13 (Figure 3.22C). This correlation was also found to be non-significant with a two-tailed P-value of 0.77.

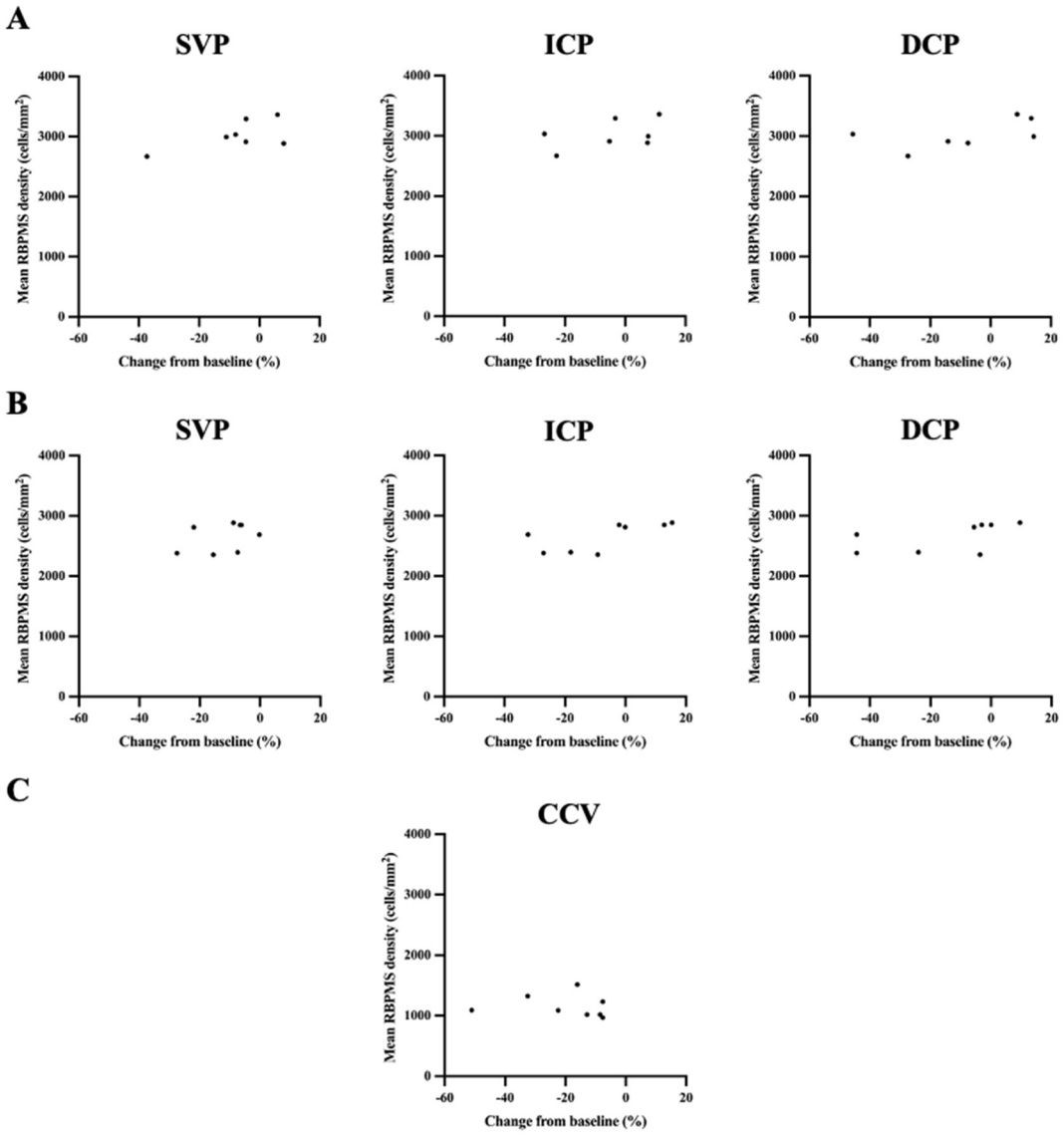

Figure 3.22. Correlation of day 10 PD and RGC density. A, B) For all mice in the 15- and 30-minute elevated IOP groups, respectively, day 10 PD values from the SVP, ICP and DCP were correlated to their corresponding RGC density values using pearson correlation with two-tailed significance tests. All plexuses for both the 15- and 30-minute elevated IOP groups were found to have positive correlations; n= 7, 8 for the 15- and 30-minute groups, respectively. C) For all mice in the 45-minute elevated IOP group, day 10 PD values from the CCV were correlated to their corresponding RGC density values using pearson correlation with two-tailed significance tests. Correlation in the 45-minute groups was found to be slightly negative; n= 8. A, B, C) Assume non-significance unless otherwise stated.

3.4. Comparison of Changes in Retinal Perfusion Between Vascular Plexuses

3.4.1. Longitudinal Comparison of Changes in Perfusion Density Between Plexuses

We longitudinally compared *in vivo* changes in PD between vascular plexuses, for each group following acute I/R injury. *In vivo* retinal PD was computed from OCTA images of the repeatability group and the 15- and 30-minute elevated IOP groups, across all time points. At each time point, mean retinal PD (reported as percent change respective to baseline) was statistically compared between the SVP, ICP and DCP vascular volumes. The 45-minute elevated IOP group was not included in analyses here (see 2.7.3).

In the repeatability group, there was no significant difference in mean change from baseline (and thus, mean PD) between the SVP, ICP and DCP at all time points post-baseline imaging (Figure 3.23). For both the 15- and 30-minute elevated IOP groups, there was no significant difference in mean PD between the SVP, ICP and DCP across all time points post-I/R injury (Figures 3.24 and 3.25, respectively). Variability in the 15- and 30-minute elevated IOP groups was lowest in the SVP and highest in the DCP, as group SDs in the SVP and DCP were lowest and highest at all time points post-I/R injury, respectively. This was shown by the increasing dispersion of change from baseline values around the mean from the SVP to the DCP. (Figures 3.24 and 3.25).

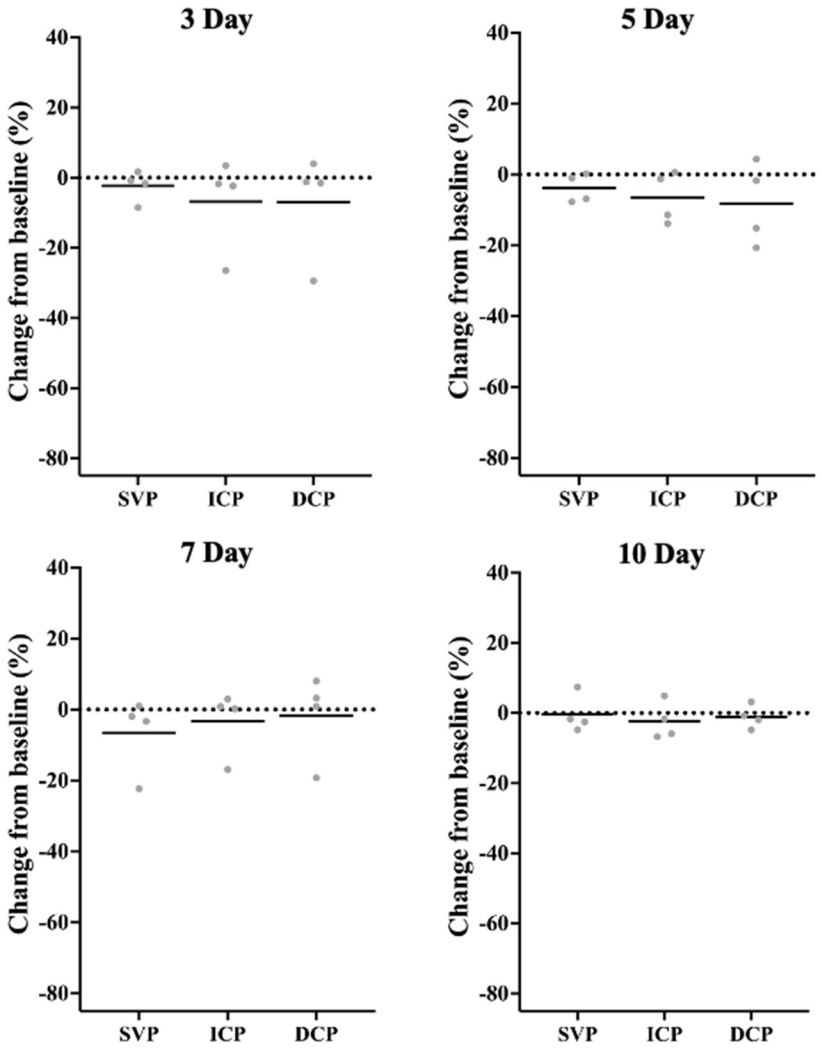

Figure 3.23. Longitudinal inter-plexus comparison of PD in the repeatability group. *In vivo* quantification of PD was computed from OCTA images of the SVP, ICP and DCP. At all time points, mean change respective to baseline for each plexus were compared for significance, using an ordinary one-way ANOVA with multiple comparisons. There was no significant difference between the SVP, ICP and DCP in the repeatability group, at any time point; n= 4 for each of the SVP, ICP and DCP. Assume non-significance unless otherwise stated. Black bars indicate group mean and grey symbols indicate individual values.

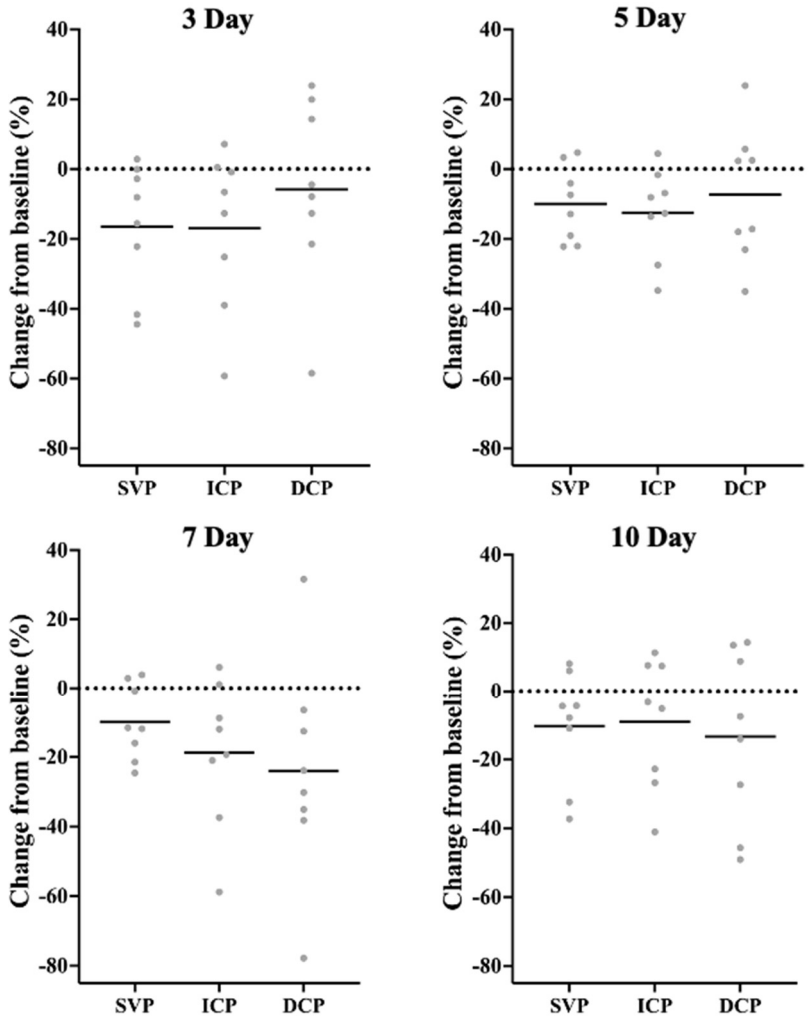

Figure 3.24. Longitudinal inter-plexus comparison of PD in the 15-minute elevated IOP group. *In vivo* quantification of PD was computed from OCTA images of the SVP, ICP and DCP. At all time points, mean change respective to baseline for each plexus were compared for significance, using an ordinary one-way ANOVA with multiple comparisons. There was no significant difference between the SVP, ICP and DCP in the 15-minute elevated IOP group, at any time point; n= 8 for each of the SVP, ICP and DCP. Assume non-significance unless otherwise stated. Black bars indicate group mean and grey symbols indicate individual values.

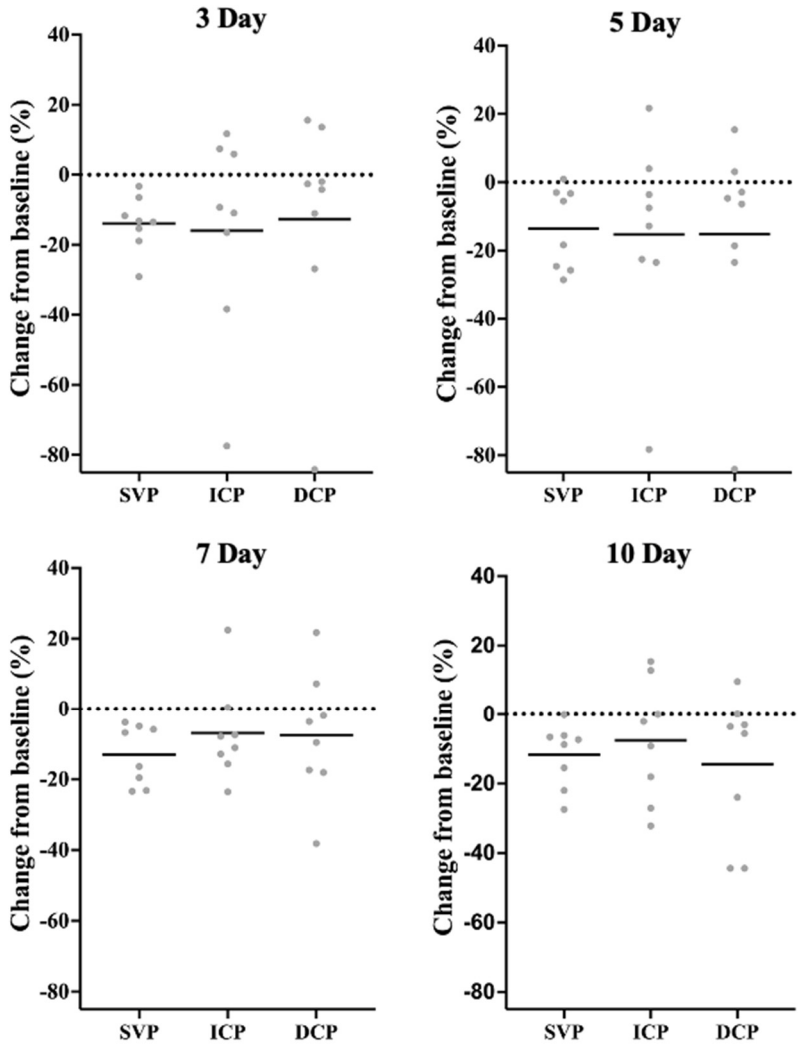

Figure 3.25. Longitudinal inter-plexus comparison of PD in the 30-minute elevated IOP group. *In vivo* quantification of PD was computed from OCTA images of the SVP, ICP and DCP. At all time points, mean change respective to baseline for each plexus were compared for significance, using an ordinary one-way ANOVA with multiple comparisons. There was no significant difference between the SVP, ICP and DCP in the 30-minute elevated IOP group, at any time point; n= 8 for each of the SVP, ICP and DCP. Assume non-significance unless otherwise stated. Black bars indicate group mean and grey symbols indicate individual values.

CHAPTER 4. Discussion

4.1. Summary of Key Findings

The overarching goal of this study was to initiate acute retinal I/R injury in mice and explore the longitudinal relationship between retinal perfusion, structure and RGC density. Using *in vivo* OCTA and OCT imaging longitudinally and post-mortem IHC, our objectives were to record the time course of changes in retinal PD and GCC thickness, compare the impact varying durations of ischemia had on PD, GCC thickness and RGC density and compare the impact each duration of ischemia had on PD between the vascular plexuses.

In the repeatability group, we observed minimal change in the time course of retinal perfusion and GCC thickness. For our first objective, we were able to track and observe the time course of retinal PD in each of the SVP, ICP and DCP after 15 and 30 minutes of ischemia, however, after 45 minutes of ischemia the CCV was needed. We were also able to concurrently track and observe the time course of GCC thickness for all durations of ischemia. For our second objective, we found that although PD was decreased at all time points after 15- or 30-minutes of ischemia, changes were not significantly different when compared to the repeatability group. Similarly, longitudinal changes in GCC thickness induced by 15- or 30-minutes of ischemia were not significantly different when compared to the repeatability group. Cumulative RGC density after 15- or 30-minutes of ischemia was not significantly different when compared to a control group. After 45-minutes of ischemia, PD was significantly decreased at all time points beginning 3 days after I/R injury, GCC thickness was

significantly increased at 1 day, then significantly decreased from 5 days post-I/R injury onwards and RGC density was significantly decreased at 10 days post-I/R injury. For our last objective, we found no significant difference longitudinally between the SVP, ICP and DCP in any of the repeatability, 15- or 30-minute elevated IOP groups.

To the best of our knowledge, this is the first work to report using OCTA in mice to track retinal perfusion longitudinally following acute I/R injury induced by elevated IOP and compare *in vivo* retinal perfusion between plexuses and varying ischemic groups

4.2. Interpretation of Results

4.2.1. OCTA and OCT Repeatability

Aside from our main objectives, we found results indicating good inter-sessional repeatability of OCTA and OCT measurements. These findings are significant within the context of this thesis, since the purpose of the repeatability group was to serve as a comparison to groups of mice with acute I/R injury, thereby accounting for the normal inter-sessional variability in OCTA and OCT measurements.

High OCTA and OCT repeatability has been shown previously in rodents. Smith and colleagues measured OCTA quantitative parameters in healthy mice and found no significant difference in median PD for the SVP, ICP and DCP across imaging sessions spanning the course of a month, concluding that longitudinal OCTA imaging was feasible in mice and repeatability values could be useful in determination of true changes in retinal perfusion (Smith et al., 2019). Additionally, Yang *et al.* measured OCT intra- and inter-sessional repeatability in healthy rats. Using circular peripapillary OCT B-scans they found no significant difference in total retinal thickness and RNFL thickness

between imaging sessions on the same day or one day later (Yang et al., 2016).

Good OCTA repeatability has also been shown previously in humans. In a clinical study, You and colleagues measured the repeatability of OCTA in both healthy and diseased human eyes. They found good intra- (same day) and inter-sessional (2 weeks later) repeatability of superficial density values, concluding that OCTA is a reliable method for assessing macular microcirculation (You et al., 2017).

4.2.2. Time Course of Retinal Perfusion and Structure Following Ischemia

The findings from our first objective are significant, as they detail the utility of OCTA/OCT and could potentially expand their use in the longitudinal evaluation of acute retinal I/R injuries. Furthermore, the assessment of retinal perfusion at the individual capillary plexus level may be critical to improving our understanding of the pathophysiology of acute I/R disease. These findings were in line with our hypothesis, as we expected to be able to track the time course of retinal perfusion using OCTA and OCT *in vivo* following acute I/R injury.

The results from objective one may also indicate a practical limitation for the experimental use of OCTA, as we were surprised about the inability to resolve the 3 plexuses after prolonged durations of ischemia. One of the main strengths of OCTA compared to other imaging techniques is the ability to segregate each vascular plexus. Although we were still able to longitudinally track PD following prolonged durations of ischemia, the necessity to combine the three plexuses into the CCV limited the depth to which we could assess perfusion, similar to what imaging modalities like FA or ICGA could offer.

4.2.2.1. Assessing Retinal Perfusion and Thickness with OCTA and OCT in Ischemia

Previous experimental research has used OCTA to assess changes in retinal perfusion during, or immediately following acute ischemia. In rat, Zhao and colleagues incrementally raised IOP, immediately assessed vessel density using OCTA and found that OCTA could be used to track vessel density in all vascular plexuses as it declines with IOP elevation (Zhao et al., 2020). Similarly, Choi and colleagues incrementally raised IOP in macaque monkeys, assessed macular perfusion immediately with OCTA and found that OCTA could be used to track vessel density in the superficial and deep capillaries of the macular region, even when significantly reduced following pressures exceeding 40mmHg (Choi et al., 2021). In both studies, however, retinal perfusion was assessed only briefly (2 and 30 minutes, respectively) following the initiation of reperfusion, therefore information on the longitudinal impact of acute I/R injury was not available.

OCT has been used previously to assess the longitudinal impact of I/R injury on retinal thickness. In mice, Lee *et al.* unilaterally occluded the common carotid artery via suture to induce retinal I/R injury, then used *in vivo* OCT imaging to assess the longitudinal impact of I/R injury on retinal thickness. For over a period of two weeks following I/R injury, the researchers found that they were able to track retinal thickness with OCT (Lee et al., 2021).

4.2.2.2. Assessing Retinal Perfusion with OCTA in Other Disease Models

Using OCTA to assess perfusion in the retina has not been limited to I/R injury

models. Previous experimental uses of OCTA include assessing retinal perfusion in models of retinal disease such as AMD, O_2-induced retinopathy and DR (Alnawaiseh et al., 2016; Kim et al., 2018; Park et al., 2016; Uehara et al., 2019). In an experimental mouse model of AMD, Alnawaiseh and colleagues used OCTA to assess outer retinal perfusion following laser-induced choroidal neovascularization (CNV). At 1- and 3-weeks following laser photocoagulation, they found CNV through the detection of new vessels in the outer retina, concluding that OCTA was able to be used longitudinally to assess retinal perfusion and that it may be useful to improve their understanding of neovascular pathologies (Alnawaiseh et al., 2016).

4.2.2.3. Assessing Perfusion with OCTA Outside the Eye

The use of OCTA in experimental research has extended beyond the retina. Researchers have used invasive techniques to record cortical blood perfusion with OCTA following disease models such as ischemic stroke. Yang *et al.* created a long-term transparent optical window to the mouse brain, permitting photothrombotic occlusion of the middle cerebral artery and subsequent OCTA imaging. They found that they were able to track cerebral perfusion longitudinally over a period of 13 days post- I/R injury, concluding that OCTA is useful in improving the understanding of ischemic stroke (Yang et al., 2019).

4.2.3. Retinal Perfusion, Structure and RGCs After Varying Ischemic Durations

4.2.3.1. Continuum of Damage Following I/R Injury

The findings from objective two may suggest that damage resulting from I/R

injury exists on a continuum associated with a threshold that influences the magnitude of ischemic injury. This may support our hypothesis, as we originally anticipated that 15-, 30- and 45-minutes of ischemia would represent mild, moderate and extensive time points for damage and that loss would increase with duration of ischemia.

Our data tends to suggest that 15 and 30 minutes of ischemia induces some mild damage to PD, GCC thickness and RGC density prior to the catastrophic damage observed after 45 minutes of ischemia. After 15 and 30 minutes of ischemia, PD was decreased across all imaging time points and at 10 days following 30 minutes of ischemia, GCC thickness and RGC density appeared to decrease as well. This may be in line with previous work that studied I/R injury and found damage to retinal thickness and RGCs after 30 minutes of ischemia (Lafuente et al., 2002; Zhu et al., 2002). Furthermore, PD and RGC density appeared to be positively correlated after 15 and 30 minutes of ischemia, suggesting a longitudinal relationship wherein PD reductions in the SVP are related to RGC density reductions. This may be consistent physiologically, considering that the SVP is intimately connected with the GCL and nourishes the RGCs (Paques et al., 2003). Interestingly, similar relationships were found with the ICP and DCP, though this may not imply causality but rather reflect the ICP and DCP's interconnected relationship with the SVP. Importantly, all changes observed after 15 and 30 minutes of ischemia were found to be not statistically significant, however, the low sample size may have resulted in underpowered data and the inability to find significance.

4.2.3.2. Threshold For Irreversible Damage in the Retina

The findings from objective two further suggest that there is a threshold for

irreversible retinal perfusion, thickness and RGC density damage, which exists between 30 and 45 minutes of ischemia. This information could contribute to our understanding of critical time periods during ischemic injury and the pathophysiology of disease progression afterwards.

Previous work in rodents following I/R injury found results regarding an ischemic damage threshold point similar to ours. Hughes elevated IOP in rats for a variety of durations, finding significant reductions in retinal thickness and RGC population after 60 minutes of ischemia, but not after 30 minutes, suggesting a threshold for irreversible damage between 30 and 60 minutes of ischemia (Hughes, 1991). Faberowski and colleagues ligated the ON for periods of 60-240 minutes, finding significant cell loss after 60 minutes of ischemia (and all time points after), suggesting a threshold for irreversible damage prior to 60 minutes (Faberowski et al., 1989). Our work may build upon this knowledge base, perhaps introducing a more accurate time frame estimate for where the threshold for irreversible damage might be, following acute I/R injury.

Other work in rodents following I/R injury found results that contrast ours. Zhu and colleagues elevated IOP in mice, finding extensive histological damage to retinal thickness and GCL cells after 30, 45 or 60 minutes, suggesting a threshold for irreversible damage prior to 30 minutes of ischemia (Zhu et al., 2002). Similarly, Lafuente *et al.* ligated the ophthalmic vessels in rats for various durations, finding a significant decrease in RGC density after both 30 and 45 minutes of ischemia, further suggesting a threshold for irreversible damage prior to 30 minutes of ischemia (Lafuente et al., 2002). A possible reason why our results after 30 minutes of ischemia are incongruent with Zhu and colleagues is the difference in analysis, as they measured total retinal thickness and

IPL thickness histologically, while we measured GCC thickness with OCT. Furthermore, differences could be attributed to low sample size, as 5 mice were used in their research, while 8 mice were included in the 30-minute elevated IOP group in our study. Other reasons may be due to the method of RGC density quantification - they retrogradely labelled RGCs with the lipophilic dye, diAsp, whereas we labelled RGCs with the IHC marker anti-RBPMS. The discrepancies in findings could also be attributed to inter-species differences, which has been reported previously for the threshold of irreversible damage (Osborne et al., 2004).

4.2.3.3. Threshold For Irreversible Damage in the Brain

Both the retina and brain have relatively high O_2 demands for metabolism when compared to the rest of the body and use the NT glutamate (proposed to contribute to excitotoxic damage during ischemia in the retina and brain), thus comparisons of the threshold for irreversible ischemic damage between the two have naturally arisen (Lee et al., 2000). Evidence on cerebral ischemia in humans and retinal ischemia in monkeys indicates irreversible tissue damage after just 5 minutes of complete occlusion of blood flow to the brain, whereas, at least around 100 minutes of blood flow occlusion is needed to induce irreversible damage in the retina (Hayreh & Weingeist, 1980; Lee et al., 2000). In rabbit, Ames and colleagues induced cerebral ischemia via clamping of the common carotid arteries and found histological evidence for cerebral vascular defects in up to 95% of the brain after just 15 minutes of ischemia, suggesting a short threshold for permanent damage of less than 15 minutes of ischemia, contrasting our findings in the mouse retina (Ames et al., 1968). The findings, taken together, may suggest that the brain has a lower

threshold for irreversible tissue damage and is therefore less resistant to ischemic damage than the retina.

The per-gram usage of O_2 in the retina has been reported to exceed that of the brain, therefore it is surprising to find the brain more susceptible to ischemic damage (Wright et al., 2020). Researchers have attributed this finding to the no-reflow phenomenon, where following restoration of blood flow, neural tissue edema generated by initial ischemic injury increases the brain volume and pushes against the skull, increasing pressure and inducing a second ischemic period. In contrast, the no-reflow phenomenon does not exist in the retina, since edema generated during ischemia can be absorbed in the vitreous body (Hayreh & Weingeist, 1980).

4.2.3.4. Altered Retinal Perfusion and the Perfusion-Thickness Relationship

The findings from our second objective also suggest that there is longitudinal depression of retinal perfusion following prolonged durations of acute I/R injury and that perfusion loss may initially precede thickness loss. This information is significant, as it could further our understanding of the role microcirculation plays in glaucoma and the perfusion-thickness relationship that ensues following acute I/R injury.

Glaucoma is a chronic optic neuropathy well known to be associated with increased IOP that leads to RGC death via the mechanical stress put on the posterior structures of the eye, including RGC axons (Weinreb et al., 2014). However, the pathogenesis of glaucoma is not completely understood and recent clinical studies using OCTA have investigated the role of microcirculation during glaucoma, finding significantly reduced retinal vessel density in both patients with primary open angle

glaucoma (POAG) and PACG (Liu et al., 2015; Rao et al., 2020; Zhang et al., 2017). Zhang and colleagues used OCTA to assess retinal peripapillary vessel density following acute angle-closure attack in PACG patients, finding that vessel density was reduced by ~20% when compared to non-glaucomatous controls and that decreases in vessel density were positively correlated with thinning of the GCC (Zhang et al., 2017). Though direct translation of results is limited, the elevation of IOP used in our work may closely model PACG- where IOP can rapidly increase to pressures around 70mmHg, therefore it is possible within the context of our findings, that the longitudinal decrease we observed in perfusion and thickness values after 45 minutes of ischemia resembles what has been reported in clinical PACG populations (Garala & Bansal, 2019).

Importantly, while perfusion deficits have been observed in glaucoma, the causal relationship of altered perfusion and RGC death is still unknown and there is currently no evidence to suggest altered perfusion directly leads to RGC death. Contrasting our findings, there is histological evidence in rodents following elevated IOP-induced I/R injury, that suggests neuronal cell and thickness loss precedes capillary degeneration, although the incongruency in our results may be due to differing analyses (Zheng et al., 2007). Additionally, there is conflicting clinical evidence on whether changes in retinal perfusion precede changes in thickness. A variety of cross-sectional clinical studies on patients with POAG have used OCTA and OCT or optical microangiography to assess retinal perfusion and thickness. Pradhan *et al.* found in the upper temporal retinal sector that perfusion loss may precede structural loss, but *vice-versa* in the superotemporal sector (Pradhan et al., 2018). Comparing retinal perfusion and thickness in healthy and glaucomatous eyes, Chen and colleagues found that changes in perfusion may precede

changes in structure (Chen et al., 2017). In contrast, Akagi *et al.* found evidence suggesting that RNFL thinning preceded changes in perfusion (Akagi et al., 2016).

4.2.3.5. Blood-Retinal-Barrier Breakdown

Before decreasing at 5-days, GCC thickness in the 45-minute elevated IOP group was significantly increased 1 day following acute I/R injury. We believe the reason for this is the development of intraretinal edema, which could be observed in the 1-day OCT B-scans of some mice in the 45-minute elevated IOP group (Figure 3.15A). This has been shown previously in pig, where retinal thickness was significantly increased 20 hours after acute retinal I/R injury due to fluid accumulation in the RNFL (Zadeh et al., 2019). After finding an increase in ROS in the retinal arterioles, Zadeh and colleagues suggested that acute I/R injury induced endothelial cell dysfunction of the retinal arterioles and subsequent inner BRB disruption, indicated by the presence of retinal edema. It is possible in the context of our findings then, that 45 minutes of ischemia induced endothelial cell disruption of the retinal arterioles and subsequent BRB disruption, which caused the observed retinal edema and significant increase in GCC thickness at 1 day following acute I/R injury. In the porcine study, however, they used a model wherein the left and right carotid arteries were clamped to induce ocular ischemia, therefore it is also possible that our mechanism of damage is not directly correlated to theirs. In the literature, BRB disruption has been associated with ischemic retinopathies, so it is possible that BRB breakdown could be a potential cause for the significant longitudinal decrease in retinal PD and GCC thickness we observed following acute I/R injury (Vinores, 2010).

Significant intraretinal edema was observed after 45 minutes of ischemia, in contrast to the 15 or 30 minute conditions. It is therefore possible that the edema itself, as opposed to the ischemic injury, induced, or contributed to the significant longitudinal decreases in PD, GCC thickness and RGC density after 45 minutes of ischemia. A limitation of our work is that we are unable to attribute PD changes and RGC loss to either ischemia or edema, or a combination of the two.

Interestingly, Marmor postulated that edema itself does not always result in neuronal degeneration, and that the underlying cause of the edema could impact the retinal neurons independently of edema (Marmor, 1999). When contextualized with our findings, it is possible that the longitudinal damage seen after 45 minutes of ischemia was due to the initial ischemic insult and worked independently of the subsequent edema. Contrastingly, Reichenbach and colleagues state that in edema-based retinal disorders, such as diabetic macular edema, the fluid accumulation associated with macular edema directly leads to degeneration of the retina via compression of the neurons and nerve fibres (Reichenbach et al., 2007). While mice do not have a macula and translatability with clinical disease is low, it is still possible that the retinal edema generated after 45 minutes of ischemia in our work resulted in compression of the RGCs and nerve fibres, leading to the longitudinal decreases in GCC thickness and RGC density that was observed. Likely, the ischemic insult and resultant edema worked in concert to produce our findings, however, our analyses were not able to distinguish their respective contributions.

4.2.4. Differences in Retinal Perfusion Between Inner Retinal Vascular Plexuses

4.2.4.1. Plexus-Specific Impact After Acute Ischemic Injury

Results from our third objective suggest that perfusion in any of the SVP, ICP and DCP are not preferentially impacted longitudinally following short or medium durations of acute I/R injury. The findings appear to be as expected, since we hypothesized that there would be no longitudinal difference in perfusion changes between the vascular plexuses following I/R injury. This information may better inform our understanding of the longitudinal plexus-specific pathological perfusion response to acute I/R injury in the retina. Importantly, OCTA images from the CCV were used for the 45-minute elevated IOP group, therefore, we were unable to distinguish or compare PDs from the SVP, ICP and DCP at any time point, leaving our inter-plexus analyses incomplete. It is possible that we could have seen preferential damage to any of the vascular plexuses following 45 minutes of ischemia.

Previous research has compared the immediate effect of acute ischemia on the individual vascular plexuses. In rat, Zhao *et al.* found evidence suggesting that the DCP was more impacted by high elevations of IOP, while Pi and colleagues contrastingly did not report preferential attenuation between plexuses after high elevations of IOP (Pi et al., 2019; Zhao et al., 2020). In monkey, Choi *et al.* found evidence that suggested the deep vascular complex was more attenuated than the superficial vascular complex at 30mmHg, but not at any higher IOPs (Choi et al., 2021). In contrast, Cheung and colleagues found evidence suggesting the deep vascular complex was more attenuated at ~100mmHg and recovered less than other plexuses 40 minutes after reperfusion (Cheung et al., 2020). By contextualizing with our findings, it is possible that any immediate plexus-specific preferential attenuation from high IOPs does not propagate to longitudinal time points

after short or medium durations of acute I/R injury.

4.2.4.2. Plexus-Specific Impact in Diabetic Retinopathy

Recent research using a model of DR has suggested that the DCP is preferentially impacted at longitudinal time points. Uehara *et al.* used OCTA to assess retinal perfusion in mice that had diabetes for 2 and 6 months. After 6 months of diabetes, vessel density in the DCP was significantly lower than age-matched controls, while the SVP and ICP were not different (Uehara et al., 2019). As our work modeled diseases such as CRAO or PACG, it is possible within the context of our findings that experimental models of DR and CRAO/PACG generate different longitudinal plexus-specific pathologies.

4.3 Limitations of Thesis Research

4.3.1. Sample Size

The groups utilized in this study consisted of 4, 8, 8 and 8 mice for the repeatability, 15-, 30- and 45-minute elevated IOP groups, respectively. As such, the low sample size could have given rise to the high variability in OCTA measurements we observed in the groups of mice that received ischemia. The presence of high variability in results may also have impacted our ability to detect statistical significance in some groups.

4.3.2. Current OCTA Technology

Poor scan quality was observed at certain time points. We omitted the 1-day OCTA measurements, as we found that image quality was poorer at this time point due to

edema, yielding artifactually low PD measurements. Omission of these data is potentially limiting, since the most immediate time point post-I/R injury was not available for analyses. A possible reason for the poor-quality scans is that edema induced the presence of inflammatory cells in the vitreous, causing an opacity known as vitreous haze, which was observed in the OCT B-scans in the eyes of some mice at this time point (Figures 3.14A and 3.15A). In all cases, observations of the OCT B-scans at the 3-day imaging time point indicated the vitreous haze was resolved and poor-quality OCTA scans were no longer acquired.

Automatic OCTA segmentation errors in the 45-minute elevated IOP group were evident upon visualizing volume projections of the SVP, ICP and DCP. Errors were likely due to the gross degeneration of the inner retina, which we observed in the peripapillary OCT B-scans (Figure 3.15A) and prevented us from manually segmenting the individual layers. It was thus necessary to use the CCV for analysis of PD in the 45-minute elevated IOP group, however this limited our investigation of retinal perfusion at the individual plexus level. The failure of automatic segmentation due to diseases that induce retinal layer alteration is a limitation noted by the manufacturer of the OCTA device used in this thesis (Rocholz et al., 2018).

A general limitation of OCTA technology is that automatic segmentation of the retinal vasculature and OCTA image generation algorithms can vary across different OCTA devices (Rao et al., 2020). This could make comparison of results to the literature more difficult.

4.3.3. Elevated IOP Model of Retinal Ischemia

To induce an acute I/R injury, we utilized a technique wherein IOP is elevated, however, this technique may introduce a mechanical damage element since the high pressure needed to collapse the retinal vessels is also exerted on the retina and causes decreases in retinal layer thickness (Zhao et al., 2020). Furthermore, it has been reported that the induction of ischemia with elevated IOP induces more retinal injury than other techniques that directly occlude the vessels, such as vessel ligation (Barnett & Osborne, 1995; Gehlbach & Purple, 1994). The introduction of further damage may potentially confound the results, as the changes in retinal perfusion, structure and RGC population we observed may be due in part to mechanical damage rather than purely ischemic damage.

4.4. Future Directions

There are a variety of experiments that could be performed to build upon and expand the findings presented in this thesis, including the extension of current work, comparing different techniques of inducing acute I/R injury and assessing the longitudinal impact of age, or preconditioning on retinal perfusion and thickness.

Increasing sample size, lengthening the imaging period following I/R injury and imaging at closer intervals between 30 and 45 minutes may yield beneficial results. There is evidence showing good OCTA inter-sessional reliability up to 1 month following baseline imaging, therefore, future work could extend past the 10-day imaging endpoint we used, in contribution towards further elucidating the time course of changes in retinal perfusion following acute I/R injury (Smith et al., 2019). Additionally, the period between the 30 and 45 minutes of ischemia we used, is a relatively long period of time,

therefore future work could introduce a variety of time points in that 15-minute span to better distinguish the threshold for irreversible damage and further our understanding of critical time periods following acute ischemic injury.

The limitation regarding mechanical damage for the elevated IOP technique has been noted above, therefore future work could compare retinal perfusion and thickness longitudinally after using the elevated IOP technique and an alternative technique, such as the ligature of the ON or CRA and CRV, which have been used previously (Faberowski et al., 1989; Lafuente et al., 2002). This potential study could directly determine the extent to which mechanical damage contributed to the changes in structure, perfusion and RGC population we found with the elevated IOP technique, however, it may require additional expertise and experience, as the ligature of the ON or CRA and CRV is more invasive and technically challenging.

Age is a significant risk factor for both POAG and PACG (Amerasinghe & Aung, 2008; Gordon et al., 2002). As a model of PACG, the elevated IOP technique may be useful in assessing the effect of aging on longitudinal changes in retinal perfusion, which could further inform our understanding of the pathophysiology of glaucoma. Recently, Jiang *et al.* assessed the impact of age on retinal perfusion in response to elevated IOP in rat using optical microangiography and found that retinal perfusion is attenuated at lower IOPs in elderly rats, when compared to adult rats (Jiang et al., 2018). It would be interesting then, for future research to compare elderly and adult mice with OCTA following acute I/R injury, to see the longitudinal impact age has on changes in retinal perfusion and thickness.

Preconditioning is defined as a period of ischemia or hypoxia that is brief and

non-lethal in nature, designed to mimic endogenous protective mechanisms (Zhu et al., 2002). In the rat and mouse retina, preconditioning periods of ischemia or hypoxia have been shown to provide significant protection against histological damage induced by mild and severe ischemic injury for up to 4 weeks following the ischemic event (Roth et al., 1998; Zhu et al., 2002). It would be interesting then, for future research to employ an ischemic or hypoxic mouse preconditioning model characterized by Zhu and colleagues, to assess the benefit it may have on longitudinal changes in retinal perfusion, thickness or RGC loss following acute I/R injury.

4.5. Conclusions

Retinal ischemia is common pathology in many retinal diseases that ultimately lead to vision loss, therefore, research investigating the time course of disease progression is increasingly needed to better understand and potentially treat in the future. While there is a plethora of imaging techniques that assess retinal perfusion *in vivo*, few can compare to OCTA in terms of providing the depth resolution necessary to assess perfusion at the level of the individual vascular plexuses. Recently, OCTA has become increasingly utilized in clinical and experimental research for the investigation of perfusion after acute I/R injury.

The results of the work presented in this research describe the successful use of *in vivo* OCTA and OCT imaging to track and observe the longitudinal time course of changes in retinal PD and GCC thickness following acute I/R injury. Information derived from OCTA and OCT analysis was invaluable in the description of a threshold for irreversible damage, the indication of longitudinal disruptions in retinal perfusion and

structure, the evaluation of temporal relationships between perfusion and structure and finally, the indication of the lack of longitudinal preferential impact between the vascular plexuses. This research has shown the utility of OCTA in the study of vascular disorders in the retina. Future research on the longitudinal impact of age and ischemic preconditioning will lead to more clinically relevant insights.

References

Abdel-Hamid, K. M., & Tymianski, M. (1997). Mechanisms and Effects of Intracellular Calcium Buffering on Neuronal Survival in Organotypic Hippocampal Cultures Exposed to Anoxia/Aglycemia or to Excitotoxins. *Journal of Neuroscience*, *17*(10), 3538–3553. https://doi.org/10.1523/JNEUROSCI.17-10-03538.1997

Akagi, T., Iida, Y., Nakanishi, H., Terada, N., Morooka, S., Yamada, H., Hasegawa, T., Yokota, S., Yoshikawa, M., & Yoshimura, N. (2016). Microvascular Density in Glaucomatous Eyes With Hemifield Visual Field Defects: An Optical Coherence Tomography Angiography Study. *American Journal of Ophthalmology*, *168*, 237–249. https://doi.org/https://doi.org/10.1016/j.ajo.2016.06.009

Albrecht May, C. (2008). Comparative anatomy of the optic nerve head and inner retina in non-primate animal models used for glaucoma research. *The Open Ophthalmology Journal*, *2*, 94–101. https://doi.org/10.2174/1874364100802010094

Alex, A. F., Alnawaiseh, M., Heiduschka, P., & Eter, N. (2019). *Retinal Fundus Imaging in Mouse Models of Retinal Diseases BT - Retinal Degeneration: Methods and Protocols* (B. H. F. Weber & T. Langmann (eds.); pp. 253–283). Springer New York. https://doi.org/10.1007/978-1-4939-8669-9_17

Allingham, M. J., Tserentsoodol, N., Saloupis, P., Mettu, P. S., & Cousins, S. W. (2018). Aldosterone exposure causes increased retinal edema and severe retinopathy following laser-induced retinal vein occlusion in mice. *Investigative Ophthalmology & Visual Science*, *59*(8), 3355–3365.

Alm, A., & Bill, A. (1972). The oxygen supply to the retina. II. Effects of high intraocular pressure and of increased arterial carbon dioxide tension on uveal and retinal blood flow in cats. A study with radioactively labelled microspheres including flow determinations in brain an. *Acta Physiologica Scandinavica*, *84*(3), 306–319. https://doi.org/10.1111/j.1748-1716.1972.tb05182.x

Alm, A., & Bill, A. (1973). Ocular and optic nerve blood flow at normal and increased intraocular pressures in monkeys (Macaca irus): a study with radioactively labelled microspheres including flow determinations in brain and some other tissues. *Experimental Eye Research*, *15*(1), 15–29. https://doi.org/10.1016/0014-4835(73)90185-1

Alnawaiseh, M., Rosentreter, A., Hillmann, A., Alex, A. F., Niekämper, D., Heiduschka, P., Pap, T., & Eter, N. (2016). OCT angiography in the mouse: A novel evaluation method for vascular pathologies of the mouse retina. *Experimental Eye Research*, *145*, 417–423. https://doi.org/https://doi.org/10.1016/j.exer.2016.02.012

Alterman, M., & Henkind, P. (1968). Radial peripapillary capillaries of the retina. II. Possible role in Bjerrum scotoma. *The British Journal of Ophthalmology*, *52*(1), 26–31. https://doi.org/10.1136/bjo.52.1.26

Amerasinghe, N., & Aung, T. (2008). Angle-closure: risk factors, diagnosis and treatment. *Progress in Brain Research*, *173*, 31–45. https://doi.org/10.1016/S0079-6123(08)01104-7

Ames, A. 3rd, Wright, R. L., Kowada, M., Thurston, J. M., & Majno, G. (1968). Cerebral ischemia. II. The no-reflow phenomenon. *The American Journal of Pathology*, *52*(2), 437–453.

Anand-Apte, B., & Hollyfield, J. G. (2010). *Developmental Anatomy of the Retinal and Choroidal Vasculature* (D. A. B. T.-E. of the E. Dartt (ed.); pp. 9–15). Academic Press. https://doi.org/https://doi.org/10.1016/B978-0-12-374203-2.00169-X

Andersen, B. J., & Saltzman, H. A. (1964). RETINAL OXYGEN UTILIZATION MEASURED BY HYPERBARIC BLACKOUT. *Archives of Ophthalmology (Chicago, Ill. : 1960)*, *72*, 792–795. https://doi.org/10.1001/archopht.1964.00970020794009

Anderson, B. J., & McIntosh, H. D. (1967). Retinal circulation. *Annual Review of Medicine*, *18*, 15–26. https://doi.org/10.1146/annurev.me.18.020167.000311

Ang, M., Tan, A. C. S., Cheung, C. M. G., Keane, P. A., Dolz-Marco, R., Sng, C. C. A., & Schmetterer, L. (2018). Optical coherence tomography angiography: a review of current and future clinical applications. *Graefe's Archive for Clinical and Experimental Ophthalmology*, *256*(2), 237–245. https://doi.org/10.1007/s00417-017-3896-2

Bakhoum, M. F., Freund, K. B., Dolz-Marco, R., Leong, B. C. S., Baumal, C. R., Duker, J. S., & Sarraf, D. (2018). Paracentral acute middle maculopathy and the ischemic cascade associated with retinal vascular occlusion. *American Journal of Ophthalmology*, *195*, 143–153.

Balaratnasingam, C., Inoue, M., Ahn, S., McCann, J., Dhrami-Gavazi, E., Yannuzzi, L. A., & Freund, K. B. (2016). Visual acuity is correlated with the area of the foveal avascular zone in diabetic retinopathy and retinal vein occlusion. *Ophthalmology*, *123*(11), 2352–2367.

Balendra, S. I., Normando, E. M., Bloom, P. A., & Cordeiro, M. F. (2015). Advances in retinal ganglion cell imaging. *Eye (London, England)*, *29*(10), 1260–1269. https://doi.org/10.1038/eye.2015.154

Barlow, H. B., Hill, R. M., & Levick, W. R. (1964). RETINAL GANGLION CELLS RESPONDING SELECTIVELY TO DIRECTION AND SPEED OF IMAGE MOTION IN THE RABBIT. *The Journal of Physiology*, *173*(3), 377–407. https://doi.org/10.1113/jphysiol.1964.sp007463

Barnett, N. L., & Osborne, N. N. (1995). Prolonged bilateral carotid artery occlusion induces electrophysiological and immunohistochemical changes to the rat retina without causing histological damage. *Experimental Eye Research*, *61*(1), 83–90. https://doi.org/10.1016/s0014-4835(95)80061-1

Baylor, D. A., Fuortes, M. G., & O'Bryan, P. M. (1971). Receptive fields of cones in the retina of the turtle. *The Journal of Physiology*, *214*(2), 265–294. https://doi.org/10.1113/jphysiol.1971.sp009432

Beatty, S., Koh, H., Phil, M., Henson, D., & Boulton, M. (2000). The role of oxidative stress in the pathogenesis of age-related macular degeneration. *Survey of Ophthalmology*, *45*(2), 115–134. https://doi.org/10.1016/s0039-6257(00)00140-5

Beck, S., Schaeferhoff, K., Michalakis, S., Fischer, M. D., Huber, G., Rieger, N., Riess, O., Wissinger, B., Biel, M., Bonin, M., Seeliger, M., & Tanimoto, N. (2009). In Vivo Analysis of Cone Survival in Mice. *Investigative Ophthalmology & Visual Science*, *51*, 493–497. https://doi.org/10.1167/iovs.09-4003

Belforte, N., Sande, P. H., de Zavalía, N., Fernandez, D. C., Silberman, D. M., Chianelli, M. S., & Rosenstein, R. E. (2011). Ischemic Tolerance Protects the Rat Retina from Glaucomatous Damage. *PLOS ONE*, *6*(8), e23763. https://doi.org/10.1371/journal.pone.0023763

Benveniste, H., Drejer, J., Schousboe, A., & Diemer, N. H. (1984). Elevation of the Extracellular Concentrations of Glutamate and Aspartate in Rat Hippocampus During Transient Cerebral Ischemia Monitored by Intracerebral Microdialysis. *Journal of Neurochemistry*, *43*(5), 1369–1374. https://doi.org/https://doi.org/10.1111/j.1471-4159.1984.tb05396.x

Bok, D. (1993). The retinal pigment epithelium: a versatile partner in vision. *Journal of Cell Science. Supplement*, *17*, 189–195. https://doi.org/10.1242/jcs.1993.supplement_17.27

Bowmaker, J. K., & Dartnall, H. J. (1980). Visual pigments of rods and cones in a human retina. *The Journal of Physiology*, *298*, 501–511. https://doi.org/10.1113/jphysiol.1980.sp013097

Brandstätter, J. H., Hartveit, E., Sassoè-Pognetto, M., & Wässle, H. (1994). Expression of NMDA and high-affinity kainate receptor subunit mRNAs in the adult rat retina. *European Journal of Neuroscience*, *6*(7), 1100–1112.

Bubis, E., Sher, I., Skaat, A., Sharvit-Ginon, I., Szalapak, A. M., Moroz, I., Kalter-Leibovici, O., & Rotenstreich, Y. (2019). Blue Autofluorescence Fundus Imaging for Monitoring Retinal Degeneration in Royal College of Surgeons Rats. *Translational Vision Science & Technology*, *8*(1), 26. https://doi.org/10.1167/tvst.8.1.26

Büchi, E. R., Suivaizdis, I., & Fu, J. (1991). Pressure-Induced Retinal Ischemia in Rats: An Experimental Model for Quantitative Study. *Ophthalmologica*, *203*(3), 138–147. https://doi.org/10.1159/000310240

Büchi, E. R. (1992). Cell death in the rat retina after a pressure-induced ischaemia-reperfusion insult: an electron microscopic study. I. Ganglion cell layer and inner nuclear layer. *Experimental Eye Research*, *55*(4), 605–613.

Calkins, D. J. (2012). Critical pathogenic events underlying progression of neurodegeneration in glaucoma. *Progress in Retinal and Eye Research*, *31*(6), 702–719. https://doi.org/10.1016/j.preteyeres.2012.07.001

Campbell, J. P., Zhang, M., Hwang, T. S., Bailey, S. T., Wilson, D. J., Jia, Y., & Huang, D. (2017). Detailed Vascular Anatomy of the Human Retina by Projection-Resolved Optical Coherence Tomography Angiography. *Scientific Reports*, *7*, 42201. https://doi.org/10.1038/srep42201

Cao, W., Zaharia, M., Drumheller, A., Casanova, C., Lafond, G., Brunette, J. R., & Jolicoeur, F. B. (1994). Effects of dextromethorphan on ischemia induced electroretinogram changes in rabbit. *Current Eye Research*, *13*(2), 97–102. https://doi.org/10.3109/02713689409042403

Carter-Dawson, L. D., & LaVail, M. M. (1979). Rods and cones in the mouse retina. I. Structural analysis using light and electron microscopy. *The Journal of Comparative Neurology*, *188*(2), 245–262. https://doi.org/10.1002/cne.901880204

Chan, G., Balaratnasingam, C., Xu, J., Mammo, Z., Han, S., Mackenzie, P., Merkur, A., Kirker, A., Albiani, D., Sarunic, M. V, & Yu, D.-Y. (2015). In vivo optical imaging of human retinal capillary networks using speckle variance optical coherence tomography with quantitative clinico-histological correlation. *Microvascular Research*, *100*, 32–39. https://doi.org/10.1016/j.mvr.2015.04.006

Chan, G., Balaratnasingam, C., Yu, P. K., Morgan, W. H., McAllister, I. L., Cringle, S. J., & Yu, D.-Y. (2012). Quantitative morphometry of perifoveal capillary networks in the human retina. *Investigative Ophthalmology & Visual Science*, *53*(9), 5502–5514. https://doi.org/10.1167/iovs.12-10265

Chauhan, B. C., Stevens, K. T., Levesque, J. M., Nuschke, A. C., Sharpe, G. P., O'Leary, N., Archibald, M. L., & Wang, X. (2012). Longitudinal In Vivo Imaging of Retinal Ganglion Cells and Retinal Thickness Changes Following Optic Nerve Injury in Mice. *PLOS ONE*, *7*(6), 1–9. https://doi.org/10.1371/journal.pone.0040352

Chen, C.-L., Bojikian, K. D., Wen, J. C., Zhang, Q., Xin, C., Mudumbai, R. C., Johnstone, M. A., Chen, P. P., & Wang, R. K. (2017). Peripapillary Retinal Nerve Fiber Layer Vascular Microcirculation in Eyes With Glaucoma and Single-Hemifield Visual Field Loss. *JAMA Ophthalmology*, *135*(5), 461–468. https://doi.org/10.1001/jamaophthalmol.2017.0261

Chen, F. K., Viljoen, R. D., & Bukowska, D. M. (2016). Classification of image artefacts in optical coherence tomography angiography of the choroid in macular diseases. *Clinical & Experimental Ophthalmology*, *44*(5), 388–399.

Cheung, C. M. G., Teo, K. Y. C., Tun, S. B. B., Busoy, J. M., Veluchamy, A. B., & Spaide, R. F. (2020). Differential reperfusion patterns in retinal vascular plexuses following increase in intraocular pressure an OCT angiography study. *Scientific Reports*, *10*(1), 16505. https://doi.org/10.1038/s41598-020-73585-0

Choi, M., Kim, S.-W., Vu, T. Q. A., Kim, Y.-J., Jung, H., Shin, D., Eom, H., Kim, Y. H., Yun, C., & Kim, Y. Y. (2021). Analysis of Microvasculature in Nonhuman Primate Macula With Acute Elevated Intraocular Pressure Using Optical Coherence Tomography Angiography. *Investigative Ophthalmology & Visual Science*, *62*(15), 18. https://doi.org/10.1167/iovs.62.15.18

Corradetti, G., Au, A., Borrelli, E., Xu, X., Freund, K. B., & Sarraf, D. (2019). Analysis of hyperreflective dots within the central fovea in healthy eyes using en face optical coherence tomography. *Investigative Ophthalmology & Visual Science*, *60*(13), 4451–4461.

Cunha-Vaz, J. G., Shakib, M., & Ashton, N. (1966). Studies on the permeability of the blood-retinal barrier. I. On the existence, development, and site of a blood-retinal barrier. *The British Journal of Ophthalmology*, *50*(8), 441–453. https://doi.org/10.1136/bjo.50.8.441

Curcio, C. A., & Allen, K. A. (1990). Topography of ganglion cells in human retina. *The Journal of Comparative Neurology*, *300*(1), 5–25. https://doi.org/10.1002/cne.903000103

Dacheux, R. F., & Miller, R. F. (1976). Photoreceptor-bipolar cell transmission in the perfused retina eyecup of the mudpuppy. *Science (New York, N.Y.)*, *191*(4230), 963–964. https://doi.org/10.1126/science.175443

Daugeliene, L., Niwa, M., Hara, A., Matsuno, H., Yamamoto, T., Kitazawa, Y., & Uematsu, T. (2000). Transient Ischemic Injury in the Rat Retina Caused by Thrombotic Occlusion–Thrombolytic Reperfusion. *Investigative Ophthalmology & Visual Science*, *41*(9), 2743–2747.

De Flora, A., Franco, L., Guida, L., Bruzzone, S., & Zocchi, E. (1998). Ectocellular CD38-catalyzed synthesis and intracellular Ca2+-mobilizing activity of cyclic ADP-ribose. *Cell Biochemistry and Biophysics*, *28*(1), 45–62.

Dessi, F., Charriaut-Marlangue, C., Khrestchatisky, M., & Ben-Ari, Y. (1993). Glutamate-induced neuronal death is not a programmed cell death in cerebellar culture. *Journal of Neurochemistry*, *60*(5), 1953–1955.

Di Pierdomenico, J., Henderson, D. C. M., Giammaria, S., Smith, V. L., Jamet, A. J., Smith, C. A., Hooper, M. L., & Chauhan, B. C. (2022). Age and intraocular pressure in murine experimental glaucoma. *Progress in Retinal and Eye Research*, *88*, 101021. https://doi.org/https://doi.org/10.1016/j.preteyeres.2021.101021

Donaldson, P. J., Grey, A. C., Maceo Heilman, B., Lim, J. C., & Vaghefi, E. (2017). The physiological optics of the lens. *Progress in Retinal and Eye Research*, *56*, e1–e24. https://doi.org/10.1016/j.preteyeres.2016.09.002

Drexler, W., & Fujimoto, J. G. (2008). State-of-the-art retinal optical coherence tomography. *Progress in Retinal and Eye Research*, *27*(1), 45–88.

Drexler, W., Liu, M., Kumar, A., Kamali, T., Unterhuber, A., & Leitgeb, R. A. (2014). Optical coherence tomography today: speed, contrast, and multimodality. *Journal of Biomedical Optics*, *19*(7), 71412.

Dugan, L. L., Sensi, S. L., Canzoniero, L. M., Handran, S. D., Rothman, S. M., Lin, T.-S., Goldberg, M. P., & Choi, D. W. (1995). Mitochondrial production of reactive oxygen species in cortical neurons following exposure to N-methyl-D-aspartate. *Journal of Neuroscience*, *15*(10), 6377–6388.

Faberowski, N., Stefansson, E., & Davidson, R. C. (1989). Local hypothermia protects the retina from ischemia. A quantitative study in the rat. *Investigative Ophthalmology & Visual Science*, *30*(11), 2309–2313.

Flammer, J. (1994). The vascular concept of glaucoma. *Survey of Ophthalmology*, *38 Suppl*, S3-6. https://doi.org/10.1016/0039-6257(94)90041-8

Fogel-Levin, M., Sadda, S. R., Rosenfeld, P. J., Waheed, N., Querques, G., Freund, B. K., & Sarraf, D. (2022). Advanced retinal imaging and applications for clinical practice: A consensus review. *Survey of Ophthalmology*, *67*(5), 1373–1390. https://doi.org/https://doi.org/10.1016/j.survophthal.2022.02.004

Fontaine, V., Mohand-Said, S., Hanoteau, N., Fuchs, C., Pfizenmaier, K., & Eisel, U. (2002). Neurodegenerative and Neuroprotective Effects of Tumor Necrosis Factor (TNF) in Retinal Ischemia: Opposite Roles of TNF Receptor 1 and TNF Receptor 2. *Journal of Neuroscience*, *22*(7), RC216--RC216. https://doi.org/10.1523/JNEUROSCI.22-07-j0001.2002

Fu, Y., & Yau, K.-W. (2007). Phototransduction in mouse rods and cones. *Pflügers Archiv - European Journal of Physiology*, *454*(5), 805–819. https://doi.org/10.1007/s00424-006-0194-y

Fujimoto, J. G., Pitris, C., Boppart, S. A., & Brezinski, M. E. (2000). Optical coherence tomography: an emerging technology for biomedical imaging and optical biopsy. *Neoplasia*, *2*(1–2), 9–25.

Funk, R. H. (1997). Blood supply of the retina. *Ophthalmic Research*, *29*(5), 320–325. https://doi.org/10.1159/000268030

Gao, S. S., Jia, Y., Zhang, M., Su, J. P., Liu, G., Hwang, T. S., Bailey, S. T., & Huang, D. (2016). Optical coherence tomography angiography. *Investigative Ophthalmology & Visual Science*, *57*(9), OCT27–OCT36.

Garala, P., & Bansal, A. (2019). Acute Secondary Optic Neuropathy as a Complication of a Single Episode of Acutely Raised Intraocular Pressure: A Case Series. *Journal of Glaucoma*, *28*(1), e10–e13. https://doi.org/10.1097/IJG.0000000000001094

Gehlbach, P. L., & Purple, R. L. (1994). A paired comparison of two models of experimental retinal ischemia. *Current Eye Research*, *13*(8), 597–602. https://doi.org/10.3109/02713689408999893

Germer, A., Biedermann, B., Wolburg, H., Schuck, J., Grosche, J., Kuhrt, H., Reichelt, W., Schousboe, A., Paasche, G., Mack, A. F., & Reichenbach, A. (1998). Distribution of mitochondria within Müller cells--I. Correlation with retinal vascularization in different mammalian species. *Journal of Neurocytology*, *27*(5), 329–345. https://doi.org/10.1023/a:1006934724566

Gilgun-Sherki, Y., Rosenbaum, Z., Melamed, E., & Offen, D. (2002). Antioxidant Therapy in Acute Central Nervous System Injury: Current State. *Pharmacological Reviews*, *54*(2), 271–284. https://doi.org/10.1124/pr.54.2.271

Glasser, A., & Kaufman, P. L. (1999). The mechanism of accommodation in primates. *Ophthalmology*, *106*(5), 863–872. https://doi.org/10.1016/S0161-6420(99)00502-3

Gordon, M. O., Beiser, J. A., Brandt, J. D., Heuer, D. K., Higginbotham, E. J., Johnson, C. A., Keltner, J. L., Miller, J. P., Parrish, R. K. 2nd, Wilson, M. R., & Kass, M. A. (2002). The Ocular Hypertension Treatment Study: baseline factors that predict the onset of primary open-angle glaucoma. *Archives of Ophthalmology (Chicago, Ill. : 1960)*, *120*(6), 714–730. https://doi.org/10.1001/archopht.120.6.714

Govetto, A., Sarraf, D., Hubschman, J.-P., Tadayoni, R., Couturier, A., Chehaibou, I., Au, A., Grondin, C., Virgili, G., & Romano, M. R. (2020). Distinctive mechanisms and patterns of exudative versus tractional intraretinal cystoid spaces as seen with multimodal imaging. *American Journal of Ophthalmology*, *212*, 43–56.

Greig, E. C., Duker, J. S., & Waheed, N. K. (2020). A practical guide to optical coherence tomography angiography interpretation. *International Journal of Retina and Vitreous*, *6*(1), 1–17.

Groh, J., Stadler, D., Buttmann, M., & Martini, R. (2014). Non-invasive assessment of retinal alterations in mouse models of infantile and juvenile neuronal ceroid lipofuscinosis by spectral domain optical coherence tomography. *Acta Neuropathologica Communications*, *2*, 54. https://doi.org/10.1186/2051-5960-2-54

Guyer, D., Schachat, A., & Green, W. (2006). *The Choroid: Structural Considerations* (pp. 33–42). https://doi.org/10.1016/B978-0-323-02598-0.50009-4

Hargrave, P. A., & McDowell, J. H. (1992). Rhodopsin and phototransduction. *International Review of Cytology*, *137B*, 49–97. https://doi.org/10.1016/s0074-7696(08)62600-5

Hartline, H. K. (1938). The response of single optic nerve fibers of the vertebrate eye to illumination of the retina. *American Journal of Physiology*, *121*, 400–415.

Hartsock, M. J., Cho, H., Wu, L., Chen, W.-J., Gong, J., & Duh, E. J. (2016). A Mouse Model of Retinal Ischemia-Reperfusion Injury Through Elevation of Intraocular Pressure. *Journal of Visualized Experiments : JoVE*, *113*. https://doi.org/10.3791/54065

Hartveit, E., Brandstätter, J. H., Enz, R., & Wässle, H. (1995). Expression of the mRNA of Seven Metabotropic Glutamate Receptors (mGluR1 to 7) in the Rat Retina. An In Situ Hybridization Study on Tissue Sections and Isolated Cells. *European Journal of Neuroscience*, *7*(7), 1472–1483. https://doi.org/https://doi.org/10.1111/j.1460-9568.1995.tb01142.x

Hawes, N. L., Smith, R. S., Chang, B., Davisson, M., Heckenlively, J. R., & John, S. W. (1999). Mouse fundus photography and angiography: a catalogue of normal and mutant phenotypes. *Molecular Vision*, *5*, 22.

Hayreh, S. S. (1974). Anatomy and physiology of the optic nerve head. *Transactions - American Academy of Ophthalmology and Otolaryngology. American Academy of Ophthalmology and Otolaryngology*, *78*(2), OP240-54.

Hayreh, S. S., & Weingeist, T. A. (1980). Experimental occlusion of the central artery of the retina. IV: Retinal tolerance time to acute ischaemia. *British Journal of Ophthalmology*, *64*(11), 818–825. https://doi.org/10.1136/bjo.64.11.818

Hejtmancik, J. F., & Shiels, A. (2015). Overview of the Lens. In *Progress in molecular biology and translational science* (Vol. 134, pp. 119–127). https://doi.org/10.1016/bs.pmbts.2015.04.006

Henkind, P. (1967). Radial peripapillary capillaries of the retina. I. Anatomy: human and comparative. *The British Journal of Ophthalmology*, *51*(2), 115–123. https://doi.org/10.1136/bjo.51.2.115

Hickham, J. B., Frayser, R., & Ross, J. C. (1963). A study of retinal venous blood oxygen saturation in human subjects by photographic means. *Circulation*, *27*, 375–385. https://doi.org/10.1161/01.cir.27.3.375

Hirano, A. A., Brandstätter, J. H., Vila, A., & Brecha, N. C. (2007). Robust syntaxin-4 immunoreactivity in mammalian horizontal cell processes. *Visual Neuroscience*, *24*(4), 489–502. https://doi.org/10.1017/S0952523807070198

Hoon, M., Okawa, H., Della Santina, L., & Wong, R. O. L. (2014). Functional architecture of the retina: development and disease. *Progress in Retinal and Eye Research*, *42*, 44–84. https://doi.org/10.1016/j.preteyeres.2014.06.003

Huber, G., Beck, S. C., Grimm, C., Sahaboglu-Tekgoz, A., Paquet-Durand, F., Wenzel, A., Humphries, P., Redmond, T. M., Seeliger, M. W., & Fischer, M. D. (2009). Spectral domain optical coherence tomography in mouse models of retinal degeneration. *Investigative Ophthalmology & Visual Science*, *50*(12), 5888–5895. https://doi.org/10.1167/iovs.09-3724

Hughes, W. F. (1991). Quantitation of ischemic damage in the rat retina. *Experimental Eye Research*, *53*(5), 573–582. https://doi.org/https://doi.org/10.1016/0014-4835(91)90215-Z

Jaffe, G. J., & Caprioli, J. (2004). Optical coherence tomography to detect and manage retinal disease and glaucoma. *American Journal of Ophthalmology*, *137*(1), 156–169. https://doi.org/10.1016/s0002-9394(03)00792-x

Janáky, M., Grósz, A., Tóth, E., Benedek, K., & Benedek, G. (2007). Hypobaric hypoxia reduces the amplitude of oscillatory potentials in the human ERG. *Documenta Ophthalmologica*, *114*(1), 45–51.

Jeon, C. J., Strettoi, E., & Masland, R. H. (1998). The major cell populations of the mouse retina. *The Journal of Neuroscience : The Official Journal of the Society for Neuroscience*, *18*(21), 8936–8946. https://doi.org/10.1523/JNEUROSCI.18-21-08936.1998

Jia, Y., Wei, E., Wang, X., Zhang, X., Morrison, J. C., Parikh, M., Lombardi, L. H., Gattey, D. M., Armour, R. L., Edmunds, B., Kraus, M. F., Fujimoto, J. G., & Huang, D. (2014). Optical coherence tomography angiography of optic disc perfusion in glaucoma. *Ophthalmology*, *121*(7), 1322–1332. https://doi.org/10.1016/j.ophtha.2014.01.021

Jiang, X., Johnson, E., Cepurna, W., Lozano, D., Men, S., Wang, R. K., & Morrison, J. (2018). The effect of age on the response of retinal capillary filling to changes in intraocular pressure measured by optical coherence tomography angiography. *Microvascular Research*, *115*, 12–19. https://doi.org/10.1016/j.mvr.2017.08.001

Johnson, N. F. (1974). Effects of acute ischemia on the structure of the rabbit retina. *Trans Ophthal Soc UK*, *94*, 394–405.

Ju, W.-K., Kim, K.-Y., & Neufeld, A. H. (2003). Increased activity of cyclooxygenase-2 signals early neurodegenerative events in the rat retina following transient ischemia. *Experimental Eye Research*, *77*(2), 137–145.

Kaur, C., Foulds, W. S., & Ling, E.-A. (2008). Hypoxia-ischemia and retinal ganglion cell damage. *Clinical Ophthalmology (Auckland, N.Z.)*, *2*(4), 879–889. https://doi.org/10.2147/opth.s3361

Keane, P. A., & Sadda, S. R. (2014). Retinal imaging in the twenty-first century: state of the art and future directions. *Ophthalmology*, *121*(12), 2489–2500.

Kiel, J. W. (2010). *The Ocular Circulation*. Morgan & Claypool Life Sciences. https://doi.org/10.4199/C00024ED1V01Y201012ISP012

Kim, Y., Hong, H. K., Park, J. R., Choi, W., Woo, S. J., Park, K. H., & Oh, W.-Y. (2018). Oxygen-Induced Retinopathy and Choroidopathy: In Vivo Longitudinal Observation of Vascular Changes Using OCTA. *Investigative Ophthalmology & Visual Science*, *59*(10), 3932–3942. https://doi.org/10.1167/iovs.18-24320

Kolb, H., & Nelson, R. (1993). OFF-alpha and OFF-beta ganglion cells in cat retina: II. Neural circuitry as revealed by electron microscopy of HRP stains. *The Journal of Comparative Neurology*, *329*(1), 85–110. https://doi.org/10.1002/cne.903290107

Kolb, H, Nelson, R., Ahnelt, P., & Cuenca, N. (2001). Cellular organization of the vertebrate retina. *Progress in Brain Research*, *131*, 3–26. https://doi.org/10.1016/s0079-6123(01)31005-1

Kolb, H. (2011). *Simple Anatomy of the Retina by Helga Kolb*. Webvision. Moran Eye Center. https://webvision.med.utah.edu/book/part-i-foundations/simple-anatomy-of-the-retina/

Kurokawa, K., Sasaki, K., Makita, S., Hong, Y.-J., & Yasuno, Y. (2012). Three-dimensional retinal and choroidal capillary imaging by power Doppler optical coherence angiography with adaptive optics. *Optics Express*, *20*(20), 22796–22812. https://doi.org/10.1364/OE.20.022796

Lafuente, M., Villegas-Perez, M. P., Selles-Navarro, I., Mayor-Torroglosa, S., De Imperial, J. M., & Vidal-Sanz, M. (2002). Retinal ganglion cell death after acute retinal ischemia is an ongoing process whose severity and duration depends on the duration of the insult. *Neuroscience*, *109*(1), 157–168.

LaVail, M. M. (1983). Outer segment disc shedding and phagocytosis in the outer retina. *Transactions of the Ophthalmological Societies of the United Kingdom*, *103 (Pt 4*, 397–404.

Lee, D., Jeong, H., Miwa, Y., Shinojima, A., Katada, Y., Tsubota, K., & Kurihara, T. (2021). Retinal dysfunction induced in a mouse model of unilateral common carotid artery occlusion. *PeerJ*, *9*, e11665. https://doi.org/10.7717/peerj.11665

Lee, J. M., Grabb, M. C., Zipfel, G. J., & Choi, D. W. (2000). Brain tissue responses to ischemia. *The Journal of Clinical Investigation*, *106*(6), 723–731. https://doi.org/10.1172/JCI11003

Leitgeb, R. A., Werkmeister, R. M., Blatter, C., & Schmetterer, L. (2014). Doppler optical coherence tomography. *Progress in Retinal and Eye Research*, *41*, 26–43.

Lettvin, J. Y., Maturana, H. R., McCulloch, W. S., & Pitts, W. H. (1959). What the Frog's Eye Tells the Frog's Brain. *Proceedings of the IRE*, *47*(11), 1940–1951. https://doi.org/10.1109/JRPROC.1959.287207

Leung, C. K. S., Lindsey, J. D., Crowston, J. G., Ju, W.-K., Liu, Q., Bartsch, D.-U., & Weinreb, R. N. (2008). In vivo imaging of murine retinal ganglion cells. *Journal of Neuroscience Methods*, *168*(2), 475–478. https://doi.org/https://doi.org/10.1016/j.jneumeth.2007.10.018

Linsenmeier, R. A., Braun, R. D., McRipley, M. A., Padnick, L. B., Ahmed, J., Hatchell, D. L., McLeod, D. S., & Lutty, G. A. (1998). Retinal hypoxia in long-term diabetic cats. *Investigative Ophthalmology & Visual Science*, *39*(9), 1647–1657.

Lipton, P. (1999). Ischemic cell death in brain neurons. *Physiological Reviews*, *79*(4), 1431–1568.

Liu, L., Jia, Y., Takusagawa, H. L., Pechauer, A. D., Edmunds, B., Lombardi, L., Davis, E., Morrison, J. C., & Huang, D. (2015). Optical Coherence Tomography Angiography of the Peripapillary Retina in Glaucoma. *JAMA Ophthalmology*, *133*(9), 1045–1052. https://doi.org/10.1001/jamaophthalmol.2015.2225

Louzada-Junior, P., Dias, J. J., Santos, W. F. dos, Lachat, J. J., Bradford, H. F., & Coutinho-Netto, J. (1992). Glutamate release in experimental ischaemia of the retina: an approach using microdialysis. *Journal of Neurochemistry*, *59*(1), 358–363.

Lund, R. D. (1965). Uncrossed Visual Pathways of Hooded and Albino Rats. *Science (New York, N.Y.)*, *149*(3691), 1506–1507. https://doi.org/10.1126/science.149.3691.1506

Manivannan, A., Sharp, P. F., Phillips, R. P., & Forrester, J. V. (1993). Digital fundus imaging using a scanning laser ophthalmoscope. *Physiological Measurement*, *14*(1), 43–56. https://doi.org/10.1088/0967-3334/14/1/006

Marmor, M. F. (1999). Mechanisms of fluid accumulation in retinal edema. *Documenta Ophthalmologica. Advances in Ophthalmology*, *97*(3–4), 239–249. https://doi.org/10.1023/a:1002192829817

May, C. A., & Lütjen-Drecoll, E. (2002). Morphology of the murine optic nerve. *Investigative Ophthalmology & Visual Science*, *43*(7), 2206–2212.

McNabb, R. P., Polans, J., Keller, B., Jackson-Atogi, M., James, C. L., Vann, R. R., Izatt, J. A., & Kuo, A. N. (2019). Wide-field whole eye OCT system with demonstration of quantitative retinal curvature estimation. *Biomedical Optics Express*, *10*(1), 338–355. https://doi.org/10.1364/BOE.10.000338

Mehmet, H., Yue, X., Squier, M. V, Lorek, A., Cady, E., Penrice, J., Sarraf, C., Wylezinska, M., Kirkbride, V., & Cooper, C. (1994). Increased apoptosis in the cingulate sulcus of newborn piglets following transient hypoxia-ischaemia is related to the degree of high energy phosphate depletion during the insult. *Neuroscience Letters*, *181*(1–2), 121–125.

Minhas, G., Morishita, R., & Anand, A. (2012). Preclinical models to investigate retinal ischemia: Advances and drawbacks. *Frontiers in Neurology*, *3*. https://doi.org/10.3389/fneur.2012.00075

Mosinger, J. L., & Olney, J. W. (1989). Photothrombosis-induced ischemic neuronal degeneration in the rat retina. *Experimental Neurology*, *105*(1), 110–113. https://doi.org/10.1016/0014-4886(89)90178-7

Nakajima, W., Ishida, A., Lange, M. S., Gabrielson, K. L., Wilson, M. A., Martin, L. J., Blue, M. E., & Johnston, M. V. (2000). Apoptosis has a prolonged role in the neurodegeneration after hypoxic ischemia in the newborn rat. *Journal of Neuroscience*, *20*(21), 7994–8004.

Nastos, C., Kalimeris, K., Papoutsidakis, N., Tasoulis, M.-K., Lykoudis, P. M., Theodoraki, K., Nastou, D., Smyrniotis, V., & Arkadopoulos, N. (2014). Global consequences of liver ischemia/reperfusion injury. *Oxidative Medicine and Cellular Longevity*, *2014*.

Nuschke, A. C. (2017). *Spatiotemporal Assessment of Axonal Transport and Cytoskeletal Structure in Retinal Ganglion Cells Following Acute Elevated Intraocular Pressure in the Rat [Dissertation]*. Dalhousie University.

Olver, J. M., Spalton, D. J., & McCartney, A. C. (1994). Quantitative morphology of human retrolaminar optic nerve vasculature. *Investigative Ophthalmology & Visual Science*, *35*(11), 3858–3866.

Osborne, N. N., Casson, R. J., Wood, J. P. M., Chidlow, G., Graham, M., & Melena, J. (2004). Retinal ischemia: mechanisms of damage and potential therapeutic strategies. *Progress in Retinal and Eye Research*, *23*(1), 91–147. https://doi.org/https://doi.org/10.1016/j.preteyeres.2003.12.001

Osborne, N. N., & Larsen, A. K. (1996). ANTIGENS ASSOCIATED WITH SPECIFIC RETINAL CELLS ARE AFFECTED BY ISCHAEMIA CAUSED BY RAISED INTRAOCULAR PRESSURE: EFFECT OF GLUTAMATE ANTAGONISTS **Part of the work reported in this original communication was presented at the symposium entitled Excitatory. *Neurochemistry International*, *29*(3), 263–270. https://doi.org/https://doi.org/10.1016/0197-0186(96)00005-8

Otori, Y., Shimada, S., Morimura, H., Ishimoto, I., Tohyama, M., & Tang, Y. (1997). Expression of c-fos and c-jun mRNA Following Transient Retinal Ischemia: An Approach Using Ligation of the Retinal Central Artery in the Rat. *Survey of Ophthalmology*, *42*, S96–S104. https://doi.org/https://doi.org/10.1016/S0039-6257(97)80032-X

Paques, M., Tadayoni, R., Sercombe, R., Laurent, P., Genevois, O., Gaudric, A., & Vicaut, E. (2003). Structural and hemodynamic analysis of the mouse retinal microcirculation. *Investigative Ophthalmology & Visual Science*, *44*(11), 4960–4967. https://doi.org/10.1167/iovs.02-0738

Park, J. R., Choi, W., Hong, H. K., Kim, Y., Jun Park, S., Hwang, Y., Kim, P., Joon Woo, S., Hyung Park, K., & Oh, W.-Y. (2016). Imaging Laser-Induced Choroidal Neovascularization in the Rodent Retina Using Optical Coherence Tomography Angiography. *Investigative Ophthalmology & Visual Science*, *57*(9), OCT331–OCT340. https://doi.org/10.1167/iovs.15-18946

Pepperberg, D. R., Okajima, T. L., Wiggert, B., Ripps, H., Crouch, R. K., & Chader, G. J. (1993). Interphotoreceptor retinoid-binding protein (IRBP). Molecular biology and physiological role in the visual cycle of rhodopsin. *Molecular Neurobiology*, *7*(1), 61–85. https://doi.org/10.1007/BF02780609

Perry, V. H. (1981). Evidence for an amacrine cell system in the ganglion cell layer of the rat retina. *Neuroscience*, *6*(5), 931–944. https://doi.org/10.1016/0306-4522(81)90174-3

Pi, S., Hormel, T. T., Wei, X., Cepurna, W., Camino, A., Guo, Y., Huang, D., Morrison, J., & Jia, Y. (2019). Monitoring retinal responses to acute intraocular pressure elevation in rats with visible light optical coherence tomography. *Neurophotonics*, *6*(4), 41104. https://doi.org/10.1117/1.NPh.6.4.041104

Pinilla, I., Fernández-Sánchez, L., Segura, F. J., Sánchez-Cano, A. I., Tamarit, J. M., Fuentes-Broto, L., Eells, J. T., Lax, P., & Cuenca, N. (2016). Long time remodeling during retinal degeneration evaluated by optical coherence tomography, immunocytochemistry and fundus autofluorescence. *Experimental Eye Research*, *150*, 122–134. https://doi.org/10.1016/j.exer.2015.10.012

Pokki, J., Ergeneman, O., Sevim, S., Enzmann, V., Torun, H., & Nelson, B. J. (2015). Measuring localized viscoelasticity of the vitreous body using intraocular microprobes. *Biomedical Microdevices*, *17*(5), 85. https://doi.org/10.1007/s10544-015-9988-z

Pradhan, Z. S., Dixit, S., Sreenivasaiah, S., Rao, H. L., Venugopal, J. P., Devi, S., & Webers, C. A. B. (2018). A Sectoral Analysis of Vessel Density Measurements in Perimetrically Intact Regions of Glaucomatous Eyes: An Optical Coherence Tomography Angiography Study. *Journal of Glaucoma*, *27*(6), 525–531. https://doi.org/10.1097/IJG.0000000000000950

Ramos, D., Carretero, A., Navarro, M., Mendes-Jorge, L., Nacher, V., Rodriguez-Baeza, A., & Ruberte, J. (2013). Mimicking microvascular alterations of human diabetic retinopathy: a challenge for the mouse models. *Current Medicinal Chemistry*, *20*(26), 3200–3217. https://doi.org/10.2174/09298673113209990028

Rao, H. L., Pradhan, Z. S., Suh, M. H., Moghimi, S., Mansouri, K., & Weinreb, R. N. (2020). Optical Coherence Tomography Angiography in Glaucoma. *Journal of Glaucoma*, *29*(4), 312–321. https://doi.org/10.1097/IJG.0000000000001463

Reichenbach, A., Wurm, A., Pannicke, T., Iandiev, I., Wiedemann, P., & Bringmann, A. (2007). Müller cells as players in retinal degeneration and edema. *Graefe's Archive for Clinical and Experimental Ophthalmology*, *245*(5), 627–636. https://doi.org/10.1007/s00417-006-0516-y

Renner, M., Stute, G., Alzureiqi, M., Reinhard, J., Wiemann, S., Schmid, H., Faissner, A., Dick, H. B., & Joachim, S. C. (2017). Optic Nerve Degeneration after Retinal Ischemia/Reperfusion in a Rodent Model. *Frontiers in Cellular Neuroscience*, *11*. https://doi.org/10.3389/fncel.2017.00254

Rocholz, R., Teussink, M. M., Dolz-Marco, R., Holzhey, C., Dechent, J. F., Tafreshi, A., & Schulz, S. (2018). SPECTRALIS Optical Coherence Tomography Angiography (OCTA): Principles and Clinical Applications. In *Heidelburg Engineering Academy*. https://www.heidelbergengineering.com/media/e-learning/Totara/Dateien/pdf-tutorials/210111-001_SPECTRALIS OCTA - Principles and Clinical Applications_EN.pdf

Romano, C., Price, M., Bai, H. Y., & Olney, J. W. (1993). Neuroprotectants in Honghua: glucose attenuates retinal ischemic damage. *Investigative Ophthalmology & Visual Science*, *34*(1), 72–80.

Roth, S., Li, B., Rosenbaum, P. S., Gupta, H., Goldstein, I. M., Maxwell, K. M., & Gidday, J. M. (1998). Preconditioning provides complete protection against retinal ischemic injury in rats. *Investigative Ophthalmology & Visual Science*, *39*(5), 777–785.

Salinas-Navarro, M., Jiménez-López, M., Valiente-Soriano, F. J., Alarcón-Martínez, L., Avilés-Trigueros, M., Mayor, S., Holmes, T., Lund, R. D., Villegas-Pérez, M. P., & Vidal-Sanz, M. (2009). Retinal ganglion cell population in adult albino and pigmented mice: a computerized analysis of the entire population and its spatial distribution. *Vision Research*, *49*(6), 637–647. https://doi.org/10.1016/j.visres.2009.01.010

Salz, D. A., Talisa, E., Adhi, M., Moult, E., Choi, W., Baumal, C. R., Witkin, A. J., Duker, J. S., Fujimoto, J. G., & Waheed, N. K. (2016). Select features of diabetic retinopathy on swept-source optical coherence tomographic angiography compared with fluorescein angiography and normal eyes. *JAMA Ophthalmology*, *134*(6), 644–650.

Schmid, H., Renner, M., Dick, H. B., & Joachim, S. C. (2014). Loss of Inner Retinal Neurons After Retinal Ischemia in Rats. *Investigative Ophthalmology & Visual Science*, *55*(4), 2777–2787. https://doi.org/10.1167/iovs.13-13372

Sharma, S., Ang, M., Najjar, R. P., Sng, C., Cheung, C. Y., Rukmini, A. V, Schmetterer, L., & Milea, D. (2017). Optical coherence tomography angiography in acute non-arteritic anterior ischaemic optic neuropathy. *The British Journal of Ophthalmology*, *101*(8), 1045–1051. https://doi.org/10.1136/bjophthalmol-2016-309245

Sher, I., Moverman, D., Ketter-Katz, H., Moisseiev, E., & Rotenstreich, Y. (2020). In vivo retinal imaging in translational regenerative research. *Annals of Translational Medicine*, *8*(17), 1096. https://doi.org/10.21037/atm-20-4355

Shi, Y., Zhang, Q., Zhou, H., Wang, L., Chu, Z., Jiang, X., Shen, M., Thulliez, M., Lyu, C., & Feuer, W. (2021). Correlations between choriocapillaris and choroidal measurements and the growth of geographic atrophy using swept source OCT imaging. *American Journal of Ophthalmology*, *224*, 321–331.

Shirai, H., Mandai, M., Matsushita, K., Kuwahara, A., Yonemura, S., Nakano, T., Assawachananont, J., Kimura, T., Saito, K., Terasaki, H., Eiraku, M., Sasai, Y., & Takahashi, M. (2016). Transplantation of human embryonic stem cell-derived retinal tissue in two primate models of retinal degeneration. *Proceedings of the National Academy of Sciences of the United States of America*, *113*(1), E81-90. https://doi.org/10.1073/pnas.1512590113

Siliprandi, R., Canella, R., Carmignoto, G., Schiavo, N., Zanellato, A., Zanoni, R., & Vantini, G. (1992). N-methyl-D-aspartate-induced neurotoxicity in the adult rat retina. *Visual Neuroscience*, *8*(6), 567–573. https://doi.org/DOI: 10.1017/S0952523800005666

Smith, C. A., Hooper, M. L., & Chauhan, B. C. (2019). Optical Coherence Tomography Angiography in Mice: Quantitative Analysis After Experimental Models of Retinal Damage. *Investigative Ophthalmology & Visual Science*, *60*(5), 1556–1565. https://doi.org/10.1167/iovs.18-26441

Smith, G. G., & Baird, C. D. (1952). Survival Time of Retinal Cells When Deprived of Their Blood Supply by Increased Intraocular Pressure*. *American Journal of Ophthalmology*, *35*(5, Part 2), 133–136. https://doi.org/https://doi.org/10.1016/0002-9394(52)90266-3

Snodderly, D. M., Weinhaus, R. S., & Choi, J. C. (1992). Neural-vascular relationships in central retina of macaque monkeys (Macaca fascicularis). *The Journal of Neuroscience : The Official Journal of the Society for Neuroscience*, *12*(4), 1169–1193. https://doi.org/10.1523/JNEUROSCI.12-04-01169.1992

Soares, M., Neves, C., Marques, I. P., Pires, I., Schwartz, C., Costa, M. Â., Santos, T., Durbin, M., & Cunha-Vaz, J. (2017). Comparison of diabetic retinopathy classification using fluorescein angiography and optical coherence tomography angiography. *British Journal of Ophthalmology*, *101*(1), 62–68.

Soares, R. O. S., Losada, D. M., Jordani, M. C., Évora, P., & Castro-E-Silva, O. (2019). Ischemia/Reperfusion Injury Revisited: An Overview of the Latest Pharmacological Strategies. *International Journal of Molecular Sciences*, *20*(20). https://doi.org/10.3390/ijms20205034

Spaide, R. F. (2015). Optical Coherence Tomography Angiography Signs of Vascular Abnormalization With Antiangiogenic Therapy for Choroidal Neovascularization. *American Journal of Ophthalmology*, *160*(1), 6–16. https://doi.org/10.1016/j.ajo.2015.04.012

Spaide, R. F., Klancnik, J. M., & Cooney, M. J. (2015). Retinal vascular layers imaged by fluorescein angiography and optical coherence tomography angiography. *JAMA Ophthalmology*, *133*(1), 45–50.

Sridhar, M. S. (2018). Anatomy of cornea and ocular surface. *Indian Journal of Ophthalmology*, *66*(2), 190–194. https://doi.org/10.4103/ijo.IJO_646_17

Stefánsson, E., Wilson, C. A., Schoen, T., & Kuwabara, T. (1988). Experimental ischemia induces cell mitosis in the adult rat retina. *Investigative Ophthalmology & Visual Science*, *29*(7), 1050–1055.

Stone, J., Maslim, J., Valter-Kocsi, K., Kyle Mervin, Bowers, F., Chu, Y., Barnett, N., Provis, J., Lewis, G., Fisher, S. K., Bisti, S., Gargini, C., Cervetto, L., Merin, S., & Pe'er, J. (1999). Mechanisms of photoreceptor death and survival in mammalian retina. *Progress in Retinal and Eye Research*, *18*(6), 689–735. https://doi.org/https://doi.org/10.1016/S1350-9462(98)00032-9

Stryer, L. (1991). Visual excitation and recovery. *The Journal of Biological Chemistry*, *266*(17), 10711–10714.

Sulzbacher, F., Pollreisz, A., Kaider, A., Kickinger, S., Sacu, S., & Schmidt-Erfurth, U. (2017). Identification and clinical role of choroidal neovascularization characteristics based on optical coherence tomography angiography. *Acta Ophthalmologica*, *95*(4), 414–420. https://doi.org/10.1111/aos.13364

Szabo, M. E., Droy-Lefaix, M. T., Doly, M., & Braquet, P. (1991). Free radical-mediated effects in reperfusion injury: a histologic study with superoxide dismutase and EGB 761 in rat retina. *Ophthalmic Research*, *23*(4), 225–234.

Tan, P. E. Z., Yu, P. K., Balaratnasingam, C., Cringle, S. J., Morgan, W. H., McAllister, I. L., & Yu, D.-Y. (2012). Quantitative confocal imaging of the retinal microvasculature in the human retina. *Investigative Ophthalmology & Visual Science*, *53*(9), 5728–5736. https://doi.org/10.1167/iovs.12-10017

Tinjust, D., Kergoat, H., & Lovasik, J. V. (2002). Neuroretinal function during mild systemic hypoxia. *Aviation, Space, and Environmental Medicine*, *73*(12), 1189–1194.

Toyoda, J. (1973). Membrane resistance changes underlying the bipolar cell response in the carp retina. *Vision Research*, *13*(2), 283–294. https://doi.org/10.1016/0042-6989(73)90107-7

Tsin, A., Betts-Obregon, B., & Grigsby, J. (2018). Visual cycle proteins: Structure, function, and roles in human retinal disease. *The Journal of Biological Chemistry*, *293*(34), 13016–13021. https://doi.org/10.1074/jbc.AW118.003228

Uehara, F., Matthes, M. T., Yasumura, D., & LaVail, M. M. (1990). Light-evoked changes in the interphotoreceptor matrix. *Science (New York, N.Y.)*, *248*(4963), 1633–1636. https://doi.org/10.1126/science.2194288

Uehara, H., Lesuma, T., Stocking, P., Jensen, N., Kumar, S. R., Zhang, M. A., Choi, S., Zhang, X., Archer, B., Carroll, L., & Ambati, B. K. (2019). Detection of microvascular retinal changes in type I diabetic mice with optical coherence tomography angiography. *Experimental Eye Research*, *178*, 91–98. https://doi.org/10.1016/j.exer.2018.09.017

Vidal-Sanz, M., Lafuente, M. P., Mayor, S., de Imperial, J. M., & Villegas-Pérez, M. P. (2001). Retinal Ganglion Cell Death Induced by Retinal Ischemia: Neuroprotective Effects of Two Alpha-2 Agonists. *Survey of Ophthalmology*, *45*, S261–S267. https://doi.org/https://doi.org/10.1016/S0039-6257(01)00205-3

Vinores, S. A. (2010). Breakdown of the Blood–Retinal Barrier. In *Encyclopedia of the Eye* (pp. 216–222). https://doi.org/10.1016/B978-0-12-374203-2.00137-8

Virgili, G., Menchini, F., Casazza, G., Hogg, R., Das, R. R., Wang, X., & Michelessi, M. (2015). Optical coherence tomography (OCT) for detection of macular oedema in patients with diabetic retinopathy. *Cochrane Database of Systematic Reviews*, *1*.

Vorwerk, C. K., Lipton, S. A., Zurakowski, D., Hyman, B. T., Sabel, B. A., & Dreyer, E. B. (1996). Chronic low-dose glutamate is toxic to retinal ganglion cells. Toxicity blocked by memantine. *Investigative Ophthalmology & Visual Science*, *37*(8), 1618—1624. http://europepmc.org/abstract/MED/8675405

Wang, Q., Swärdh, A., & Sjöquist, P. (2001). Relationship between ischaemic time and ischaemia/reperfusion injury in isolated Langendorff-perfused mouse hearts. *Acta Physiologica Scandinavica*, *171*(2), 123–128.

Wangsa-Wirawan, N. D., & Linsenmeier, R. A. (2003). Retinal oxygen: fundamental and clinical aspects. *Archives of Ophthalmology (Chicago, Ill. : 1960)*, *121*(4), 547–557. https://doi.org/10.1001/archopht.121.4.547

Wässle, H., Heinze, L., Ivanova, E., Majumdar, S., Weiss, J., Harvey, R. J., & Haverkamp, S. (2009). Glycinergic transmission in the Mammalian retina. *Frontiers in Molecular Neuroscience*, *2*, 6. https://doi.org/10.3389/neuro.02.006.2009

Webb, R. H., Hughes, G. W., & Delori, F. C. (1987). Confocal scanning laser ophthalmoscope. *Applied Optics*, *26*(8), 1492–1499. https://doi.org/10.1364/AO.26.001492

Weinreb, R. N., Aung, T., & Medeiros, F. A. (2014). The pathophysiology and treatment of glaucoma: a review. *JAMA*, *311*(18), 1901–1911. https://doi.org/10.1001/jama.2014.3192

Werblin, F. S., & Dowling, J. E. (1969). Organization of the retina of the mudpuppy, Necturus maculosus. II. Intracellular recording. *Journal of Neurophysiology*, *32*(3), 339–355. https://doi.org/10.1152/jn.1969.32.3.339

Werns, S. W., Shea, M. J., & Lucchesi, B. R. (1985). Free radicals in ischemic myocardial injury. *Journal of Free Radicals in Biology & Medicine*, *1*(2), 103–110.

Wiesel, T. N. (1959). Recording inhibition and excitation in the cat's retinal ganglion cells with intracellular electrodes. *Nature*, *183*(4656), 264–265. https://doi.org/10.1038/183264a0

Winkler, B. S., Boulton, M. E., Gottsch, J. D., & Sternberg, P. (1999). Oxidative damage and age-related macular degeneration. *Molecular Vision*, *5*, 32.

Winkler, B. S. (1972). The electroretinogram of the isolated rat retina. *Vision Research*, *12*(6), 1183–1198. https://doi.org/https://doi.org/10.1016/0042-6989(72)90106-X

Wojtkowski, M., Srinivasan, V., Fujimoto, J. G., Ko, T., Schuman, J. S., Kowalczyk, A., & Duker, J. S. (2005). Three-dimensional retinal imaging with high-speed ultrahigh-resolution optical coherence tomography. *Ophthalmology*, *112*(10), 1734–1746. https://doi.org/10.1016/j.ophtha.2005.05.023

Wright, W. S., Eshaq, R. S., Lee, M., Kaur, G., & Harris, N. R. (2020). Retinal Physiology and Circulation: Effect of Diabetes. *Comprehensive Physiology*, *10*(3), 933–974. https://doi.org/10.1002/cphy.c190021

Wu, H.-H., Huang, C.-C., Chang, C.-P., Lin, M.-T., Niu, K.-C., & Tian, Y.-F. (2018). Heat shock protein 70 (HSP70) reduces hepatic inflammatory and oxidative damage in a rat model of liver ischemia/reperfusion injury with hyperbaric oxygen preconditioning. *Medical Science Monitor: International Medical Journal of Experimental and Clinical Research*, *24*, 8096.

Yang, J. H., Yu, S.-Y., Kim, T. G., Seo, K. H., & Kwak, H. W. (2016). Repeatability and Reproducibility of Spectral-Domain Optical Coherence Tomography Measurements of Retinal Thickness in Rats. *Current Eye Research*, *41*(10), 1346–1352. https://doi.org/10.3109/02713683.2015.1114651

Yang, S., Liu, K., Ding, H., Gao, H., Zheng, X., Ding, Z., Xu, K., & Li, P. (2019). Longitudinal in vivo intrinsic optical imaging of cortical blood perfusion and tissue damage in focal photothrombosis stroke model. *Journal of Cerebral Blood Flow and Metabolism : Official Journal of the International Society of Cerebral Blood Flow and Metabolism*, *39*(7), 1381–1393. https://doi.org/10.1177/0271678X18762636

Yang, Y., Ng, T. K., Ye, C., Yip, Y. W. Y., Law, K., Chan, S.-O., & Pang, C. P. (2014). Assessing sodium iodate-induced outer retinal changes in rats using confocal scanning laser ophthalmoscopy and optical coherence tomography. *Investigative Ophthalmology & Visual Science*, *55*(3), 1696–1705. https://doi.org/10.1167/iovs.13-12477

Yau, K. W. (1994). Phototransduction mechanism in retinal rods and cones. The Friedenwald Lecture. *Investigative Ophthalmology & Visual Science*, *35*(1), 9–32.

You, Q., Freeman, W. R., Weinreb, R. N., Zangwill, L., Manalastas, P. I. C., Saunders, L. J., & Nudleman, E. (2017). REPRODUCIBILITY OF VESSEL DENSITY MEASUREMENT WITH OPTICAL COHERENCE TOMOGRAPHY ANGIOGRAPHY IN EYES WITH AND WITHOUT RETINOPATHY. *Retina (Philadelphia, Pa.)*, *37*(8), 1475–1482. https://doi.org/10.1097/IAE.0000000000001407

Yu, D.-Y., & Cringle, S. J. (2001). Oxygen Distribution and Consumption within the Retina in Vascularised and Avascular Retinas and in Animal Models of Retinal Disease. *Progress in Retinal and Eye Research*, *20*(2), 175–208. https://doi.org/https://doi.org/10.1016/S1350-9462(00)00027-6

Yu, D.-Y., Cringle, S. J., & Su, E.-N. (2005). Intraretinal oxygen distribution in the monkey retina and the response to systemic hyperoxia. *Investigative Ophthalmology & Visual Science*, *46*(12), 4728–4733. https://doi.org/10.1167/iovs.05-0694

Yu, P. K., Balaratnasingam, C., Morgan, W. H., Cringle, S. J., McAllister, I. L., & Yu, D.-Y. (2010). The structural relationship between the microvasculature, neurons, and glia in the human retina. *Investigative Ophthalmology & Visual Science*, *51*(1), 447–458. https://doi.org/10.1167/iovs.09-3978

Zadeh, J. K., Garcia-Bardon, A., Hartmann, E. K., Pfeiffer, N., Omran, W., Ludwig, M., Patzak, A., Xia, N., Li, H., & Gericke, A. (2019). Short-Time Ocular Ischemia Induces Vascular Endothelial Dysfunction and Ganglion Cell Loss in the Pig Retina. *International Journal of Molecular Sciences*, *20*(19). https://doi.org/10.3390/ijms20194685

Zhang, A., Zhang, Q., Chen, C.-L., & Wang, R. K. (2015). Methods and algorithms for optical coherence tomography-based angiography: a review and comparison. *Journal of Biomedical Optics*, *20*(10), 100901. https://doi.org/10.1117/1.JBO.20.10.100901

Zhang, S., Wu, C., Liu, L., Jia, Y., Zhang, Y., Zhang, Y., Zhang, H., Zhong, Y., & Huang, D. (2017). Optical Coherence Tomography Angiography of the Peripapillary Retina in Primary Angle-Closure Glaucoma. *American Journal of Ophthalmology*, *182*, 194–200. https://doi.org/10.1016/j.ajo.2017.07.024

Zhao, D., He, Z., Wang, L., Fortune, B., Lim, J. K. H., Wong, V. H. Y., Nguyen, C. T. O., & Bui, B. V. (2020). Response of the Trilaminar Retinal Vessel Network to Intraocular Pressure Elevation in Rat Eyes. *Investigative Ophthalmology & Visual Science*, *61*(2), 2. https://doi.org/10.1167/iovs.61.2.2

Zheng, L., Gong, B., Hatala, D. A., & Kern, T. S. (2007). Retinal Ischemia and Reperfusion Causes Capillary Degeneration: Similarities to Diabetes. *Investigative Ophthalmology & Visual Science*, *48*(1), 361–367. https://doi.org/10.1167/iovs.06-0510

Zhu, Y., Ohlemiller, K. K., McMahan, B. K., & Gidday, J. M. (2002). Mouse Models of Retinal Ischemic Tolerance. *Investigative Ophthalmology & Visual Science*, *43*(6), 1903–1911.

Zipfel, G. J., Babcock, D. J., Lee, J.-M., & Choi, D. W. (2000). Neuronal Apoptosis After CNS Injury: The Roles of Glutamate and Calcium. *Journal of Neurotrauma*, *17*(10), 857–869. https://doi.org/10.1089/neu.2000.17.857

Appendix A: Copyright Permissions

Figure 1.3.

ELSEVIER LICENSE
TERMS AND CONDITIONS

Jan 17, 2023

This Agreement between Ryan Matthews ("You") and Elsevier ("Elsevier") consists of your license details and the terms and conditions provided by Elsevier and Copyright Clearance Center.

License Number	5471390297011
License date	Jan 17, 2023
Licensed Content Publisher	Elsevier
Licensed Content Publication	Elsevier Books
Licensed Content Title	Encyclopedia of the Eye
Licensed Content Author	B. Anand-Apte,J.G. Hollyfield
Licensed Content Date	Jan 1, 2010
Licensed Content Pages	7
Start Page	9
End Page	15
Type of Use	reuse in a thesis/dissertation
Portion	figures/tables/illustrations
Number of figures/tables/illustrations	1

Figure 1.5.

CCC Marketplace

Order Number: 1311907
Order Date: 17 Feb 2023

Payment Information

Ryan Matthews
Ryan.Matthews@dal.ca
Payment method: Invoice

Billing Address:
Ryan Matthews
41 Wakefield Court
Middle Sackville, NS B4E 0 H1
Canada

+1 (905) 870-0208
ryan.matthews@dal.ca

Customer Location:
Ryan Matthews
41 Wakefield Court
Middle Sackville, NS B4E 0 H1
Canada

Order Details

1. CURRENT MEDICINAL CHEMISTRY

Billing Status: Open

Article: Mimicking Microvascular Alterations of Human Diabetic Retinopathy: A Challenge for the Mouse Models

Order License ID	1311907-1	**Type of use**	Republish in a thesis/dissertation
Order detail status	Completed		
ISSN	0929-8673	**Publisher**	BENTHAM SCIENCE PUBLISHERS LTD.
		Portion	Image/photo/illustration

0.00 CAD
Republication Permission

LICENSED CONTENT

Publication Title	CURRENT MEDICINAL CHEMISTRY	**Publication Type**	Journal
		Start Page	3200
Article Title	Mimicking Microvascular Alterations of Human Diabetic Retinopathy: A Challenge for the Mouse Models	**End Page**	3217
		Issue	26
		Volume	20
Date	01/01/1994		
Language	English		
Country	Netherlands		
Rightsholder	EUREKA SCIENCE (FZC)		

REQUEST DETAILS